7. SITE 738[1]

Shipboard Scientific Party[2]

HOLE 738A

Date occupied: 10 January 1988

Date departed: 10 January 1988

Time on hole: 13 hr, 45 min

Position: 62°42.54'S, 82°47.25'E

Bottom felt (rig floor; m, drill-pipe measurement): 2263.2

Distance between rig floor and sea level (m): 10.5

Water depth (drill-pipe measurement from sea level, m): 2252.7

Total depth (rig floor, m): 2266.0

Penetration (m): 2.8

Number of cores: 1

Total length of cored section (m): 2.8

Total core recovered (m): 2.76

Core recovery (%): 98

Oldest sediment cored:
    Depth sub-bottom (m): 2.8
    Nature: diatom ooze
    Earliest age: Quaternary
    Measured velocity (km/s): 1.57

HOLE 738B

Date occupied: 10 January 1988

Date departed: 11 January 1988

Time on hole: 1 day, 2 hr, 45 min

Position: 62°42.54'S, 82°47.25'E

Bottom felt (rig floor; m, drill-pipe measurement): 2263.0

Distance between rig floor and sea level (m): 10.5

Water depth (drill-pipe measurement from sea level, m): 2252.5

Total depth (rig floor, m): 2477.3

Penetration (m): 214.3

Number of cores: 24

Total length of cored section (m): 214.3

Total core recovered (m): 170.85

Core recovery (%): 79

Oldest sediment cored:
    Depth sub-bottom (m): 214.3
    Nature: nannofossil chalk
    Earliest age: middle Eocene
    Measured velocity (km/s): 1.73

HOLE 738C

Date occupied: 11 January 1988

Date departed: 17 January 1988

Time on hole: 5 days, 11 hr

Position: 62°42.54'S, 82°47.25'E

Bottom felt (rig floor; m, drill-pipe measurement): 2263.0

Distance between rig floor and sea level (m): 10.5

Water depth (drill-pipe measurement from sea level, m): 2252.5

Total depth (rig floor, m): 2796.8

Penetration (m): 533.8

Number of cores: 36

Total length of cored section (m): 533.8

Total core recovered (m): 146.29

Core recovery (%): 27

Oldest sediment cored:
    Depth sub-bottom (m): 485.9
    Nature: limestone
    Earliest age: early Turonian
    Measured velocity (km/s): 3.04

Hard rock:
    Depth sub-bottom (m): 533.8
    Nature: volcanic breccia, volcaniclastic rocks, and aphyric basalt
    Measured velocity (km/s): 4.395

Principal results: A 486-m-thick lower Turonian through Quaternary sediment section overlying 38 m of volcaniclastic rocks and altered basalt was cored at Site 738 (62°42.54'S, 82°47.25'E; 2252.5 m water depth), on the southern tip of the Kerguelen Plateau.

Eight provisional lithologic units are recognized at Site 738:

Unit I: 0–16.8 m below seafloor (mbsf), Quaternary to uppermost Miocene diatom ooze;

Unit II: 16.8–17.7 mbsf, upper Miocene nannofossil ooze containing a minor percentage of diatoms;

Unit III: 17.7–120.8 mbsf, lower Oligocene to middle Eocene homogeneous nannofossil ooze;

Unit IV: 120.8–254.4 mbsf, middle and lower Eocene nannofossil ooze and chalk containing thin chert layers and chert concretions;

Unit V: 254.4–418.6 mbsf, lower Eocene to Campanian chalk containing chert nodules and fragments, with bioturbation in the Cretaceous;

Unit VI: 418.6–479.7 mbsf, Campanian to lower Turonian silicified limestone, partially laminated and containing burrows;

Unit VII: 479.7–495.6 mbsf, calciclastic limestone containing basalt pebbles;

Unit VII: 495.6–533.8 mbsf, volcaniclastic rocks and altered basalt.

The sequence documents a series of paleoceanographic and geological changes in the area, including (1) algal calciclastic limestone with basalt pebbles indicating inner shelf deposition during or before the early Turonian; (2) Upper Cretaceous chalks, although primarily pelagic, containing indications from trace fossil assemblages, benthic shelly faunas, and omission surfaces associated with glauconite of a seafloor depth shallower than at present; (3) gradual change through the upper Miocene and lower Pliocene in the pelagic facies, from nannofossil ooze to diatom ooze; and (4) deposition of ice-

[1] Barron, J., Larsen, B., et al., 1989. *Proc. ODP, Init. Repts.*, 119: College Station, TX (Ocean Drilling Program).

[2] Shipboard Scientific Party is as given in the list of Participants preceding the contents.

rafted debris of gneissic/granitic antarctic derivation from the upper Miocene to Holocene. The sedimentary sequence overlies altered basalts interpreted as representing basement. Diagenetic processes have transformed the Oligocene to Turonian calcareous pelagites at depth to chalks and limestones with sporadic porcellanites and cherts.

Site 738 constitutes an excellent middle Paleogene to Maestrichtian reference section for Southern Ocean calcareous microfossils because a short hiatus is present only at the middle Eocene/upper Eocene and preservation declines in sediments older than late Maestrichtian. A combination of low-latitude and middle-latitude zones can be applied to nannofossil and planktonic foraminiferal assemblages. The Cretaceous/Tertiary boundary appears to be complete, although the uppermost Cretaceous, immediately below the boundary, was poorly recovered. The Cretaceous/Tertiary boundary lies in a 15-cm-thick laminated claystone interval, which contains 95% micrite particles and few to rare nannofossils. Late Maestrichtian planktonic foraminifers include ornate specimens, which are more typical of subtropical transitional regions than cool, temperate regions. The Cenozoic benthic foraminiferal assemblages of Site 738 indicate paleodepths near or deeper than the present water depth (2252.5 m). However, the upper Maestrichtian is characterized by species indicative of outer shelf environments. Benthic foraminifers in the older Cretaceous sediments are too sparse to be definitive of paleodepth.

Diatoms and radiolarians are more common in the Neogene section and are generally absent in the Paleogene sequence. However, radiolarians show sporadic occurrences in the Eocene and Cretaceous. Surprisingly, low-latitude diatoms (*Thalassiosira miocenica*, *Thalassiosira convexa aspinosa*, and *Thalassiosira praeconvexa*) are present in the uppermost Miocene (5.8–6.1 Ma). Ice-rafted debris is restricted to the overlying Pliocene and Quaternary.

Paleomagnetic stratigraphy at Site 738 is generally poor, although it has been established for the lowermost Paleocene. As at the previous Kerguelen Plateau Sites 736 and 737, the organic carbon content is low in the Site 738 sediments and no gas was encountered.

BACKGROUND AND OBJECTIVES

Site 738 (target site SKP-6A) is on the southern part of the Kerguelen-Heard Plateau (62°42.54′S, 82°47.25′E) in a water depth of 2252.5 m. This site is north of the modern Antarctic Divergence and near the southern limit of influence of the Antarctic Circumpolar Current. As the southernmost site of the Kerguelen-Heard part of the combined Kerguelen–Prydz Bay paleoceanographic transect, Site 738 provides the southernmost pelagic record for documentation of changes in Late Cretaceous and Cenozoic paleoclimatology of East Antarctica. Sediments recovered at the site were anticipated to be free of the considerable terrigenous influence expected for the Prydz Bay sites. Such Site 738 sediments should, therefore, record the initial northward expansion of Antarctic water masses, presumably in the late Paleogene (Barker, Kennett, et al., 1988), as well as subsequent fluctuations in Antarctic water masses. Additionally, the expected good Neogene record of ice rafting at Site 738 could be used for comparison with the nature and composition of ice-rafted clasts to be recovered in Prydz Bay sediments, from which the origin of the Neogene icebergs that passed over Site 738 could be assessed.

The position of Site 738, immediately north of the constricted deep-water (>3500 m) passage separating the area from Antarctica, suggests that Site 738 sediments should record the Neogene erosive periods of Circumpolar Deep Water (CPDW) as it moved eastward around Antarctica. Such erosive periods are likely to be represented by hiatuses in the Site 738 sediments.

Site 738 was chosen near the intersection of French seismic lines MD 47-07 and MD 47-08, where volcanic basement is within 500 m of the seafloor. A second objective at Site 738 was to date the age of basement and to determine its origin and nature. Such information and the age and character of sediments immediately overlying the basement will be important in synthesizing the rifting and subsidence history of the Kerguelen-Heard Pla-

teau. When compared with the results of ODP Leg 120, it will be possible to elucidate whether the southern part of the Kerguelen-Heard Plateau had a separate tectonic history from the central and northern parts as suggested by Coffin et al. (1986).

SITE GEOPHYSICS

Site Survey

Ocean Drilling Program (ODP) geophysical survey line 119-03 was recorded on approach to Site 738 (Fig. 1) using the standard navigation, seismic, and magnetic equipment (see "Explanatory Notes" chapter, this volume). A sonobuoy was deployed about 4.5 km before crossing the proposed site and recorded to a total offset of 11 km. A beacon was dropped crossing the proposed site, which was picked at shotpoint 3900 on *Marion Dufresne* multichannel seismic-reflection line MD 47-07. The seismic line was continued 6 nmi beyond the dropped beacon to examine nearby subsurface structure. Seismic gear was then recovered, and the ship proceeded back to the beacon to commence drilling. The seismic results are discussed in "Seismic Stratigraphy" section, this chapter.

Sonobuoy Data

The sonobuoy was released before reaching the proposed drill site to acquire wide-angle reflection and refraction arrivals through the sedimentary section directly beneath the site.

Noise levels in the sonobuoy record were high because the hydrophone apparently did not deploy to the standard 17-m depth (water-gurgling noises were heard even though the seas were very calm). Consequently, the direct arrival (*D*-wave) and wide-angle
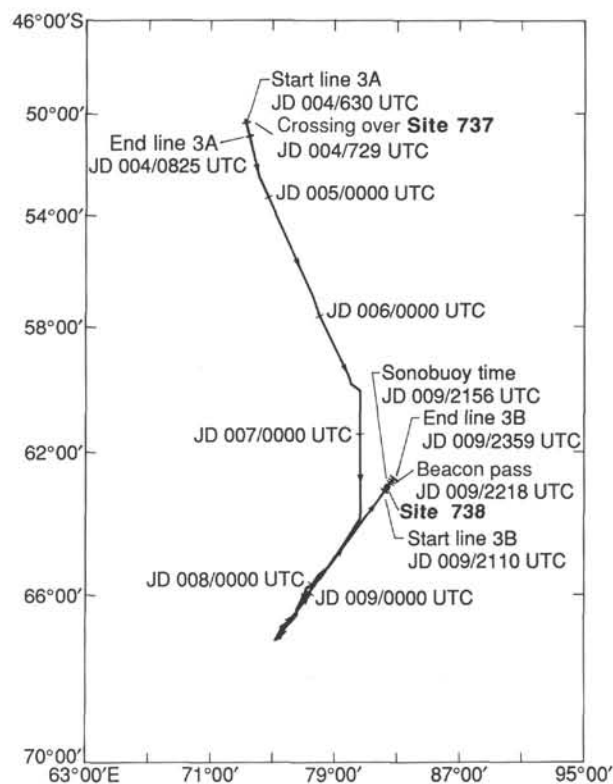

Figure 1. Index map of seismic lines recorded during the site survey for Site 738.

reflections are not strong, but five arrivals could be traced to offsets of up to 5 km (Fig. 2). Only two very weak, and questionable, refraction arrivals could be identified. Minor corrections (−70 m/s) were added to rms and refraction velocities to correct for a questionable D-wave (see the discussion of sonobuoy error, "Underway Geophysics" chapter, this volume). The interval and refraction velocities for sonobuoy 3 are given in Table 1.

The sonobuoy results indicate that low-velocity sediment (1.48 km/s), which has few coherent reflectors in the vertical-incidence seismic profile, extends from the seafloor to about 0.24 s sub-bottom. At this point, well-layered strata with interval velocities of 2.51 to 3.15 km/s extend to acoustic basement. A comparison of sonobuoy interval velocities with laboratory velocity measurements (Hamilton Frame) is given in the "Physical Properties" section of this chapter.

Acoustic basement in seismic-reflection profiles (3.6 s two-way traveltime) gives a good wide-angle reflection (Fig. 3) that is underlain by an additional 0.05 s of apparently layered rocks. A weak refraction (4.1 km/s) is recorded from the top of acoustic basement. A few coherent wide-angle reflections and diffractions are visible within acoustic basement, suggesting that an intra-basement sub-basin with up to 0.3 s of layered rocks lies between the point of sonobuoy deployment and Site 738. The sub-basin thins toward Site 738, and the high-velocity igneous basement(?) underlying the sub-basin abruptly shallows 2–3 km

Table 1. Preliminary results for sonobuoy 3, Site 738.

Horizon[a]	Vrms (km/s)	Vint (km/s)	Ti (s)	Zi (km)	Vrfr (km/s)	To (s)
AA	1.475	1.48	3.04	2.253	nr	—
BB	1.475	2.51	3.28	2.430	nr	—
CC	1.500	2.75	3.34	2.505	nr	—
DD	1.565	3.15	3.47	2.684	nr	—
EE	1.649	—	3.60	2.889	4.10 [b]5.90	3.24

Note: Vrms = rms velocity for horizon; Vint = interval velocity computed using Vrms, Ti, and Dix equation (e.g., Vint between horizons AA and BB is 1.48 km/s); Ti = vertical-incidence reflection time (two-way) to horizon; Zi = total depth from sea level to horizon computed from Vint and Ti (water depth = 2253 m); Vrfr = refraction velocity associated with horizon (e.g., Vrfr at top of acoustic basement EE is 4.10 km/s); To = intercept time for refractor associated with horizon; nr = no refractor observed.

[a] Letters of horizons do not correlate between drill sites and do not correspond to prior stratigraphic analyses.

[b] Apparent velocity for acoustic basement about 5 km northeast of Site 738.

northeast of the site. The rapid shallowing is evidenced by vertically stacked diffractions in the vertical-incidence seismic profile (Fig. 4) and by a sharp upbowing of the acoustic basement refractor (e.g., higher apparent velocities on a steep updip sur-
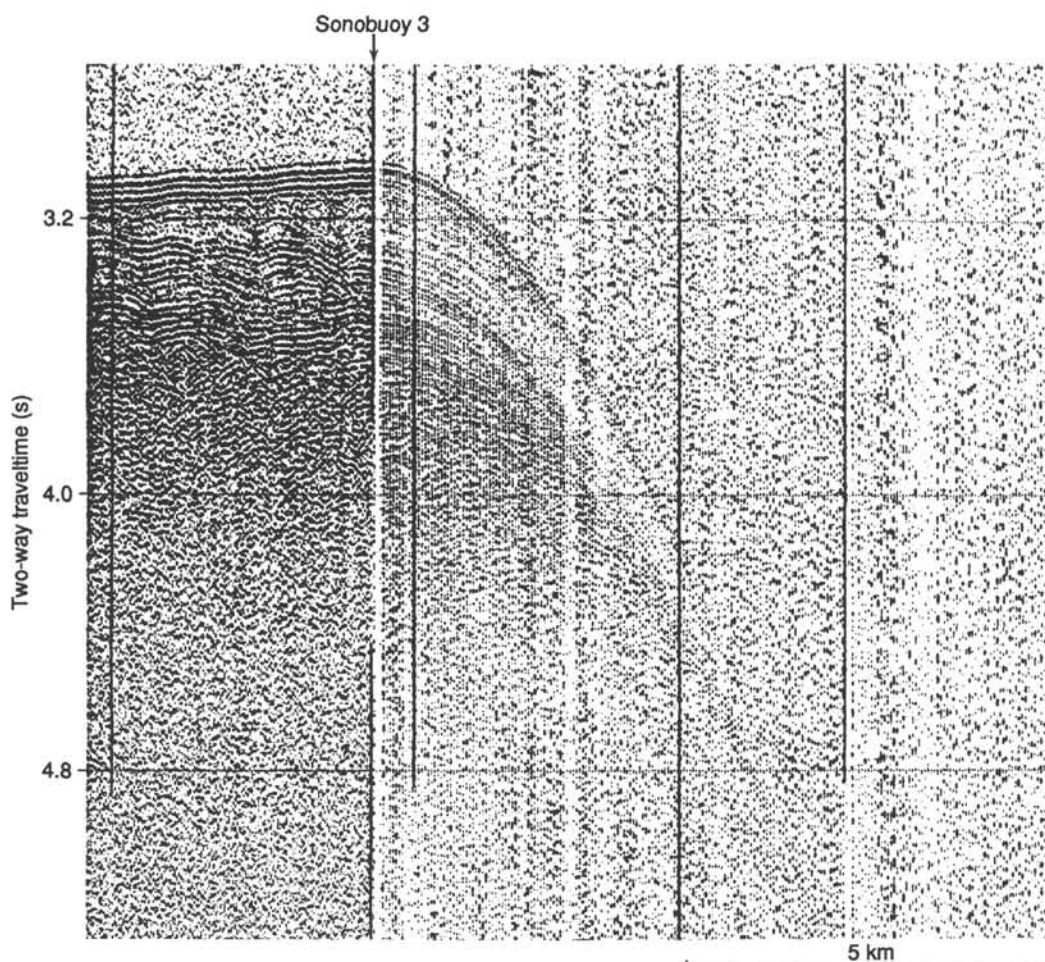

Figure 2. Vertical-incident seismic and sonobuoy seismic record for sonobuoy station 3. Site 738 is about 4.5 km northeast of where the sonobuoy was deployed. See Figure 1 for location.
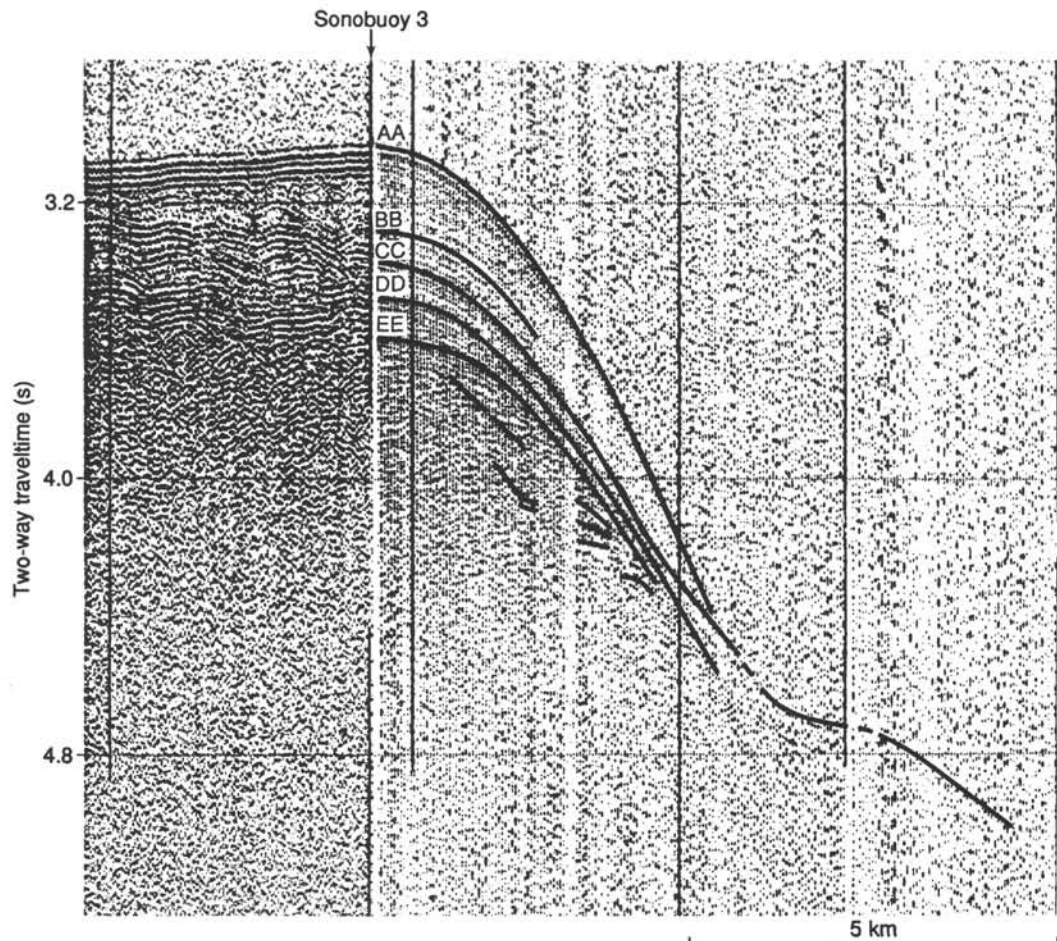
Figure 3. Vertical-incident seismic and sonobuoy seismic record for Site 738 showing wide-angle reflection and refraction interpretations. Letters denote layers in Table 1. See Figure 1 for location.

face) in the sonobuoy data (Fig. 3). The apparent velocity of the acoustic basement increases to 5.9 km/s about 5 km northeast of Site 738, where basement seems bevelled and has few internal reflections in the seismic profile (Fig. 3).

The foregoing observations indicate that acoustic basement may be composed of different rock types beneath Site 738 (volcaniclastics/altered basalt) and beneath a point 5 km to the northeast (massive basalt?). The depth to acoustic basement beneath Site 738 is 635 mbsf, based on the sonobuoy results, but volcaniclastics and altered basalt flows were encountered at 480–533 mbsf in Hole 738B. The additional 0.3 s of what are probably layered rocks within acoustic basement near Site 738 is estimated to be 623 m thick from the sonobuoy data. These rocks may be similar to those in the bottom of Hole 738B.

In summary, the sedimentary section at Site 738 is characterized by 177 m of low-velocity strata (1.48 km/s) that overlie three deeper sedimentary units with velocities of 2.51 to 3.15 km/s and a combined thickness of 458 m. Distinct velocity discontinuities between the sedimentary units (e.g., strong refraction arrivals) are not observed, but the generally poor data quality may obscure these arrivals. Acoustic basement has apparent refraction velocities of 4.1 km/s beneath Site 738 and 5.9 km/s about 5 km to the northeast. Internal layering within acoustic basement near Site 738, observed in sonobuoy and vertical-incidence seismic data, suggests that acoustic basement may be composed of layered volcaniclastic rocks beneath Site 738.

OPERATIONS

A departure profile was made across Site 737, with the drillship getting underway to the north, streaming gear and crossing the beacon on the departure course. The gear was then recovered, except for the magnetometer, and speed was increased to 12 kt for the transit south.

Good weather prevailed as the vessel ran near the center of a deep low-pressure area, and anticipated high winds did not materialize. With following winds and swells, *JOIDES Resolution* made about a good 12 kt for the first two days.

On 6 January 1988 the first iceberg of the voyage was spotted at latitude 58°47'S. The density of bergs, growlers, and bergy bits increased until between 60°30' and 61°15'S about 40 ice contacts were present at any given time on the 12 nmi range of the radar screen. With *Maersk Master* in the van, a detour of about 30 nmi to the east was made to avoid the greatest ice concentration. The density of bergs then decreased as the vessel proceeded southward on a longitude of about 80°30'E.

At latitude 65°59'S the course was changed back to the southwest toward Prydz Bay, with only a few scattered icebergs in sight. The first pack ice was encountered at about 66°30'S in two dense, but narrow, bands. Thoroughly scattered multiyear pack-ice floes persisted as target Site PB-6 was approached. Ice coverage was not greater than one-tenth, and drilling appeared feasible, although the approach survey promised to be difficult.
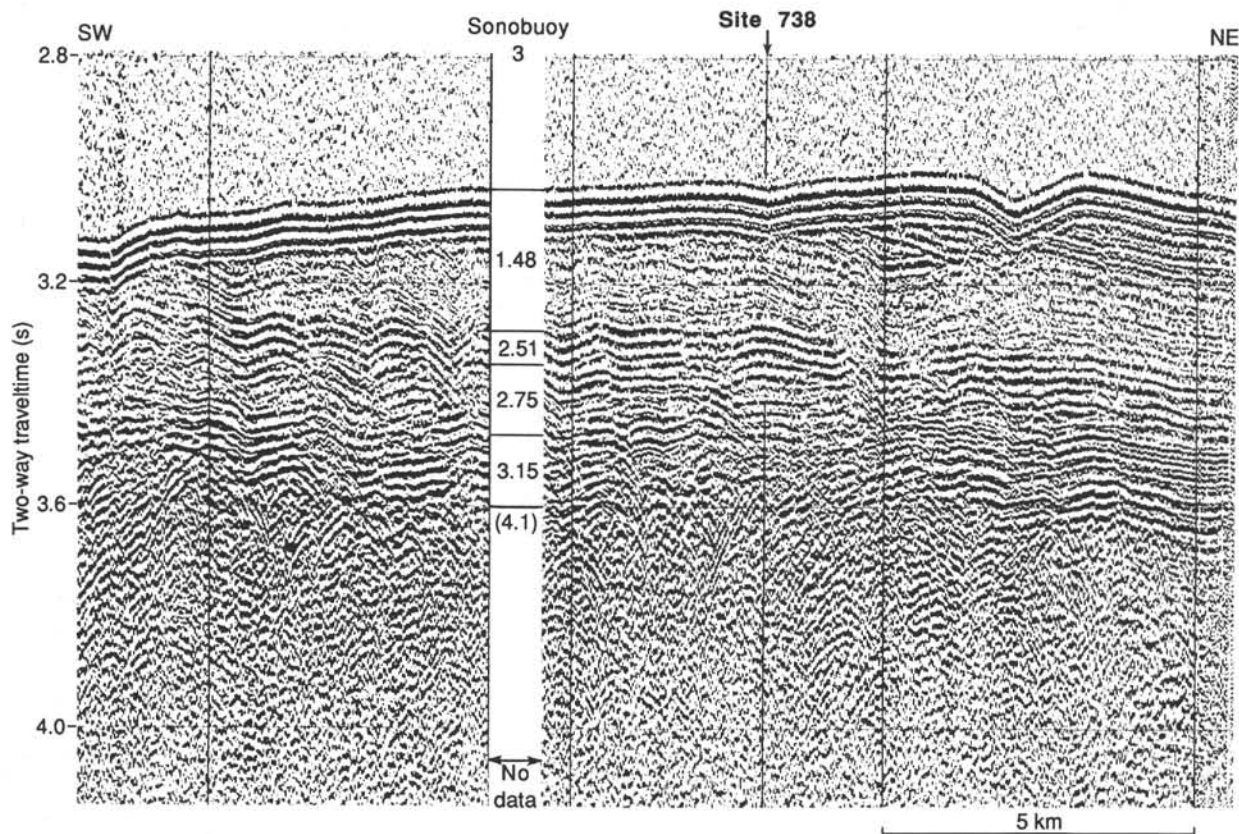
Figure 4. Vertical-incident seismic profile showing sonobuoy interval and refraction velocities at Site 738.

The seismic gear was streamed for the approach, and almost immediately, the density of the pack ice increased. The ice coverage quickly reached about three-tenths, and we found it necessary to retrieve the seismic gear after only a few minutes of profiling. *Maersk Master* scouted ahead, but saw no opening in the ice in the direction of target Site PB-6. *JOIDES Resolution* was forced to reverse course only 5 nmi from her destination and steam back toward clearer waters.

Ice information indicated that the band of pack ice was only a few miles wide and that Prydz Bay and the landward sites of the proposed transect were ice free. Because of the uncertainty as to time required to find a clear route through or around the pack ice and the plan to begin the Prydz Bay operation with profiling and drilling at the seaward sites, the consensus was to divert to target Site SKP-6A. All Leg 119 objectives, except for the Prydz Bay sites, would then be complete after about eight site days, leaving the balance of the operating time for Prydz Bay.

Because the vessel had passed fairly close to target Site SKP-6A on the southward transit, the new course was nearly reciprocal. The amount of ice encountered on the northward track seemed less than that noted just one or two days before. The drill site is only about 90 nmi south of the latitude of greatest iceberg concentration found on the voyage south, so there was little doubt that the ice management services of *Maersk Master* would be required.

The proposed site was approached from the southwest, and the gear was streamed about 7.5 nmi out. A sonobuoy was launched 1 nmi from the site, and the positioning beacon was dropped on Global Positioning System (GPS) navigation at 0218 hr, 10 January. The profile was extended 6 nmi before the ship turned and took station.

Site 738—South Kerguelen Plateau

Hole 738A

The pipe trip started slowly because the bottom-hole assembly (BHA) had to be assembled from individual drill collars and drill pipe not run on the shallower sites had to be measured and drifted. We took advantage of the good weather during the trip to transfer bulk bentonite and cement from *Maersk Master*. The advanced piston corer (APC) coring assembly was deployed for the initial core, but as the corer reached the BHA, the coring line began to bind in the oil saver, causing the line to stop and start with violent jerks. A delay of about 1.5 hr was required to clear the close tolerances of the oil saver of an accumulation of rust and tarry line coating. When the APC was finally landed and the pipe was pressured, we found that the APC shear pins had failed as a result of the earlier erratic motion. The quality of the resulting "gravity" core was suspect, so we took a second seafloor core, beginning Hole 738B.

Hole 738B

The second core confirmed that the first attempt had stroked fully, and the contents of the two cores agreed to within 20 cm. Oriented APC cores were then taken to refusal depth at 105 mbsf (Table 2). Refusal was manifested by incomplete stroke and damage to the corer caused by hard siliceous stringers in the soft nannofossil ooze. Core recovery with the APC was 97.7%.

Coring continued with the extended core barrel (XCB) to 216 mbsf. Recovery began to decrease with depth because of an increase in indurated zones and traces of chert. Because chert and basement rocks were anticipated deeper in the section, the pipe was tripped for the rotary core barrel (RCB) BHA and coring system.

Table 2. Coring summary, Site 738.

Core no.	Date (Jan. 1988)	Time	Depth top (mbsf)	Depth bottom (mbsf)	Length cored (m)	Length recovered (m)	Recovery (%)
119-738A-							
1H	10	1620	0.0	2.8	2.8	2.76	98.6
					2.8	2.76	
119-738B-							
1H	10	1715	0.0	4.0	4.0	4.05	101.0
2H	10	1815	4.0	13.5	9.5	9.77	103.0
3H	10	1910	13.5	23.0	9.5	8.93	94.0
4H	10	2000	23.0	32.5	9.5	9.86	104.0
5H	10	2055	32.5	42.0	9.5	9.88	104.0
6H	10	2150	42.0	51.5	9.5	8.99	94.6
7H	10	2245	51.5	61.0	9.5	9.82	103.0
8H	11	0000	61.0	70.5	9.5	9.78	103.0
9H	11	0100	70.5	80.0	9.5	7.00	73.7
10H	11	0200	80.0	85.0	5.0	4.61	92.2
11H	11	0250	85.0	94.5	9.5	9.42	99.1
12H	11	0330	94.5	104.0	9.5	9.51	100.0
13H	11	0415	104.0	108.2	4.2	4.23	101.0
14X	11	0540	108.2	117.8	9.6	5.36	55.8
15X	11	0620	117.8	127.5	9.7	8.90	91.7
16X	11	0710	127.5	137.2	9.7	2.47	25.4
17X	11	0755	137.2	146.8	9.6	6.69	69.7
18X	11	0845	146.8	156.5	9.7	6.77	69.8
19X	11	0930	156.5	166.2	9.7	8.95	92.2
20X	11	1010	166.2	175.8	9.6	9.04	94.1
21X	11	1045	175.8	185.4	9.6	4.46	46.4
22X	11	1135	185.4	195.0	9.6	6.14	63.9
23X	11	1230	195.0	204.6	9.6	1.93	20.1
24X	11	1315	204.6	214.3	9.7	4.29	44.2
					214.3	170.85	
119-738C-							
1W	12	0805	0.0	196.6	196.6	0.26	
2R	12	0925	196.6	206.2	9.6	1.93	20.1
3R	12	1000	206.2	215.9	9.7	0.75	7.7
4R	12	1045	215.9	225.6	9.7	4.15	42.8
5R	12	1120	225.6	235.2	9.6	2.34	24.4
6R	12	1205	235.2	244.8	9.6	1.20	12.5
7R	12	1300	244.8	254.4	9.6	3.60	37.5
8R	12	1405	254.4	264.1	9.7	1.39	14.3
9R	12	1500	264.1	273.8	9.7	0.91	9.4
10R	12	1545	273.8	283.4	9.6	5.10	53.1
11R	13	0230	283.4	293.0	9.6	3.45	35.9
12R	13	0930	293.0	302.7	9.7	0.00	0.0
13R	13	1015	302.7	312.3	9.6	0.13	1.4
14R	13	1130	312.3	321.9	9.6	0.14	1.5
15R	13	1225	321.9	331.6	9.7	0.17	1.8
16R	13	1325	331.6	341.3	9.7	9.33	96.2
17R	13	1425	341.3	350.9	9.6	10.03	104.5
18R	13	1520	350.9	360.5	9.6	9.62	100.0
19R	13	1615	360.5	370.2	9.7	4.62	47.6
20R	13	1720	370.2	379.9	9.7	7.21	74.3
21R	13	1815	379.9	389.6	9.7	0.82	8.5
22R	13	1915	389.6	399.2	9.6	8.03	83.6
23R	13	2010	399.2	408.9	9.7	4.73	48.7
24R	13	2240	408.9	418.6	9.7	4.53	46.7
25R	14	0230	418.6	428.2	9.6	5.46	56.9
26R	14	0555	428.2	437.9	9.7	4.44	45.8
27R	14	0920	437.9	447.6	9.7	7.43	76.6
28R	14	1245	447.6	457.2	9.6	5.97	62.2
29R	14	1600	457.2	466.6	9.4	3.93	41.8
30R	14	1910	466.6	476.3	9.7	3.72	38.3
31R	14	2230	476.3	485.9	9.6	3.56	37.1
32R	15	0215	485.9	495.6	9.7	0.15	1.6
33R	15	0615	495.6	505.2	9.6	7.96	82.9
34R	15	1050	505.2	514.8	9.6	7.80	81.3
35R	15	1800	514.8	524.3	9.5	7.47	78.6
36R	15	2255	524.3	533.8	9.5	3.96	41.7
(Coring)					337.2	146.03	
(Washing)					196.6	0.26	
					533.8	146.29	

Icebergs were awaiting the drillship when she arrived on site and had to be dealt with from the start of operations. *Maersk Master* had already towed a large berg by the end of the first day and was kept busy towing and prop-washing for most of the duration of site occupancy.

Hole 738C

The next hole was drilled to 197 mbsf before RCB coring began. Chert nodules in the chalky ooze had their usual disastrous effect on core recovery, with only about 25% recovery over the first 87 m of cored interval.

As Core 119-739C-10R was being cut, the iceberg situation became critical, with the unusual situation of four bergs simultaneously converging on the 2-nmi "red zone." While two new bergs approached along their plotted paths, two previously towed bergs ignored prevailing environmental forces and circled back into the zone. Coring was suspended, and the drill string was pulled to keep only the BHA in the hole. This response reduced the red zone to 1 nmi or less while *Maersk Master* busied herself with towing or prop-washing a succession of both new and persistent visitors. When the danger finally cleared, after delaying coring operations for 8 hr, the bit was run back to total depth. Only one additional core was cut before it was necessary to repeat the ice drill for a further delay of 6.5 hr.

Coring then continued in soft chalky ooze. Sporadic chert nodules and siliceous streaks obstructed the core catchers and liners, reducing core recovery. The Cretaceous/Tertiary boundary was recovered intact at about 375 mbsf. At 410 mbsf, the soft chalk abruptly turned to hard limestone, and the rate of penetration dropped sharply. Localized chert concentrations persisted, but the expected massive cherts were not found, and apart from reduced recovery, no drilling problems were caused by the chert.

The rate of penetration in coring the limestone was about 4 m/hr to 495.6 mbsf, where "basement" rocks were encountered. Although basalt fragments were an important component, the rate of penetration only dropped to about 3.5 m/hr. At 534 mbsf the scientific drilling objectives were considered complete, and coring was terminated.

Problems with hole cleaning began near total depth, probably because the soft upper 400 m of the hole became enlarged through erosion and the annular velocity was insufficient to remove drill cuttings. A wiper trip was made, and the hole was flushed with 100 bbl of high-viscosity mud to condition it for logging operations. The bit and associated components were routinely released with the hydraulic bit release, and the end of the pipe was pulled to logging depth at 128 mbsf.

The first logging tool combination, seismic stratigraphic, encountered a soft bridge only about 15 m below the pipe, but was worked past the obstruction. A second bridge, or fill, was found 79 m above total depth. A good log was recorded from that point up to the pipe. The logging tool was exchanged for the lithoporosity combination, and a second successful run was made over the same open-hole interval.

The third intended downhole instrument run was the vertical seismic profile (VSP) tool. The tool was run out the end of the pipe and encountered the same bridge at 15 m below the pipe that had stopped the first logging sonde. During attempts to work the tool past the bridge, the tool was pulled inside the top connector of the hydraulic bit release and became lodged there. When the tool could not be freed, it was necessary to deploy the Kinley crimper and cutter tools to sever the logging cable inside the BHA and save both the cable and the downhole tool.

The logging cable and the drill string were then recovered. The VSP tool was extricated from the hydraulic bit release, where one of the clamping arms had become wedged after partially opening spontaneously. The only damage was a slightly bent

arm, the loss of 8 m of cable and, of course, the opportunity for VSP or further logging operations.

After the second day of site operations, the wind had calmed and most of the surrounding icebergs had almost completely stopped moving. Nevertheless, *Maersk Master* completed 13 tows and 10 prop-washes, accounting for 67% of the time spent in ice management at the site.

JOIDES Resolution departed for the Prydz Bay operating area for the second time at 0545 hr, 17 January.

LITHOSTRATIGRAPHY, SEDIMENTOLOGY, AND IGNEOUS PETROLOGY

The three holes drilled at Site 738 are in a water depth of 2252.5 m at the southernmost part of the Kerguelen Plateau. All of the holes were drilled without any major offset. APC coring of Hole 738A was terminated at 2.8 mbsf, owing to technical problems and possible double punching of the sediment. Hole 738B was drilled to 108.2 mbsf with the APC and continued with the XCB down to 214.3 mbsf. Hole 738C was washed down to 196.6 mbsf before switching to the RCB. Drilling penetrated the entire sedimentary sequence and was terminated in basement at 533.8 mbsf. Recovery with the APC at Hole 738B was almost complete, with an average of 98%. Continuation of this hole by XCB led to 61% average recovery. At Hole 738C the average recovery rate using the RCB was 43%.

Lithology

Sediments recovered at Site 738 range in age from early Turonian to Quaternary. The sedimentary sequence is dominated by nannofossil ooze, which gradually turns into calcareous chalk and limestone. The chalk and limestone contain varying amounts of chert concretions and layers. Locally, the limestone is silicified. The upper part of the lithologic column includes coarse material originating from a terrigenous source area; thus, this far-traveled component is termed "exotic." Based on visual core descriptions and compositional analyses of smear slides (Fig. 5), the lithologic formations were divided into eight units. Between some of these units, the changes in their characteristic properties are transitional. The lithology and stratigraphic occurrence of the various units are summarized in Table 3.

Unit I

Diatom ooze

Samples 119-738B-1H-1, 0 cm, through 119-738B-3H-3, 25 cm; depth, 0–16.8 mbsf.
Age: late Miocene to Quaternary.

Unit I is a diatom ooze with varying proportions of foraminifers and neomorphic (i.e., transformed but without gross compositional changes) carbonate and minor amounts of radiolarians, clay, and nannofossils. It is predominantly pale brown (10YR 6/3), very pale brown (10YR 7/3), and brown (10YR 5/3), but there are paler and darker mottled patches that may represent burrows, as well as white (10YR 8/1) clusters of diatom ooze about 5 mm in diameter in Section 119-738B-2H-6. Parts of the sediment are soupy, having been severely disturbed during drilling. Exotic material makes up to 5% of the bulk sediment, although less than 1% is of gravel size; it becomes most abundant toward the bottom of this unit.

Very coarse sand particles, including granitic varieties, with diameters of 1–2 mm, are disseminated throughout the core. Layer components that are 1–10 mm in diameter are either manganese nodules or manganese-coated clasts; adhering to some of these are smaller grains that are also manganese coated. Larger, mainly angular clasts up to 50 mm in length are scattered throughout Samples 119-738B-2H-3, 46 cm, and 119-738B-3H-2, 70 cm, (7.4–15.7 mbsf) and Sections 119-738B-3H-1 and

119-736B-3H-2. The pebbles include granite, both white and red, and metamorphic rocks. Most are coated with manganese oxide, and some are coated only on their upper sides. This coating resulted from uneven manganese precipitation, and it obliterates any primary surface markings.

Although this unit shows little change in appearance, smear slide analysis (Fig. 5) and the carbonate content (see "Organic Geochemistry" section, this chapter) suggest that it can be subdivided into a calcareous diatom/diatom foraminiferal ooze (Subunit IA) and a diatom ooze without significant carbonate (Subunit IB).

Subunit IA

Calcareous diatom/diatom foraminiferal ooze

Samples 119-738B-1H-1, 0 cm, through 119-738B-2H-5, 20 cm; depth, 0–10.2 mbsf.
Age: late Pliocene to Quaternary.

Subunit IA mainly is calcareous diatom ooze. Calcareous foraminiferal ooze with diatoms occurs in Sample 119-738B-1H-2, 80 cm, and diatom foraminiferal ooze is found in Sample 119-738B-1H-3, 40 cm. Of the major components, diatom content ranges from 25% to 60%, foraminifers from 15% to 55%, and neomorphic carbonate (micrite and sparite) from 10% to 35%. Minor components include nannofossils (0% to 15%), radiolarians (3% to 15%), and clay (2% to 7%). The overall carbonate content reflects the balance between foraminifers and neomorphic carbonate and diatoms, and it ranges from 45% to 75% (see "Organic Geochemistry" section).

Subunit IB

Diatom ooze

Samples 119-738B-2H-5, 20 cm, through 119-738B-3H-3, 25 cm; depth, 10.2–16.8 mbsf.
Age: late Miocene to late Pliocene.

Subunit IB consists of diatom ooze. In comparison to Subunit IA, there is a sharp increase in the proportion of diatoms, although there is no obvious change in the appearance of the sediment. Diatom percentages range from 65% to 80% (Fig. 5), with the remainder consisting of radiolarians (2% to 15%), foraminifers (0% to 5%), nannofossils (0% to 5%), clay (0% to 5%), and neomorphic carbonate (0% to 10%). Overall carbonate percentages are about 25% in Sample 119-738B-2H-5, 80 cm, and <1% below (see "Organic Geochemistry" section).

Up to 10% quartz—as well as minor amounts of silicoflagellates, sponge spicules, feldspar, glauconite, zircon, and palagonite—is present in both subunits. The bulk of the sediment is silt sized (80% to 85%), with up to 10% clay-sized particles.

Unit II

Calcareous nannofossil ooze

Samples 119-738B-3H-3, 25 cm, through 119-738B-3H-3, 120 cm; depth, 16.8–17.7 mbsf.
Age: late Miocene.

Unit II consists of calcareous nannofossil ooze with minor diatoms. This well-defined unit is only 95 cm thick, dividing the diatom-rich ooze of Subunit IA and the almost pure nannofossil ooze of Unit III. The diffuse boundaries with the adjacent units, extending over a few millimeters or centimeters, probably resulted in part from disturbance of the soft sediment during drilling and cutting. However, the boundaries are marked by distinct color changes. Colors range from very pale brown (10YR 7/3) at the top of the unit to white (10YR 8/2) at the bottom as the diatom content decreases. Unit II is homogeneous, but scattered throughout is <1% exotic material, consisting of a few subangular manganese-coated pebbles and uncoated quartz granules, decreasing in proportion downward.
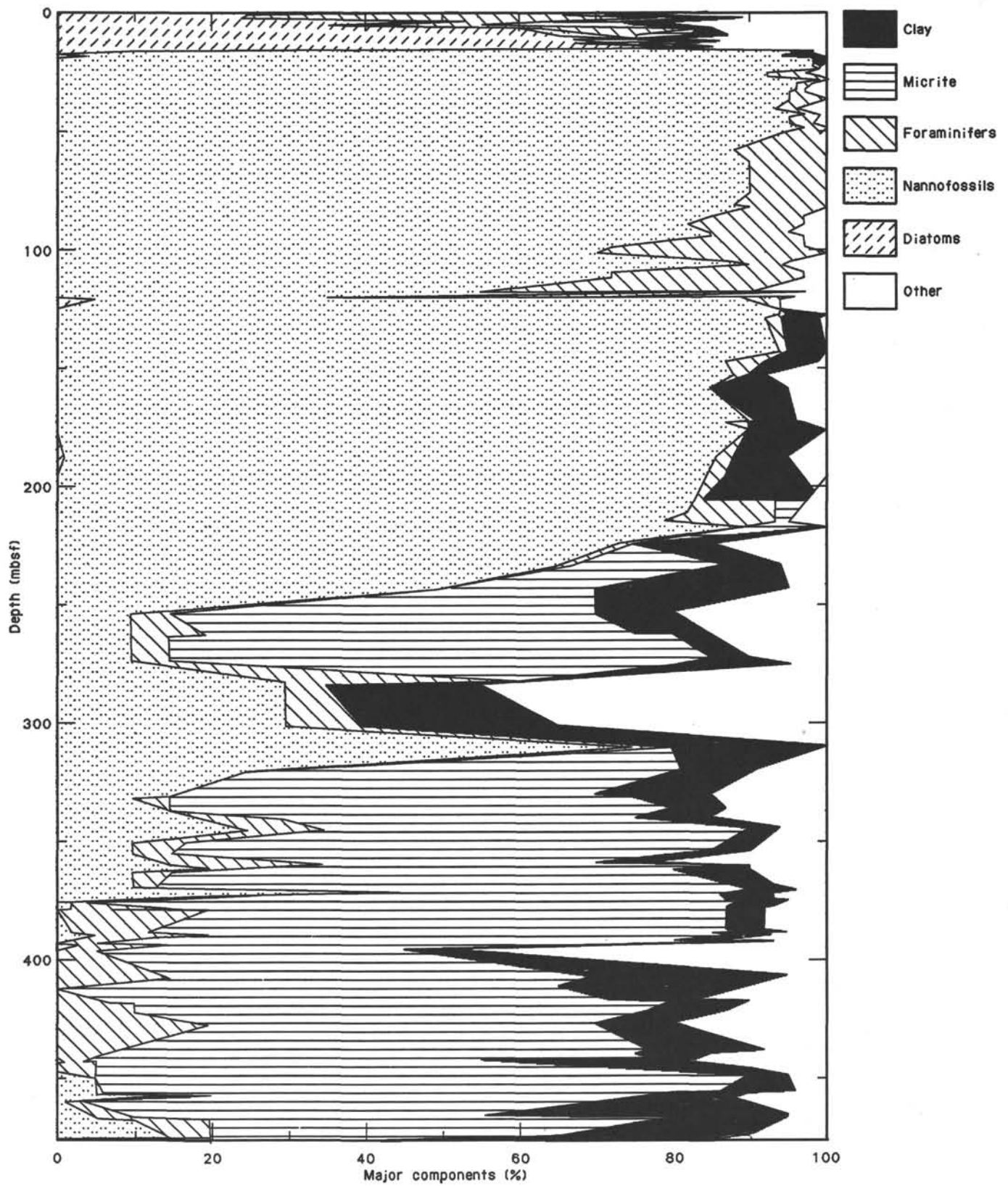
Figure 5. Smear slide compositional data, Holes 738B and 738C.

Table 3. Summary of lithologic units, Site 738.

Age	Unit	Depth (mbsf)	Hole, core, section, interval (cm)	Dominant lithologies
Quaternary–late Pliocene	IA	0–10.2	738B-1H-1, 0, to -2H-5, 20	Calcareous diatom ooze
late Pliocene–late Miocene	IB	10.2–16.8	738B-2H-5, 20, to -3H-3, 25	Diatom ooze
late Miocene	II	16.8–17.7	738B-3H-3, 25, to -3H-3, 120	Nannofossil ooze with minor diatoms
early Oligocene– middle Eocene	III	17.7–120.8	738B-3H-3, 120, to -15X-2, 150	Nannofossil ooze, homogeneous
middle Eocene– early Eocene	IV	120.8–254.4	738B-15X-3, 0, to 738C-7R-CC, 10	Nannofossil ooze and chalk, partially with chert
early Eocene–early Maestrichtian to Campanian	V	254.4–418.6	738C-8R to -24R	Calcareous chalk, partially with minor foraminifers and nannofossils and chert
early Maestrichtian to Campanian– early Turonian	VI	418.6–479.7	738C-25R-1, 0, to -31R-3, 41	Limestone with minor clay and chert
early Turonian or older	VIIA	479.7–495.5	738C-31R-CC, 7, to -32R-CC, 9	Calciclastic limestone
early Turonian or older	VIIB	495.5–495.6	738C-32R-CC, 9, to -32R-CC, 14	Basaltic breccia
early Turonian or older	VIII	495.6–533.8	738C-33R-1, 0, to -36R-3, 143	Basement

Smear slide analysis shows about 85% nannofossils, 15% radiolarians, 1% quartz, and traces of silicoflagellates, foraminifers, feldspar, and glauconite.

Unit III

Calcareous nannofossil ooze

Samples 119-738B-3H-3, 120 cm, through 119-738B-15X-2, 150 cm; depth, 17.7–120.8 mbsf.
Age: middle Eocene to early Oligocene.

Unit III consists of predominantly white (10YR 8/1) homogeneous calcareous nannofossil ooze without any visible structures. The content of nannofossils in smear slide estimates is as high as 100%, and the inorganic carbonate percentages range from 91% to 96% (see "Organic Geochemistry" section). Throughout this unit are irregularly distributed small patches of manganese micronodules (<1 mm in length).

The uppermost part (from 120 cm in Section 119-738C-3H-3 to 35 cm in Section 119-738C-3H-5) of this unit contains traces (<1%) of exotic coarse sand-size particles and a quartz grain 5 mm in length. These components mark the first appearance of significant terrigenous material within the Cenozoic at this site. The occurrence of an angular granite clast at 62–67 cm in Section 119-738B-8H-1 can be ascribed to fall-in contamination from higher in the hole. Sections 119-738B-8H-2 through 119-738B-12H-CC contain 10%–30% foraminifers.

Unit IV

Calcareous nannofossil ooze and chalk

Section 119-738B-15X-3 through Sample 119-738C-7R-CC, 10 cm; depth, 120.8–254.4 mbsf.
Age: early to middle Eocene.

Unit IV consists of white (10YR 8/1) calcareous nannofossil ooze and chalk, part of which has porcellanite chert layers and concretions. The nannofossil ooze gradually changes to chalk downcore. Parts of this unit consist of both soft ooze and firmer, more "chalky" sediment. Biscuit structures are found within the semilithified intervals of the latter. Biscuit structures, presumably induced by drilling, occur first in Section 119-738C-18X-1 and can be traced all the way to the bottom of this unit. A partially diagenetic origin cannot be completely excluded for the biscuits.

Distinct chert layers occur at 8–10 cm in Section 119-738B-15X-3 (white, 10YR 8/1) and at 52–60 cm in Section 119-738B-15X-6 (light gray, 10 YR 6/1). X-ray-diffraction (XRD) investigations on Samples 119-738B-15X-3, 8 cm, 119-738B-15X-6, 55 cm, and 119-738B-19X-4, 31 cm, identified distinct opal-CT and quartz peaks, as well as a minor amount of calcite. Small patches of manganese micronodules (<1 mm in length) are irregularly dispersed throughout this unit. Laminae-like greenish bands occur in Sections 119-738B-20X-3 through 119-738B-20X-5. It is not obvious if these greenish bands are of chemical origin or if they reflect varying concentrations of spicules, glass, or glauconite.

Percentages of inorganic carbon, based on coulometric analyses (see "Organic Geochemistry" section), range from 93% to 95%.

Unit V

Calcareous chalk

Cores 119-738C-8R through 119-738C-24R; depth, 254.4–418.6 mbsf.
Age: Campanian to early Eocene.

Unit V is a white (10YR 8/1) to light greenish gray (5GY 7/1) calcareous chalk with chert nodules and fragments, with minor foraminifers and nannofossils. The chert nodules and fragments are dark yellowish brown (10YR 4/4) to black (5Y 2.5/1). The chalk is apparently partially silicified by both opal-CT and quartz, as evidenced in XRD Sample 119-738C-24R-3, 3 cm. Some of the chert nodules have porcellanite-like rims, which in turn are surrounded by silicified white (10YR 8/1) chalk. They also usually have numerous small inclusions (chalk or silicified chalk) that give the chert a cloudy appearance. Color changes between the core and rim of the nodules are typically diffuse. Biscuit structures occur throughout unit.

From 90 cm in Section 119-738C-19R-1 to 150 cm in Section 119-738C-20R-4 the recovered chalk is severely disturbed by drilling and broken into centimeter- to millimeter-sized fragments. The chalk and chert are partially pulverized, giving the sediment a soupy appearance.

The interval from 82 to 98 cm in Section 119-738C-20R-5 contains distinct (on a submillimeter to millimeter scale) laminae. These laminae vary in shade from lighter (10GY 8/1) to

darker (10GY 5/1) greenish gray. Some laminae show evidence of microfaulting, either by internal offsets or diffuse anastomosing. Anastomosing laminae pass down into an underlying white chalk. Within Section 119-738C-21R-1 are several diffuse grayish layers (on a millimeter to centimeter scale), parts of which contain compressed burrow structures.

From Cores 119-738C-20R to 119-738C-24R, Unit V is moderately to intensively bioturbated. Burrow structures belong predominantly to the *Planolites* and *Chondrites* assemblages, and to a lesser degree to *Zoophycos*. Thin layers (<10 mm) of sand-size material consist of shelly microfaunal debris.

Percentages of inorganic carbonate (see "Organic Geochemistry" section) range from 87% to 95%.

Unit VI

Limestone

Section 119-738C-25R-1 through Sample 119-738C-31R-3, 41 cm; depth: 418.6–479.7 mbsf.
Age: early Turonian to Campanian-Maestrichtian.

Unit VI consists of light gray (5Y 7/1) to light olive gray (5Y 6/2) limestone, parts of which contain minor clay content and chert nodules and fragments. In almost all of the smear slides foraminifers are the only detectable biogenic component, usually ranging from 5% to 10%. Parts of the limestone are silicified (e.g., 20–35, 50–59, and 80–92 cm in Section 119-738C-29R-1), and silicification generally increases downhole. Within silicified intervals primary sediment structures, such as burrows or laminations, are preserved. The percentages of carbonate range from 67% to 93% ("Organic Geochemistry" section). The limestone is highly fractured along clay-rich slickenslide surfaces. At 26–27 cm in Section 119-738C-25R-3, small clasts show rotational deformation owing to microtectonism.

Another indication of tectonic influence is microfracturing. Microfracturing caused anastomose patterns (45–72 cm in Section 119-738C-27R-2) as well as single fractures and normal microfaults with displacements of up to 5 mm (e.g., 124–129 cm in Section 119-738C-29R-1). The fractures are very thin (<1 mm), mostly closed, and show clay enrichment on the surfaces. Microfracturing also caused partial brecciation of the sediment. The fractures have no preferred orientation and were probably produced during compaction, possibly in combination with pressure solution (clay enrichment).

The whole unit is moderately to intensively bioturbated. Burrow structures represent mainly the *Zoophycos/Chondrites/Planolites* assemblage. In addition, *Thalassinoides* is also found, and it seems to represent the relatively oldest trace fossil structures. In Section 119-738C-27R-2, *Thalassinoides* was burrowed by *Planolites*, which in turn was bioturbated by *Chondrites*. *Zoophycos* seems to belong to the relatively youngest generation of burrowing trace fossils. There are thin (a few millimeters) sandy layers within the bioturbated intervals. Partially compressed and elongated burrows (e.g., 119–126 cm in Section 119-738C-31R-2) cause flaser bedding-like sedimentary structures (Fig. 6). Well-preserved *Inoceramus* fragments (up to 6 cm in length) are found in Sections 119-738C-27R-4 through 119-738C-27R-5 (Fig. 7).

Unit VII

Calciclastic limestone and basaltic breccia

Samples 119-738C-31R-CC, 7 cm, through 119-738C-32R-CC, 14 cm; depth, 479.7–495.6 mbsf.
Inferred age: early Turonian or older.

Unit VII consists of two subunits composed of micrite and basaltic clasts (Fig. 8). The recovery in both subunits was poor: 17 cm in Subunit VIIA and only 5 cm in Subunit VIIB.
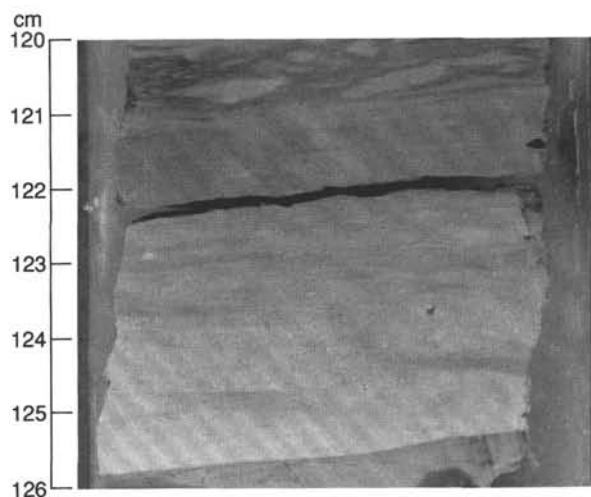

Figure 6. Flaser bedding-like sedimentary structures in bioturbated limestone, caused by the compression and elongation of burrows; Section 119-738C-31R, 120–126 cm.

Depths below seafloor of the core catchers are calculated by placing the core catcher directly below the last recovered rock or to the top of the core, if recovery is restricted to the core catcher. Subunit VIIA may occur between 479.7 and 495.55 mbsf. The uncertainty of the depth of Subunit VIIB ranges from 485.99 to 495.60 mbsf.

Subunit VIIA

Calciclastic limestone

Samples 119-738C-31R-CC, 7 cm, through 119-738C-32R-CC, 9 cm; depth, 479.7–495.5 mbsf.
Inferred age: early Turonian or older.

This subunit consists of a light brown calciclastic limestone (Fig. 8). It is characterized by mostly rounded clasts of macrofossils and basalt; some of the fossils are well preserved. The fossils include crinoids, oysters and other mollusks, bryozoans, algae, gastropods, sponges, and foraminifers (benthics and rare planktonics). One ostracode has a geopetal filling (sparry calcite above micrite) and gravitational cement (Fig. 9) (Scholle, 1978). The grain size of the fossil clasts ranges from medium to very coarse sand. Based on the >2:1 relation of micrite to sparite, the sediment can be called a packed biomicrite (Fluegel, 1982).

Some of the carbonate material is partly silicified. The basalt clasts are subangular to rounded and range from 0.5 mm to more than 20 mm in length. The groundmass consists of a highly altered dark brown mesostasis (recrystallized glass) and plagioclase microphenocrysts (<0.1 mm). Plagioclase and clinopyroxene glomerocrysts (0.2–0.4 mm) occur in Core 119-738C-32R.

The smaller basaltic clasts are thoroughly oxidized whereas the large ones only have highly oxidized margins. Small (5-mm) vesicles are rare (<1% volume) and are completely filled by secondary phases, mostly clay minerals.

Discussion. Algae and bryozoans suggest a relatively shallow water depth in close proximity during deposition as the clasts are probably parautochthonous. A near-reef environment is indicated by a reeflike structure some 50 km northwest of Site 738 (Fig. 37, "Seismic Stratigraphy" section). The gravitational cement indicates at least temporary cementation in the vadose zone (Fluegel, 1982).

The alteration of the basaltic clasts occurred in an oxidizing environment, probably subaerial to shallow marine.
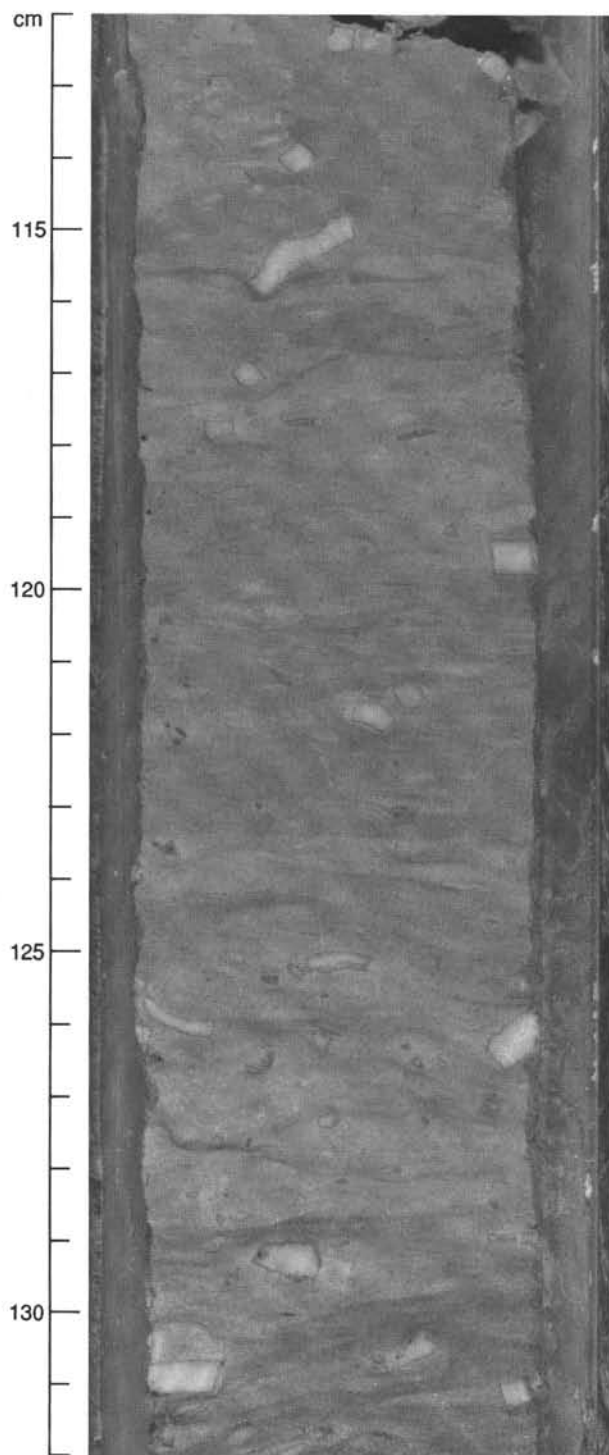
Figure 7. *Inoceramus* fragments within bioturbated limestone; Section 119-738C-27R-4, 112–132 cm.

Subunit VIIB

Basaltic breccia

Samples 119-738C-32R-CC, 9 cm, through 119-738-32R-CC, 14 cm; depth, 495.5–495.6 mbsf.
Inferred age: early Turonian or older.

Subunit VIIB is a fractured and highly vesicular basalt overlain by a limestone containing angular clasts of the basalt (Fig. 8). Glomerophyric plagioclase phenocrysts (0.5–3 mm) are in a
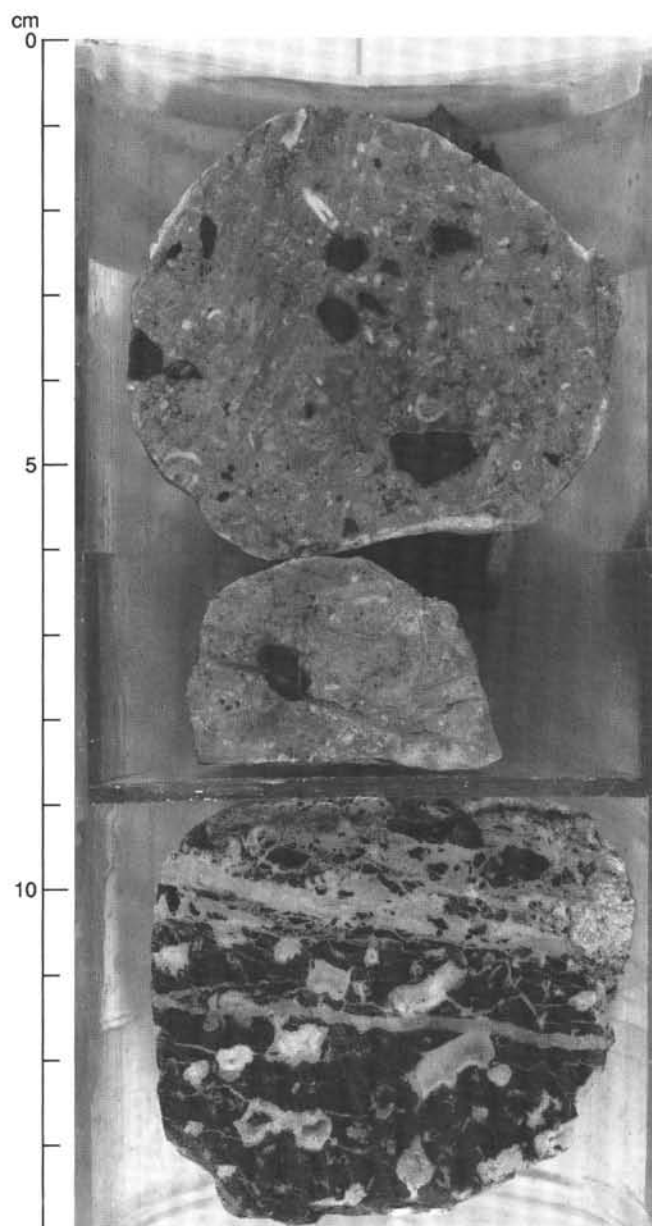

Figure 8. Calciclastic limestone with clasts of macrofossils and basalt (0–9 cm) and fractured and highly vesicular basalt overlain by limestone with angular basaltic clasts (9–14 cm); Section 119-738C-32R-CC.

groundmass of plagioclase microphenocrysts, altered mafic minerals (pyroxene and olivine), and a mesostasis of recrystallized glass with dendritic opaque minerals. Neither the basalt nor the basaltic clasts exhibit chilled margins.

The irregular vesicles, which comprise about 20% of the subunit, have a diameter of >1 cm and are rimmed by a thin (about 0.05 mm) brown layer that is probably clay minerals. Most of the vesicles are completely filled by sparry calcite, but a few have a central cavity filled by a waxlike green to orange mass. One cavity has a geopetal filling in which the lower quarter of the waxlike green mass is separated by a sharp horizontal boundary from the overlying sparry calcite.

The fractures are filled by sparry calcite. The plagioclase microphenocrysts are partly carbonatized and sericitized. Clinopyroxene and olivine are completely altered to brown clay minerals.
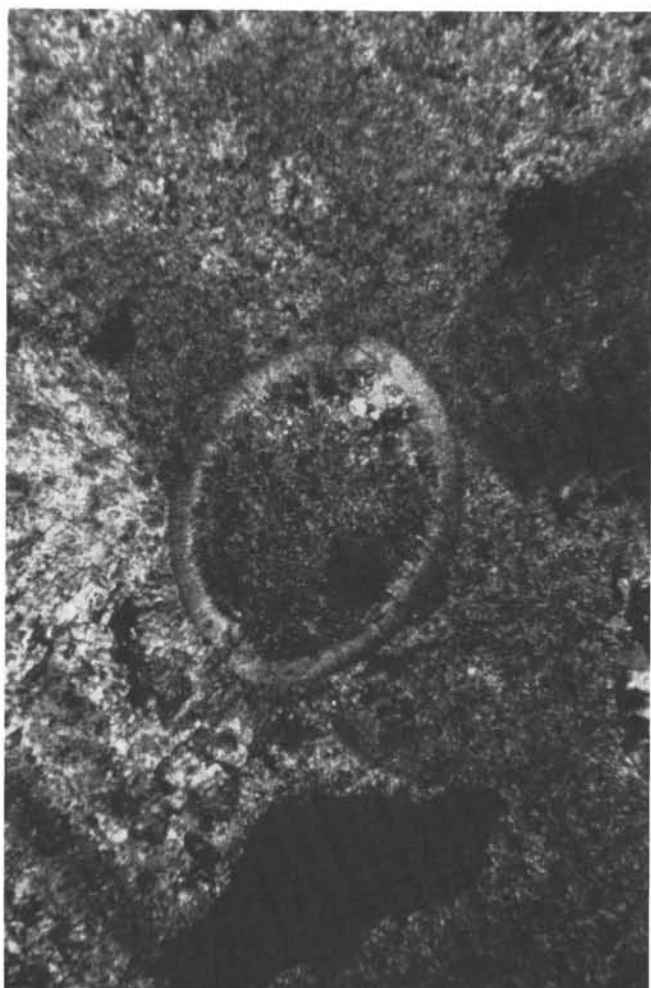
Figure 9. Ostracode filled with geopetal calcite (micrite and sparite) and gravitational cement.

The basaltic clasts are embedded either in micrite or in sparry calcite. They are angular, and some fit together like jigsaw puzzle pieces.

No fossils were observed.

Discussion. The basalt may represent the top of a lava flow, based on the large size and abundance of vesicles. The absence of glassy rinds suggests that either the flow was erupted subaerially or that the topmost part was eroded. No extensive oxidation of the basaltic clasts (autochthonous) indicates a rapid covering by sediment. A low-energy environment is suggested by the absence of any signs of transportation.

Unit VIII

Basement

Samples 119-738C-33R-1, 0 cm, through 119-738C-36R-3, 143
  cm; depth, 495.6–533.8 mbsf.
Inferred age: early Turonian or older.

Basement consists of alternating volcaniclastics and basalts (Table 4). The seven basalt layers recovered have a total thickness of 16.6 m and vary individually in thickness from 5 cm to >6 m. The six layers of volcaniclastic rocks range in thickness from 35 cm to >5 m, totaling 10.6 m. These thicknesses are minimum values because the average recovery of the cored interval (38.2 m) was 71%.

Table 4. Summary of Units VII and VIII, Hole 738C.

Unit	Petrography (color of matrix)	Recovery (m)	Core, section, interval (cm)
VIIA	Calciclastic limestone	0.17	31R-CC, 7, to 32R-CC, 9
VIIB	Basaltic breccia	0.05	32R-CC, 9–14
VIII	Basalt	0.05	33R-1, 0
	Volcaniclastic rock (green, black, and red)	5.38	33R-1, 5, to 33R-4, 112
	Basalt	2.82	33R-4, 112, to 33R-6, 103
	Volcaniclastic rock (green)	0.66	34R-1, 0–66
	Basalt	4.49	34R-1, 66, to 34R-4, 70
	Volcaniclastic rock (red)	1.96	34R-4, 70, to 34R-5, 125
	Basalt	0.54	34R-5, 125, to 34R-6, 48
	Volcaniclastic rock (red)	0.35	34R-6, 48–83
	Basalt	3.15	34R-6, 83, to 35R-2, 146
	Volcaniclastic rock (gray)	0.60	35R-3, 0–60
	Basalt	0.13	35R-3, 60–73
	Volcaniclastic rock (dull red)	2.29	35R-3, 73, to 35R-5, 37
	Basalt	6.32	35R-5, 37, to 36R-3, 143
		[a]28.74	

[a] Official recovery totals 27.19 m.

The minimum age, as inferred from the age of overlying Unit VI, is early Turonian (see "Biostratigraphy" section, this chapter).

Basalts

The basalts are aphyric to moderately plagioclase-phyric. Some show flow textures and/or coarser-grained pegmatoid schlieren. The amount of plagioclase ranges from 35% to 50%. Opaque minerals (magnetite, ilmenite, and a small amount of hematite, as identified by reflected light) amount to 10%–20% and have a diameter of up to 0.2 mm. They are regularly dispersed. The groundmass consists mostly of altered feldspar and pyroxene microlites and a dark mesostasis. Phenocrysts of pyroxene (<0.5 mm) and olivine (<0.4 mm) are very rare (<1% and <0.01% by volume, respectively). The proportion of vesicles varies from 0% to about 20%, and they usually range in size from <0.5 to 5 mm, rarely exceeding 20 mm. Most of the vesicles are round to oval shaped, although some are oblong or irregular. Sample 119-738C-34R-6 (Piece 8A) (Fig. 10) contains vertically oriented drop-shaped vesicles.

Most of the vesicles are completely filled by secondary phases (Figs. 10–12); others are partly filled. The succession from the rim to the center of the vesicles can be summarized as follows: (1) chalcedony in small round aggregates; (2) from two to rarely up to five layers of fibrous, birefringent sheet silicates in green to brown shades, with each layer from 10 to 20 μm thick; (3) one or two green or brown isotropic layers, each 20 to 40 μm thick; (4) one layer of light green to white, birefringent fibrous crystals, some externally bright green (saponite?); (5) aggregates of radially arranged crystals as described for layer (4); and (6) sparry calcite. Layers (2) to (4) constitute the concentric, macroscopically dark green rim of the vesicles that is always present. Layer (4) is missing from some of the rims, in which case the isotropic material of layer (3), macroscopically described as a light green to orange waxlike substance, may fill the vesicles completely. The aggregates and sparry calcite may occur in the cen-
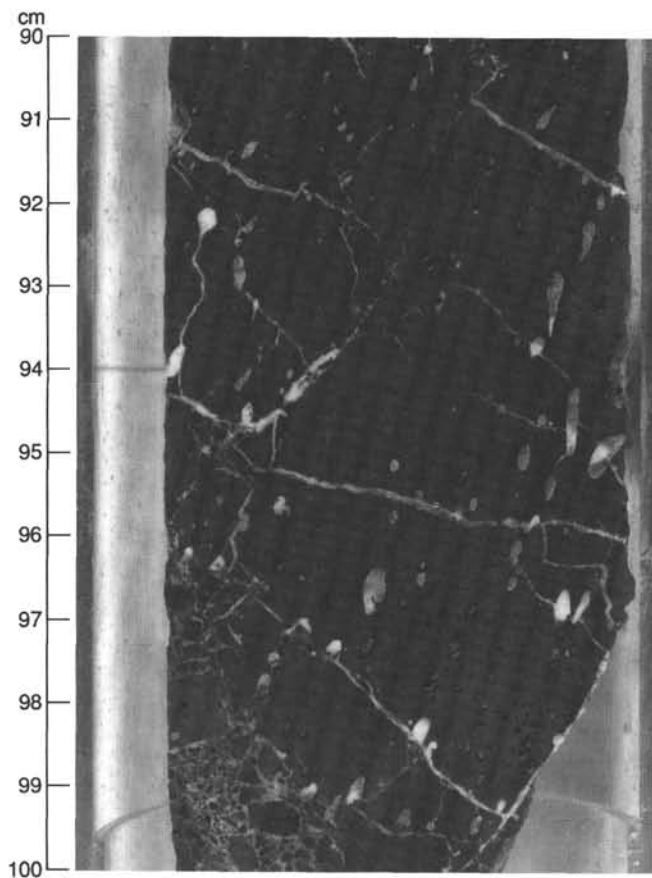
ter of the vesicle. Some vesicles have geopetal fillings that consist of radially arranged aggregates or sparry calcite in the upper part and the isotropic substance in the lower part (Fig. 12). The boundary is commonly horizontal, but also dips at up to 40°.

In general, the basalts are moderately altered. The plagioclase microphenocrysts are partly carbonatized and sericitized. Clinopyroxene microphenocrysts are highly altered, and olivine is totally altered to brown clay minerals. The glassy matrix is recrystallized.

The basalts are moderately fractured overall, with some slightly and highly fractured sections (Figs. 13 and 14). The irregular fractures have a dark green rim like the vesicles, and the wider fractures also have a sparry calcite filling in which fragments of the host rock may be embedded. The gray color varies from grayish red-brown to yellowish brown to almost black, with the latter color the freshest.

Plagioclase compositions of a moderately altered basalt (Sample 119-738C-36R-2, 143–146 cm) generally range (22 analyses) from An_{57} to An_{69}, as determined by onshore electron microprobe analysis. Compositions of An_{48} and An_{73} were found in one sample each. No significant difference among phenocrysts, microphenocrysts, and schlieren plagioclase were observed. Microprobe analysis of nine clinopyroxene crystals from Sample 119-738C-36R-2, 143–146 cm, suggests two distinct compositional types: augite (En_{44-55}, Fs_{13-23}, Wo_{25-37}; seven crystals) and pigeonite (En_{67-73}, Fs_{20-25}, Wo_{6-8}; two crystals; Morimoto, 1988).

Discussion. The presence of glassy to microlitic matrix suggests quick cooling. The absence of glassy margins may be primary and, together with the amount and size of the vesicles, probably indicates subaerial emplacement. If the glassy margins were eroded prior to burial, emplacement in shallow water is also possible.

Volcaniclastic Rocks

Several types of clasts were distinguished in the volcaniclastic rocks (Fig. 15). Comprising 40%–90% of the rocks, the clasts are rounded to angular and most are moderately to highly altered. Their size ranges from 0.5 to 80 mm. They are embedded
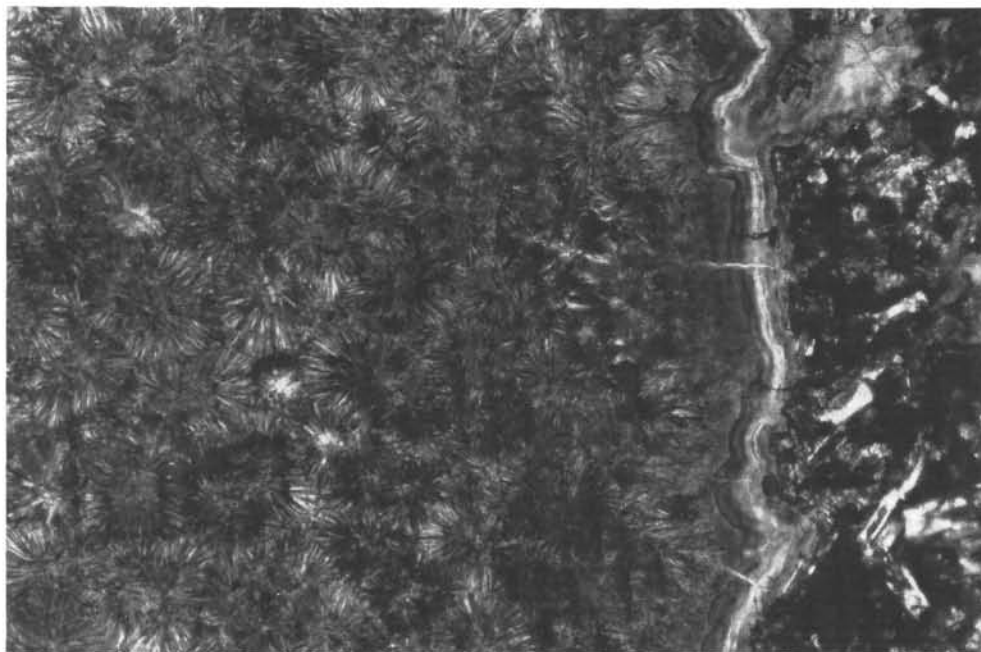

Figure 10. Drop-shaped vesicles in basalt; Section 119-738C-34R-6, 90–100 cm.

Figure 11. Section of an amygdule with different thin rims. The fibrous green crystals are radially arranged.
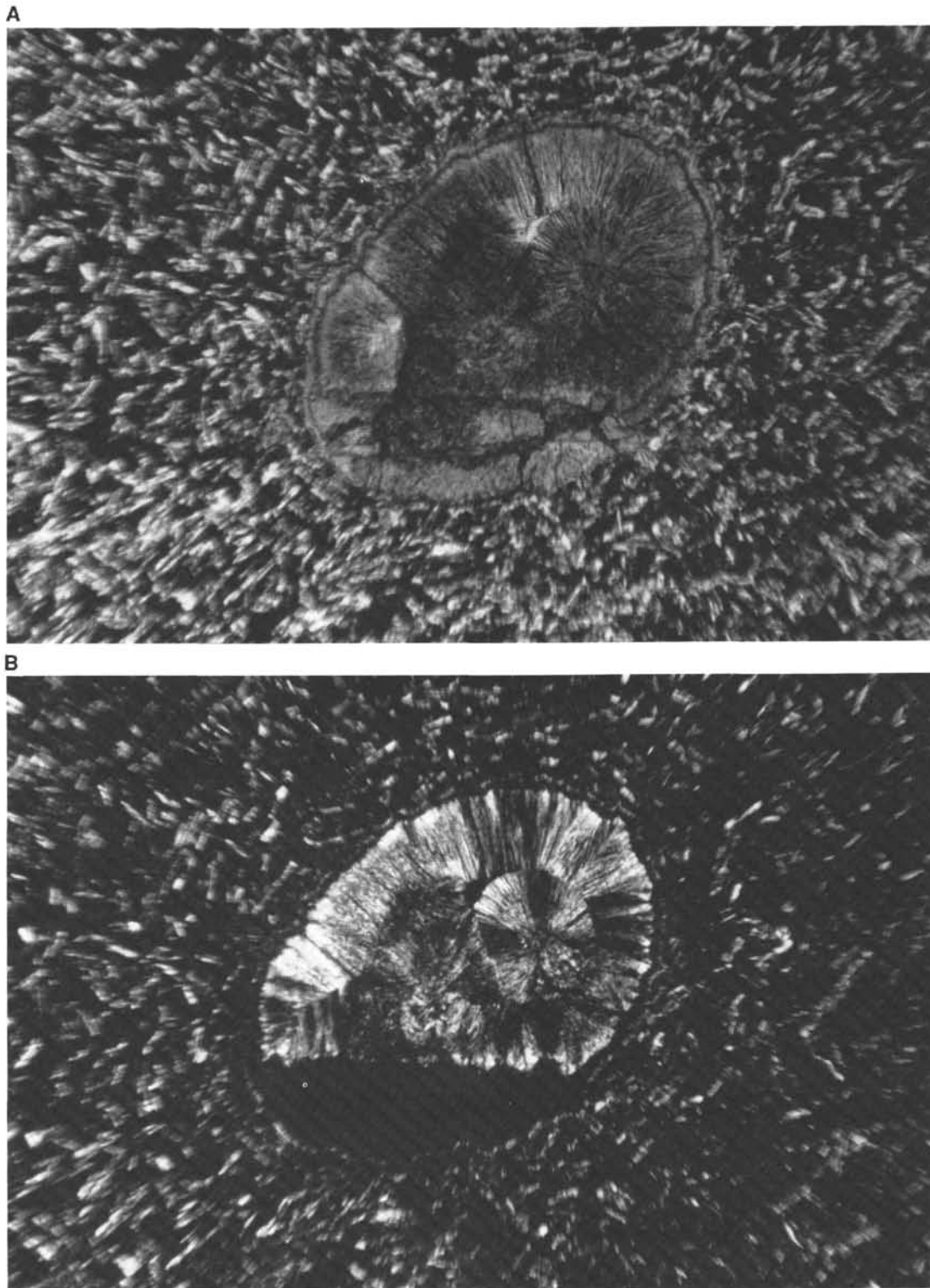
Figure 12. **A.** Vesicle filled by two different minerals, separated by a sharp boundary. **B.** Crossed nicols.

in a fine-grained varicolored red to dull red and black, with some green, matrix.

The gray to brownish black clasts are approximately 50% opaque glassy matrix and contain a relatively high content (5%–20%) of vesicles. The vesicles have a diameter of 1 to 2 mm, with some up to 5 mm. They have a dark green rim, like the alternating basalts, and are filled by white, needlelike crystals (ze-

olite?), a light green to orange, waxlike isotropic substance, and/or sparry calcite. As in the basalt vesicles, a sharp, straight boundary separates the different fillings and lies either horizontal or dips at up to 70°. A few of the boundaries between these clasts and the surrounding matrix appear unclear. As observed in thin-section Sample 119-738C-34R-5, 44–46 cm, this macroscopic appearance arises from a brecciation of the outer part of
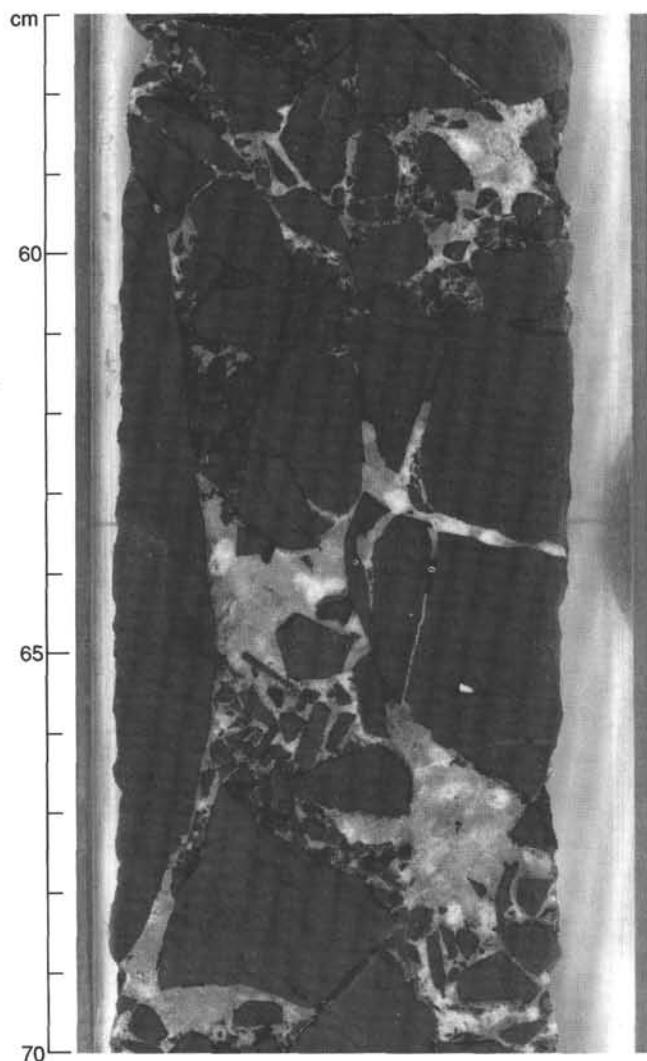
Figure 13. Fractured gray-green basalt with calcite filling and a moderate shifting noted for some of the clasts on the right side; Section 119-738C-34R-3, 57–70 cm.
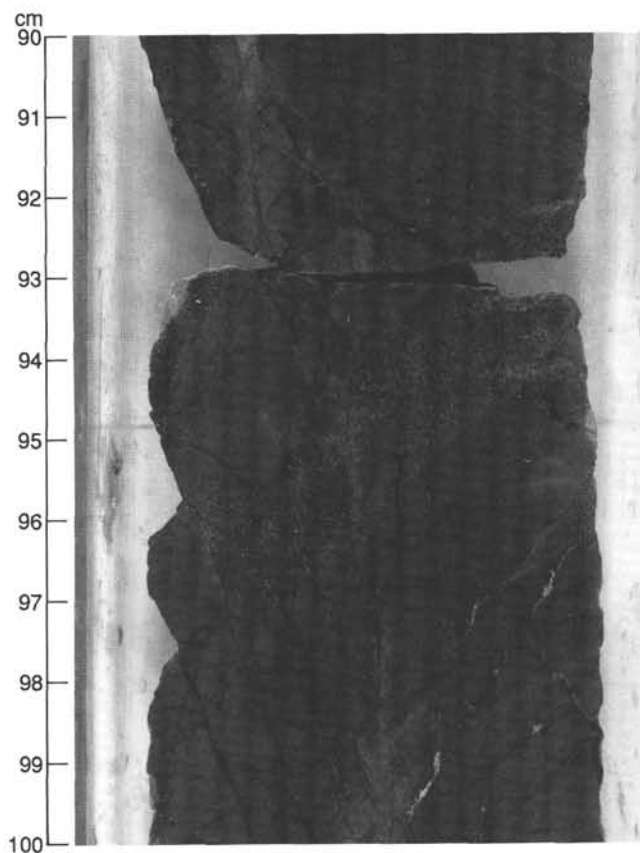

Figure 14. Irregular thin fractures filled by green clay minerals crosscut a massive gray-green basaltic sequence; Section 119-738C-34R-1, 90–100 cm.

the clast in which the size of the individual fragments of the clast decreases and the proportion of the matrix increases with increasing distance.

The greenish clasts, some of which are altered to yellowish brown to brown, resemble the alternating aphyric to sparsely plagioclase-phyric basalts. The proportions of plagioclase and opaques are similar, as is the filling of the vesicles. The distribution of vesicles appears bimodal, either low (<5%) or high (20% to 25%). Their size ranges from 0.5 to 5 mm, with some up to 13 mm.

Small (up to 4 mm), bright red angular clasts occur in Samples 119-738C-3R-2 (Piece 1A) and 119-738C-34R-6 (Piece 8A). The clasts are fine grained and nonvesicular.

Discussion. The high glass content of the black clasts suggests quenching. They are thus interpreted to represent—or be derived from—the top breccia of a lava flow. The roundness and different types of clasts indicate transportation and an epiclastic origin. The red color of part of the matrix indicates alteration under oxidizing conditions, probably resulting from subaerial weathering.

Hiatuses and Lithologic Units

Hiatuses encountered at Site 738 and their relationship to the eight lithologic units are listed in Table 5 (see "Biostratigraphy" and "Sedimentation Rates" sections, this chapter). A hiatus of at least 1 m.y. (>5.8/<4.8 Ma) of apparent duration ("Biostratigraphy" section) at the upper Miocene/lower Pliocene boundary does not coincide with lithologic unit boundaries. This hiatus, at 62–148 cm within Section 119-738B-3H-2 (15.62–16.48 mbsf), however, might correlate with the first appearance of coarse gravel in Core 119-738B-3H (Fig. 16).

The occurrence of a hiatus within the upper/uppermost Miocene at 25 cm in Section 119-738B-3H-3 (16.75 mbsf) (>8.4 to 6.1 Ma; see "Biostratigraphy" section) coincides with the lithologic boundary between Unit II and Subunit IB. This boundary is marked by a distinct color change from pale brown (10YR 7/1) to brown (10YR 5/3). The hiatus seems to correlate with a relatively gradual increase in magnetic susceptibility (Fig. 16) that is apparently not related to the gravel layers or clasts in Sections 119-738B-3H-1 and 119-738B-3H-2. The susceptibility peak might reflect a relative increase in the size and/or concentration of magnetic grains (King et al., 1982; Dorn, 1987). The apparent duration of this hiatus suggests a relationship with global hiatus events NH5 and NH6 (Barron and Keller, 1982).

A hiatus between the (middle) upper Miocene and lower Oligocene in Section 119-738B-3H-3 (16.5–17.5 mbsf) coincides with the lithologic boundary between Units III and II. The boundary is marked by a distinct color change from white (10YR 8/2) to pale brown (10YR 7/3). No changes in magnetic
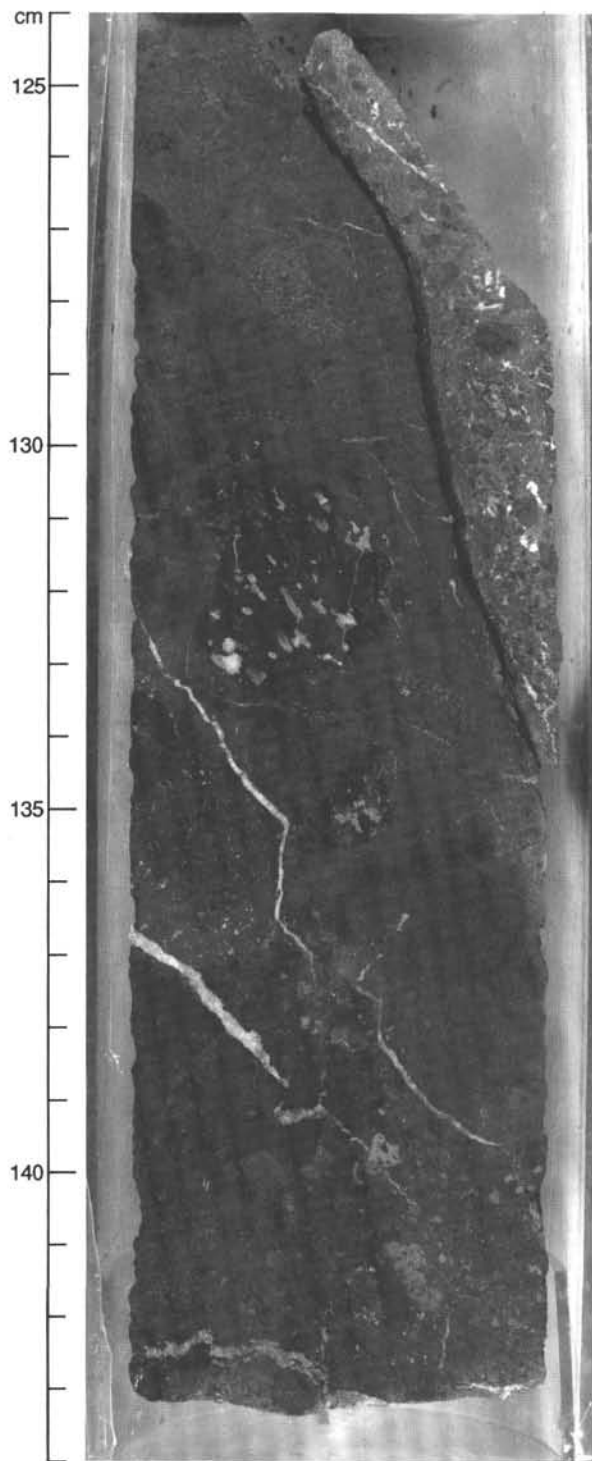
Figure 15. Red volcaniclastic rock, crosscut by calcite veins, with different types of clasts; Section 119-738C-33R-1, 124–144 cm.

susceptibility (Fig. 16) are detectable within the interval containing the hiatus (110 cm in Section 119-738B-3H-3 to the core catcher).

An apparent hiatus between the middle and upper Eocene in Core 119-738B-9H (70.5–80.0 mbsf) is not reflected lithologically. A hiatus within the lower Maestrichtian in Core 119-738C-24R (204.6–214.3 mbsf) seems to coincide with the lithologic boundary between Units VI and V.

BIOSTRATIGRAPHY

Turonian to Quaternary sediments were recovered at Site 738. The biostratigraphic zonation, recovery, lithology, abundance and preservation of the various fossil groups, and a preliminary paleomagnetic scale are summarized in Figure 17.

Calcareous nannofossils are rare to common in the Neogene section, but have a sporadic distribution. They are abundant and generally well preserved in the Paleogene. Mesozoic sediments yield few to common, poorly preserved calcareous nannofossils. Foraminifers are well preserved and abundant in almost all Maestrichtian and younger samples and are dominated by planktonic forms. Preservation in Campanian and older sediments tends to be poor.

Siliceous microfossils have a variable distribution. Diatoms are common to abundant in upper Miocene, lower Pliocene, and Quaternary sediments, but are generally not recorded in older material. Radiolarians, on the other hand, are abundant and well preserved in Miocene to Pleistocene sediments, as well as sporadically present and moderately preserved in Oligocene, Eocene, and Cretaceous sediments. Diatom assemblages consist of pelagic species characteristic of the Southern Ocean and the middle to low latitudes. The majority of radiolarians recovered are characteristic of middle to high latitudes, although tropical forms dominate some of the Eocene samples. Organic-walled microfossils were found in Cretaceous and Paleocene sediments at Site 738.

A number of important stratigraphic boundaries and disconformities have been recorded from Site 738. The youngest sediments recovered contain planktonic foraminifers such as *Neogloboquadrina pachyderma*, radiolarians characteristic of Zone NR2, and diatoms assigned to the *Coscinodiscus elliptopora/ Actinocyclus ingens* Zone, the latter forms indicating a Pleistocene age for this part of the succession. Below this, in Core 119-738B-2H, a hiatus spanning most of the upper Pliocene and lower Pleistocene is suggested by the absence of radiolarian Zones NR5 and NR6. On the basis of planktonic foraminifers, calcareous nannofossils, and diatoms, a disconformity is recognized between the lower Oligocene and the upper Miocene (Section 119-738B-3H-3). This is supported by evidence from the radiolarian distribution, although precise zonation of the latter is not possible due to the absence of tropical stratigraphic markers. The Eocene/Oligocene boundary lies between Samples 119-738B-4H-CC and 119-738B-5H-CC, according to evidence from calcareous nannofossils. A hiatus, which was also noted at Site 737, may be present at the middle/upper Eocene boundary based on the absence of the nannofossil CP14b Subzone.

The Cretaceous/Tertiary boundary was recovered in a laminated interval of Core 119-738C-20R-5, based on nannofossil and foraminifer analyses. The Upper Cretaceous chalk sequence can be subdivided using several nannofossil events. All of the main zones representing early Turonian through late Maestrichtian are represented. In addition, a number of moderately preserved radiolarians, diagnostic of the *Amphipyndax tylotus* Zone (late Campanian to Maestrichtian) were found in Samples 119-738C-23R-CC through 119-738C-26R-CC.

Calcareous Nannofossils

Calcareous nannofossils are rare to common, but sporadic, in the condensed Neogene section at Site 738. They are abundant and generally moderately well preserved in the relatively expanded Paleogene interval (170 m). The Mesozoic sediments (upper Maestrichtian to Turonian) from this site yield few to common, poorly preserved calcareous nannofossils. From preliminary shipboard examination, it seems that Site 738 recovered a relatively complete Cretaceous/Tertiary boundary. About 80% of the lower Paleogene section was recovered, and the calcareous nannofossils are abundant and well preserved. Rework-

Table 5. Tentative hiatus occurrence and relationship to lithologic boundaries, Site 738.

Hiatus	Relationship to lithologic units	Biostratigraphic indication	Occurrence in core	Remarks
upper Miocene/lower Pliocene	no	Diatoms >5.8/<4.8 Ma	738B-3H-2, 62–148 cm	First gravel occurrence
upper/uppermost Miocene	yes Units II/IB	Diatoms >8.4/6.1 Ma	738B-3H-3, 25 cm	Distinct color change; magnetic suscepti- bility increase NH5 + NH6?
lower Oligocene/(middle-) upper Miocene	yes Units III/II	CP16 (nannofossils)/ NR10 (radiolarians)	738B-3H-3	Distinct color change
?middle/upper Eocene	no	CP14b (nannofossils) missing	738B-9H	
Within lower Maestrichtian	yes Units VI/V	NC23 (nannofossils) missing	738C-24R	

ing of older calcareous nannofossils into the younger sediments is minimal. It is, therefore, a promising section in many aspects for calcareous nannofossil studies, such as detailed investigations of the evolutionary dynamics of the calcareous nannoplankton immediately following the terminal Cretaceous mass extinction and the early Paleogene interrelationship of nannoplankton evolution and the paleoceanography of the Southern Ocean. In the poorly recovered uppermost Cretaceous section (only 8% core recovery in Core 119-738C-21R) the calcareous nannofossils are generally rare, fragmented, and moderately to well preserved. The preliminary nannofossil stratigraphy is presented in Figure 17. Okada and Bukry's (1980) zonation was used for the Cenozoic, and Roth's (1978) zonation was applied in the Upper Cretaceous to facilitate correlation with low-latitude sequences.

Neogene

Sample 119-738A-1H-CC contains *Calcidiscus leptoporus*, *Coccolithus pelagicus*, *Gephyrocapsa caribbeanica*, *Helicosphaera kamptneri*, and *Pseudoemiliania lacunosa*, an assemblage of probable early Pleistocene age.

In Sample 119-738B-1H-CC, only rare *C. pelagicus* and *G. caribbeanica* were found, neither of which is very age indicative. This sample was taken at approximately the same depth as Sample 119-738A-1H-CC, but yields a different composition and abundance of the calcareous nannofossil assemblage. It appears that the calcareous nannofossil assemblages and their abundances vary greatly within the top 10 m of sediment.

Paleogene

The abundant calcareous nannofossils in Sample 119-738B-3H-CC include common *Reticulofenestra bisecta*, *Reticulofenestra hillae*, *Reticulofenestra daviesi*, *Isthmolithus recurvus*, and *Reticulofenestra oamaruensis*, in addition to abundant *C. pelagicus*. A disconformity is apparent between this sample and Sample 119-738B-2H-CC. Another disconformity is suggested between Samples 119-738B-4H-CC and 119-738B-5H-CC because there is no overlap in the ranges of *I. recurvus* and *Reticulofenestra reticulata*, or, in other words, it is not possible to recognize the *Isthmolithus recurvus* Subzone (CP15b). This disconformity includes the Eocene/Oligocene boundary. No *Discoaster saipanensis* were found at this site, although they were found at Site 737, which is about 10° north. It seems that the last-appearance datum (LAD) of *D. saipanensis* cannot be used to mark the Eocene/Oligocene boundary south of 60°. The LAD of *R. reticulata*, however, is just slightly older than the LAD of *D. saipanensis* and can be used to approximate the Eocene/Oligocene boundary (Perch-Nielsen, 1985; Martini and Müller, 1986).

The LAD of *Chiasmolithus solitus* was recognized in Sample 119-738B-9H-1, 66–68 cm, and the first-appearance datum (FAD) of *Reticulofenestra umbilica* was observed in Sample 119-

738B-15X-1, 66–68 cm. This interval is placed in the *Discoaster bifax* Subzone (CP14a). The *Discoaster saipanensis* Subzone (CP14b) is missing.

There is very low resolution in terms of calcareous nannofossil stratigraphy for the interval from Samples 119-738B-15X-CC to 119-738C-10R-CC (125–288 mbsf), where the index species of both Okada and Bukry's (1980) and Martini's (1971) zonations are absent or rare and sporadic. We tentatively place the intervals from Samples 119-738B-15X-CC through 119-738B-23X-CC in the CP13 Zone and from Samples 119-738B-26X-1, 66–68 cm, through 119-738C-6R-CC in the CP12 Zone. The FAD of *Discoaster praebifax* was found in Sample 119-738C-4R-CC. This species is present both in low and high latitudes and has a range from Zones CP12 to CP13 (Wei and Wise, in press). The interval from Samples 119-738C-7R-1, 66–68 cm, through 119-738C-8R-CC belongs to Zones CP10 to CP11, and the interval from Samples 119-738C-9R-1, 66–68 cm, through 119-738C-10R-CC belongs to Zone CP9. The FAD of *Discoaster multiradiatus* occurs in Sample 119-738C-11R-CC and marks the lower boundary of the CP8 Zone.

Samples 119-738C-13R-CC and 119-738C-14R-CC contain *Discoaster mohleri* but no *D. multiradiatus*. Because *Discoaster nobilis* is not present, which is generally the case in high latitudes, we place Samples 119-738C-13R-CC and 119-737C-14R-CC into the combined CP6 and CP7 Zone. No *D. mohleri* was found, but *Heliolithus kleinpellii* is present in Sample 119-738C-15R-CC, indicating an age of Zone CP5.

Fasciculithus tympaniformis and *Sphenolithus primus* were found in Sample 119-738C-16R-CC; thus, we can assign this sample to Zone CP4. Samples 119-738C-17R-CC and 119-738C-18R-CC contain *Chiasmolithus danicus*, *Prinsius martinii*, and a few other species, but no fasciculiths, and, thus, belong to Zones CP2 and CP3. The subdivision of the two zones is impossible because the index fossil, *Ellipsolithus macellus* (a shallow-water form) is absent at this site.

The Cretaceous/Tertiary Boundary

The Cretaceous/Tertiary boundary was recovered in Section 119-739C-20R-5, within an interval of laminated claystone about 15 cm in thickness (see the core photograph). The fine fractions consist of over 95% microcarbonate particles and few to rare calcareous nannofossils. Based on preliminary examination of smear slides, the detailed succession, with the depths as indicated on the detailed photographs (which are shifted downward by 0.5 cm relative to the visual core descriptions of Section 119-738C-20R-5), is as follows.

White mottled chalk at 97–102 cm is overlain by laminated chalk at 97.0–96.2 cm, followed by a 3-mm-thick gray clay at 95.9–96.2 cm, which is succeeded by a green to gray laminated claystone. These lithologies contain rare, strongly fragmented, and moderately well-preserved upper Maestrichtian nannofos-
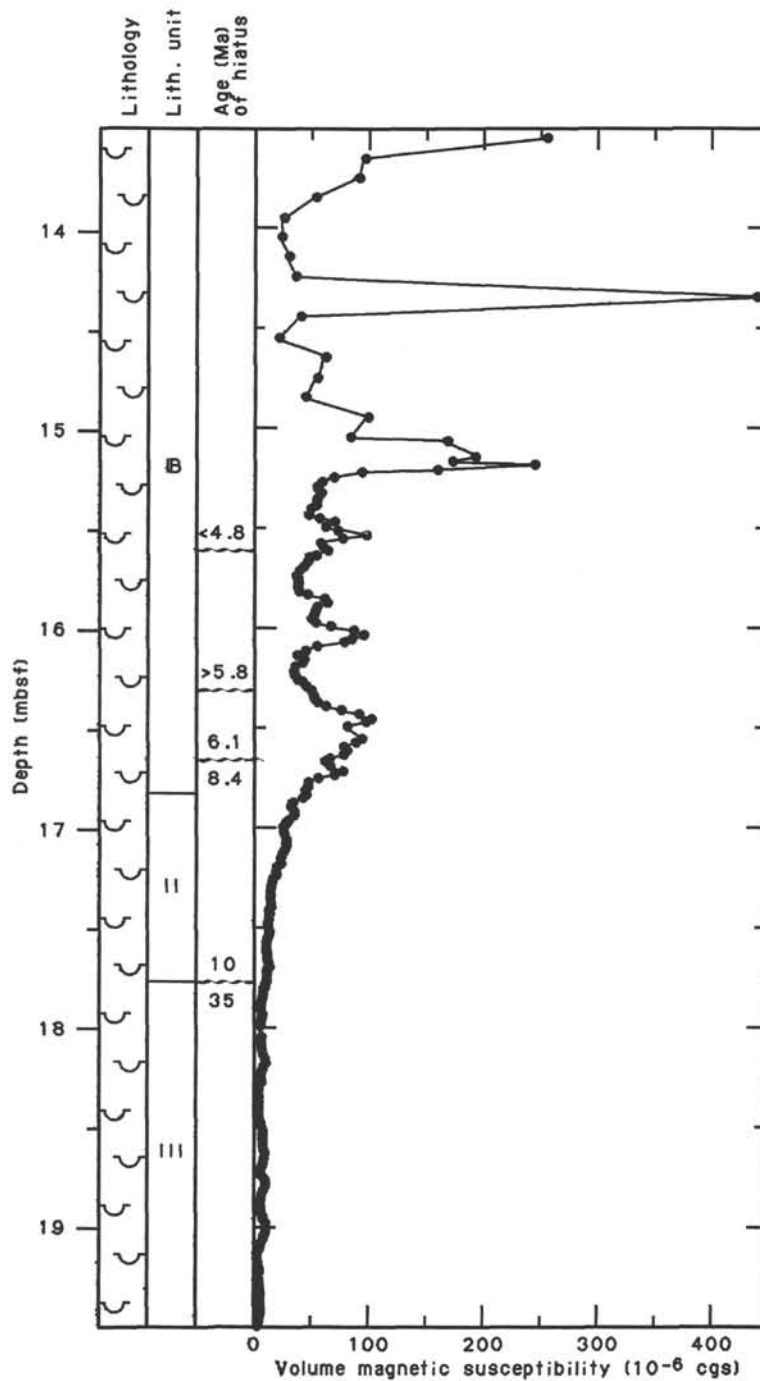
Figure 16. Neogene hiatuses and related lithology and magnetic susceptibility changes as recorded in Core 119-738B-3H.

sils, with common to abundant *Lucianorhabdus cayeuxii*, *Nephrolithus frequens*, *Prediscosphaera cretacea*, *Kamptnerius magnificus*, and *Arkhangelskiella cymbiformis* and few to rare *Cribrosphaerella ehrenbergii*, *Cribrosphaerella daniae*, *Cretarhabdus surirellus*, and *Thoracosphaera* sp. At 85.5 cm few *Markalius inversus* and *Thoracosphaera* sp. and at 85.0 cm rare *Biantholithus sparsus* were found, which palentologically defines the base of Subzone CP1a, the earliest Danian nannofossil subzone. At these two levels the proportion of Cretaceous to Danian taxa is about 100/1 and the proportion of nannofossils in the total carbonate fraction is about 1%. In the mottled interval around 80 cm the Danian taxa increase to more than 50% of the nannofossil assemblage and include abundant *M. inversus* (oval forms), common *Thoracosphaera* sp., *M. inversus* (circular), *Zygodiscus sigmoides*, and rare *Hornibrookina teuriensis*. The lowermost appearance of *Cruciplacolithus tenuis* at 70 cm defines the base of Subzone CP1b. Because the gradual replacement of Cretaceous by lower Tertiary nannofossil taxa occurs in a laminated

interval, the transition can not be explained by bioturbation processes, but must be truly gradual or due to lateral influx or older Cretaceous material.

Mesozoic

The Upper Cretaceous chalk sequence can be subdivided using several nannofossil events, some of which have been directly correlated with the geomagnetic reversal time scale in sedimentary sections (Monechi and Thierstein, 1985), and others that have been calibrated as events between the biostratigraphically correlated datums. The assemblages are dominated by *K. magnificus, Gartnerago obliquum,* and *A. cymbiformis* and contain common *C. daniae, C. ehrenbergii, N. frequens* (down to Sample 119-738C-24R-1, 24 cm), *Zygodiscus anthophorus* (down to Sample 119-738C-29R-CC), *Seribiscutum primitivum,* and *Gartnerago nanum,* all of which show high-latitude affinities. Biochronologically, the sequence can be assigned to the nannofossil zones of Roth (1978): Samples 119-738C-20R-5, 93 cm, to 119-738C-24R-1, 24 cm, NC23 (upper Maestrichtian) based on the presence of *N. frequens;* Samples 119-738C-24R-2, 64 cm, to 119-738C-24R-3, 89 cm, NC19b-22 (Campanian-Maestrichtian); Samples 119-738C-24R-CC to 119-738C-26R-CC, NC18-19a (Campanian) based on the presence of *Eiffellithus eximius* and *Broinsonia parca;* Samples 119-738C-27R-2, 22 cm, to 119-738C-28R-4, 25 cm, NC17 (upper Santonian) based on the absence of *B. parca* and *Lithastrinus floralis;* Samples 119-738C-28R-CC to 119-738C-29R-CC, NC16 (lower Santonian) based on the presence of *L. floralis* and *Z. anthophorus;* Samples 119-738C-30R-1, 103 cm, to 119-738C-30R-CC, NC13-15 (upper Turonian–Coniacian) based on the absence of *Z. anthophorus* and the presence of *Micula staurophora;* and Samples 119-738C-31R-1, 77 cm, to 119-378C-31R-CC, NC12 (lower Turonian) based on the absence of *M. staurophora, K. magnificus, Cruciellipsis chiastia,* and *Axopodorhabdus albianus* and the presence of *Ahmuellerella octoradiata.*

Foraminifers

Foraminifers are well preserved and abundant in nearly all core catchers above the disconformity separating Campanian from upper Maestrichtian sediments at 412 mbsf (Fig. 17). Planktonic foraminifers consistently dominate the late Maestrichtian age and younger samples. Recrystallization and calcite overgrowth are not apparent on any of the Cenozoic foraminifer tests, whereas the upper Maestrichtian specimens show minor calcite overgrowth, and the Campanian and older foraminifers lack primary wall structure and are commonly infilled with silica.

Planktonic Foraminifers

Neogene to Holocene

The mud-line samples from Holes 738A and 738B and Sample 119-738A-1H-CC are composed of a foraminifer sand, mainly consisting of *Neogloboquadrina pachyderma. Globigerina bulloides* occurs in low abundance. Several specimens of *Globorotalia scitula* and *Globigerina quinqueloba* were also found.

The oldest Neogene sediments at Site 738 occur at 20 mbsf, between Cores 119-738B-2H and 119-738B-3H. These are composed of a radiolarian-diatom ooze yielding rare specimens of *N. pachyderma,* indicating an age no older than late Miocene.

Paleogene

The stratigraphic position of the zonal boundaries for Holes 738B and 738C (Fig. 17) is approximated based on the occurrences of datums correlated with the Berggren et al. (1985) time scale (Table 6). The distribution of other important planktonic foraminifer marker species within the two holes (Table 7) and

Table 6. Planktonic foraminifer datums recognized at Site 738 (assigned ages from Berggren et al., 1985). The stratigraphic position of the listed events is constrained by core-catcher analysis only.

|	Datum[a]	Core	Chron	Age (Ma)
LAD	*Globigerinatheka index*	738B-5H	C13	late Eocene (36.6)
LAD	*Acarinina bullbrooki*	738B-14X	C18	late middle Eocene (43.0)
FAD	*Globigerinatheka index*	738B-19X	C21	early middle Eocene (45.0)
LAD	*Planorotalites pseudomenardii*	738C-10R	C26	latest Paleocene (58.8)
FAD	*Planorotalites pseudomenardii*	738C-13R	C26	early late Paleocene (61.0)
LAD	*Morozovella pseudobulloides*	738C-14R	C26	early late Paleocene (61.0)
LAD	*Morozovella pusilla*	738C-14R	C26	early late Paleocene (62.0)
FAD	*Morozovella pseudobulloides*	738C-17R	C29	earliest Paleocene (66.1)
LAD	*Globoconusa daubjergensis*	738C-17R	C27	middle early Paleocene (64.0)
FAD	*Globoconusa daubjergensis*	738C-19R	C29	earliest Paleocene (66.35)
LAD	*Globotruncana*	738C-21R	C29	latest Maestrichtian (66.4)

[a] FAD = first-appearance datum; LAD = last-appearance datum.

Table 7. Stratigraphic ranges and assigned ages of selected planktonic foraminifers recovered from Site 738.

Species	Core interval	Age[a]
Chiloguembelina cubensis	738B-3H to -19X	early late Eocene to late early Oligocene
Globigerina angiporoides	738B-3H to -8H	late Eocene to early Oligocene
Globigerina linaperta	738B-8H to -15X	late middle Eocene to late Eocene
Globigerina brevis	738B-6H to -7H	late Eocene to early Oligocene
Pseudohastigerina micra	738B-9H to -19X	early Eocene to latest Eocene
Planorotalites australiformis	738B-13H to -738C-11R	earliest to middle Eocene
Acarinina primitiva	738B-9H to -738C-13R	early late Paleocene to late middle Eocene
Truncorotalites collactea	738B-7H to -738C-7R	late early Eocene to early late Eocene
Acarinina bullbrooki	738B-14X to -23X	late early Eocene to latest middle Eocene
Acarinina pentacamerata	738B-20X to -738C-4R	late early Eocene to early middle Eocene
Planorotalites chapmani	738B-20X to -738C-9R	late middle Paleocene to early middle Eocene
Pseudohastigerina wilcoxensis	738B-20X to -738C-8R	latest Paleocene to early middle Eocene
Chiloguembelina crinita	738C-10R to -16R	late Paleocene
Chiloguembelina waiparoensis	738C-10R to -16R	late early to late Paleocene
Zeauvigerina tueria	738C-13R to -18R	late early Paleocene to early late Paleocene
Subbotina triloculinoides	738C-13R to -16R	early to late Paleocene

[a] Age ranges based on correlation with southern middle-latitude ranges of Jenkins (1985) and low-latitude ranges of Bolli and Saunders (1985) and Toumarkine and Luterbacher (1985).

correlation with their ranges at southern midlatitude and low-latitude sites (Jenkins, 1985; Toumarkine and Luterbacher, 1985; Bolli and Saunders, 1985) also provide the basis for these zonal correlations. Absence of low-latitude zonal markers causes uncertainty in recognition of several of the Eocene planktonic zones, and, therefore, some zones are combined and several zonal boundaries are inferred.

Figure 17. Biostratigraphic summary, Site 738.
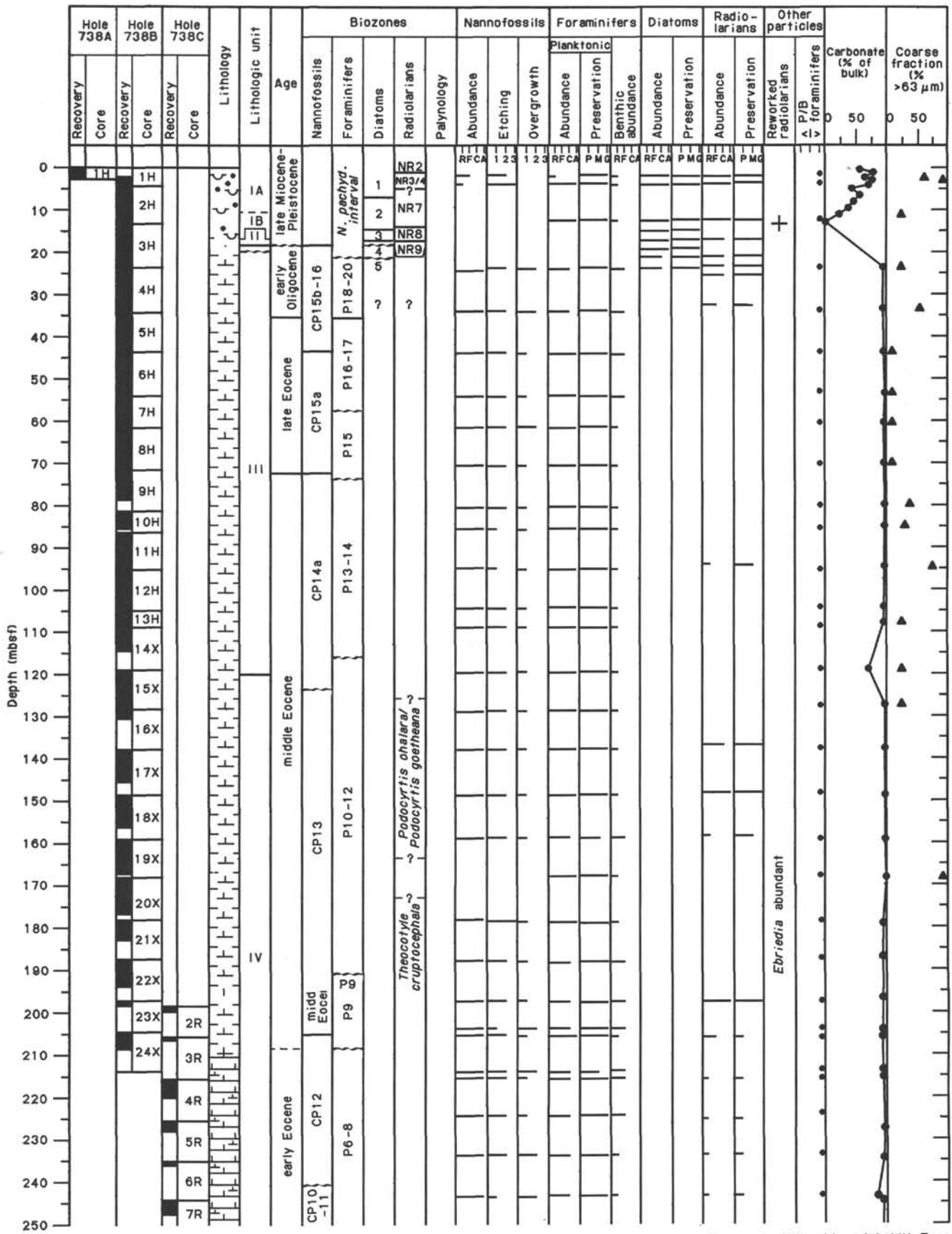
Diatom zones: 1= *Coscinodiscus elliptopora/Actinocyclus ingens* Zone   2= *Nitzschia angulata* Zone   3= *Nitzschia reinholdii* Zone
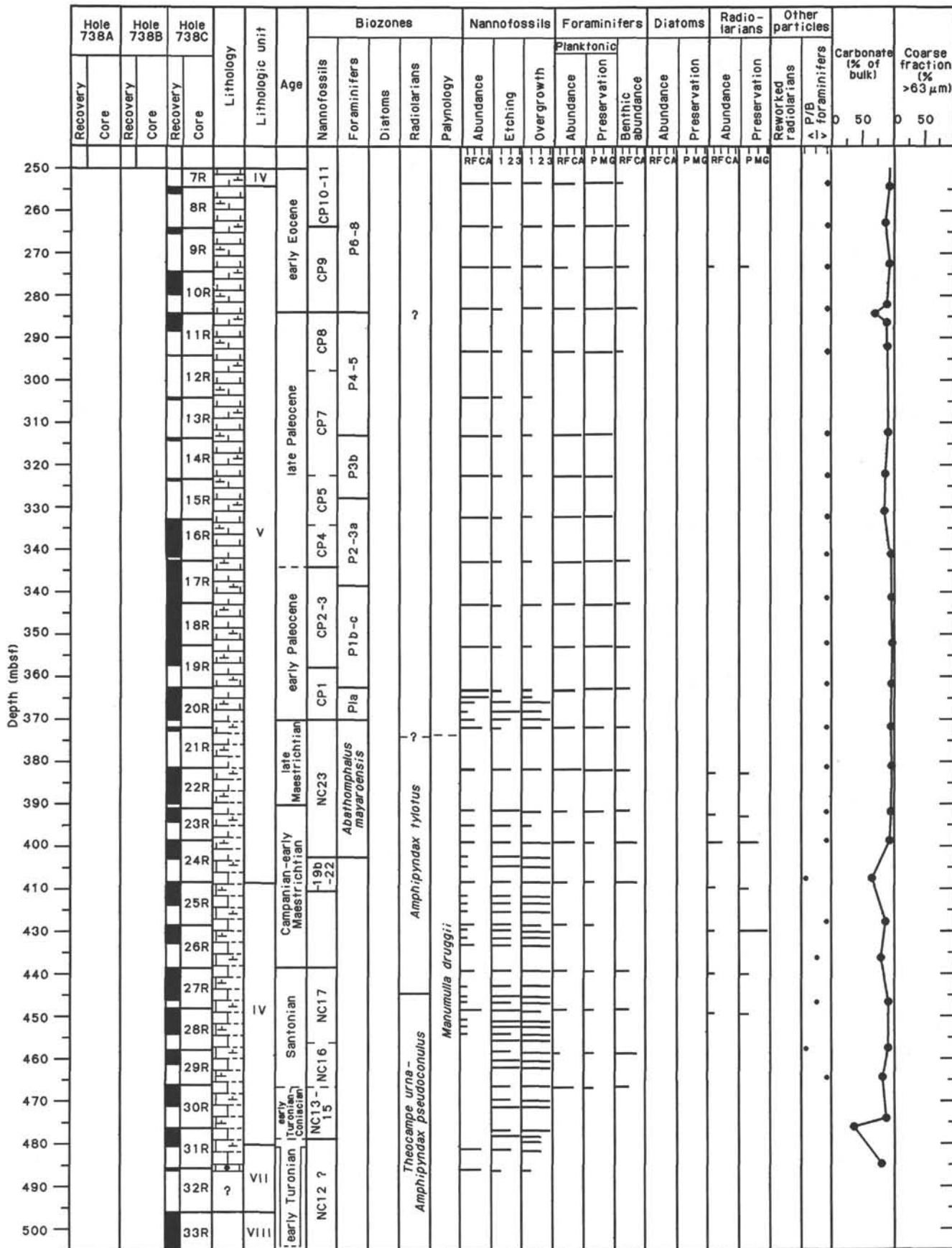4= *Denticulopsis hustedtii/Denticulopsis lauta* Zone   5= *?Cosinodiscus superbus* Zone

Figure 17 (continued).

An early Oligocene age is assigned to Sample 119-738B-3H-CC based on the presence of *Globigerina angiporoides, Globigerina euapertura, Globigerina yeguaensis, Globigerina pseudovenezuelana, Chiloguembelina cubensis,* and *Globorotalia suteri.* Thus, a disconformity separates lower Oligocene from Miocene sediments at Hole 738B. No hiatuses are apparent within the 390-m sequence of upper Maestrichtian through lower Oligocene nannofossil ooze and chalk, although verification of this awaits a more thorough shorebased study.

The LAD of *Globigerinatheka index* in Core 119-738B-5H is the basis for placing the Eocene/Oligocene boundary at 35 mbsf (Fig. 17). Also occurring in the upper Eocene sediments are *G. angiporoides, Globigerina brevis, Globigerina eocaena,* and *Globigerina ampliapertura.* Determination of the middle Eocene/late Eocene boundary (Fig. 17) is based on the LAD of *Acarinina primitiva* in Core 119-738B-9H. *Acarinina bullbrooki, Globigerina linaperta, Globigerina aculeata, G. index, Pseudohastigerina micra, Planorotalites australiformis,* and *Truncorotaloides collactea* are also important components of the middle Eocene. The FAD of *Acarinina pentacamerata* in Sample 119-738C-4R-CC and its range through Core 119-738B-20X indicate correlation with Zones P10 through P12 (early middle Eocene) for this interval. An older age is suggested for this interval based on the occurrence of *Planorotalites chapmani* from Cores 119-738B-20X through 119-738C-9R, because this species is reported to range from Zones P3b through P6 (late Paleocene through early Eocene), according to Toumarkine and Luterbacher (1985). However, this age assignment conflicts of that of co-occurring foraminifer and calcareous nannoplankton species; therefore, the range of *P. chapmani* is considered as diachronous.

The FAD of *A. bullbrooki* in Sample 119-738B-23X-CC suggests a late early Eocene age for this sample and correlation with Zone P9. This sample also yields the LAD of *Acarinina soldadoensis,* which supports the late early Eocene age assignment. However, calcareous nannoplankton distributions indicate that the early Eocene/middle Eocene boundary occurs below this sample. Until a more detailed shorebased study is completed, this boundary is tentatively placed in Core 119-738B-24X. Zones P6 through P8 are not differentiated, based on the shipboard determination of foraminifer distributions.

The Paleocene/Eocene boundary is placed between Cores 119-738C-11R and 119-738C-10R based on the LAD of *Planorotalites pseudomenardii* in Sample 119-738C-10R-CC. No sediment was recovered from Core 119-738C-12R, which may explain the absence of the uppermost Paleocene P5 Zone. The base of the P4 Zone (*Planorotalites pseudomenardii* Zone) occurs in Core 119-738C-13R, based on the FAD of the nominal taxon. Core 119-738C-14R yields the FAD of *Morozovella pusilla,* which is diagnostic of Zone P3b (lower upper Paleocene). *Globigerina triloculinoides, Planorotalites pseudobulloides, Chiloguembelina crinita,* and *Chiloguembelina waiparensis* also occur in Core 119-738C-14R.

Planktonic Zones P3a (*Morozovella angulata* Zone) and P2 (*Morozovella uncinata* Zone) are undifferentiated because of the absence of the nominal taxa. The presence of *Planorotalites compressus, Morozovella pseudobulloides,* and *Globigerina triloculinoides* and the absence of *M. pusilla* in Cores 119-738C-15R and 119-738C-16R also suggest correlation with Zones P3a and P2. The LAD of *Globoconusa daubjergensis* occurs in Core 119-738C-17R (342 mbsf), suggesting correlation with Zone P1c (*Subbotina trinidadensis* Zone). This species ranges down to Sample 119-738C-19-CC (373 mbsf), where it is considerably reduced in size and co-occurs with *Chiloguembelina* sp.

Specimens of *Zeauvigerina teuria* and *P. compressus* occur with *G. daubjergensis* in Core 119-738C-18R, and *Morozovella inconstans* was found in Core 119-738C-19R. Zone P1a (*Eoglobigerina eugubina* Zone) ranges from above the extinction of

Cretaceous planktonic foraminifers (Sample 119-738C-20R-5, 72 cm) to Sample 119-738C-19R-CC, based on the FAD of *G. daubjergensis* in Sample 119-738C-19R-CC and the presence of *Eoglobigerina fringa* and *E. eugubina* in several samples from above 72 cm in Core 119-738C-20R-5.

Cretaceous

The Cretaceous/Tertiary boundary occurs between Samples 119-738C-20R-CC, which contains the diagnostic Upper Cretaceous planktonic species *Abathomphalus mayaroensis, Globigerinelloides subcarinatus, Globigerinelloides multispinatus,* and *Heterohelix globulosa,* and 119-738C-20R-5, 72 cm, which yields minute specimens of *E. fringa* and *E.* cf. *E. eugubina,* diagnostic of lower Danian Zone P1a. Analysis of samples more proximal to the calcareous nannoplankton Cretaceous/Tertiary boundary (Section 119-738C-20R-5, 85 cm) will be undertaken during the shorebased study.

A. mayaroensis was also found in the core-catcher samples of Cores 119-738C-20R to 119-738C-23R, enabling correlation with the upper Maestrichtian *Abathomphalus mayaroensis* Zone. Also occurring within this zone are specimens of *Heterohelix glabrans, H. globulosa, Heterohelix striata, Rugoglobigerina rotundata, Globotruncanella havanensis,* and *Hedbergella* sp. Calcispheres are very abundant in the fine-fraction residues of these samples.

Benthic Foraminifers

Benthic foraminifers were studied at Site 738 from the mud-line sample and all core-catcher samples. Benthic species are rare in comparison with planktonic microfossils, although their abundance is sufficient in most intervals to perform quantitative counts. Preservation remains good throughout the Neogene and Paleogene and decreases drastically in the Cretaceous sequence. Species diversity of the benthic component is higher than at Site 737, but relatively low for a lower bathyal region. This is partly due to nonpreservation of agglutinated species in subsurface sediment; several agglutinated taxa were found in the mud-line sample whereas only the family of Ataxophragmiidae is rarely represented in sediments below. The following assemblages of benthic species are recognized in the Neogene and Paleogene.

Assemblage 1 (Quaternary to Pliocene/Miocene)

Assemblage 1 is terminated by an unconformity, making it difficult to determine the exact age of the lower boundary. Neogene sediments are represented only in the mud-line sample and in the upper three core-catcher samples (Cores 119-738A-1H, 119-738B-1H, and 119-738B-2H). The benthic assemblage is dominated by *Epistominella exigua.* Other less common species include *Oridorsalis umbonatus, Dentalina ittai, Dentalina frobisherensis, Pullenia simplex,* and *Nonionellina* sp. The agglutinated component consists of *Rhizammina algaeformis, Thurammina papillata, Eggerella bradyi,* and *Reophax scorpiurus.* Below the surface, the benthic assemblage decreases drastically in total number and species diversity. The remaining taxa in Cores 119-738B-1H and 119-737B-2H are *E. exigua, Pullenia* spp., *O. umbonatus,* and *E. bradyi. E. exigua* occurs abundantly between 3800 and 4400 m water depth in the equatorial Indian Ocean in association with cold, more oxygenated Indian Bottom Water (IBW) (Peterson, 1983, 1984). On the Southeast Indian Ridge *E. exigua* dominates the benthic fauna and is associated with IBW and in the Australian Basin with a water mass intermediate between Antarctic Bottom Water (AABW) and IBW (Corliss, 1979). IBW northward of the Polar Front reflects water-mass properties of CPDW south of the Antarctic Convergence (Corliss, 1979). At Site 738, *E. exigua* occurs at a shallower depth and may be associated with the CPDW that flows

in easterly directions south of the Kerguelen Plateau (Kolla et al., 1976).

Assemblage 2 (lower Oligocene to middle upper Eocene)

The upper boundary of this interval cannot be defined because of the existing hiatus. The lower Oligocene is represented by only two samples (119-738B-3H–CC and 119-738B-4H-CC). Species diversity is higher than in assemblage 1, and the fauna is dominated by *Stilostomella* spp., a genus that occurs abundantly within the Eocene. Additional species in assemblage 2 include *Pleurostomella subnodosa, O. umbonatus, Cibicidoides robertsonianus, Pullenia bulloides, Pullenia quinqueloba, Cibicidoides laurisae, Cibicidoides ungerianus, Osangularia* sp., and *Bolivinopsis cubensis. Stilostomella* is distributed mainly in the Atlantic (Zones P10 to P16-17), and its maximum abundance indicates a paleodepth of 2000–3500 m (Tjalsma and Lohmann, 1983). This genus dominates the benthic assemblage through Zones P18-20 at Site 738. Site 689 (Maud Rise, 2080 m water depth) shows a high abundance of *Stilostomella* into the lower Miocene (Shipboard Scientific Party, 1988). *E. exigua* is absent from this assemblage. The occurrence of *Nuttalides umbonifera* in the lower Oligocene may indicate the presence of cold, corrosive, deep bottom-water masses. In the Indian Ocean this species is associated with the AABW, which spreads in the modern ocean mainly below 4000 m (Corliss, 1979; Peterson, 1983, 1984). Based on the assumption that similar faunal and oceanographic relationships remain through time, the presence of *N. umbonifera* might imply the early Oligocene initiation of AABW. This event might be connected with an intensification of bottom current activity resulting in the hiatus in the overlying strata. Site 744, with a preserved Oligocene/Miocene sequence, shows a full development of *N. umbonifera* during the Miocene.

Assemblage 3 (lower upper Eocene to lower Eocene)

Assemblage 3 is quite similar to assemblage 2. It is characterized by the common occurrence of *Nuttalides truempyi*, which has its last appearance in Core 119-738B-7H. The last appearance of this species has been used as a marker of the Eocene/Oligocene boundary (Berggren and Aubert, 1976). The last occurrence of *N. truempyi* at Site 738, at the zonal boundary of P15/16 to P17, is comparable to its range in the Atlantic, according to Tjalsma and Lohmann (1983). On the Maud Rise this event occurs somewhat lower in the middle Eocene (Shipboard Scientific Party, 1988). Other dominant taxa of assemblage 3 include *Stilostomella* spp. and *C. ungerianus. Stilostomella* seems to have been less spinose in the early Eocene. Other characteristic species include *B. cubensis, Orthomorphina havanensis, Karreriella chapapotensis, O. umbonatus, Pleurostomella acuta,* and *Amphimorphina ignota.* A more detailed subdivision of the Eocene sequence may be possible after closer sampling and intensive identification of taxa.

Assemblage 4 (Paleocene)

Assemblage 4 has several species in common with assemblage 3, such as *N. truempyi* and *B. cubensis.* Additional taxa in the upper Paleocene include *Neoflabellina semireticulata, Nonion havanensis, Osangularia mexicana, Neoeponides hildebrandti, Gyroidinoides* sp., and *Pleurostomella* sp. The presence of *Stilostomella* is minor. The lower Paleocene is characterized by taxa such as *Coryphostoma idwayensis, Anomalina praeacuta, Bulimina callahani, Bolivina incrassata,* and *Osangularia velascoensis.*

Assemblage 5 (upper Maestrichtian)

The upper Maestrichtian benthic fauna is considerably different from the Tertiary benthic assemblages. Sample 119-738C-21-CC yields abundant specimens of *Bolivinoides draco draco*

as well as *Neoflabellina* spp., *Frondicularia* sp., *Lenticulina* spp., *Nodosaria* spp., and *Marginulina* spp. Other benthic taxa include *Gavelinella beccariformis, N. truempyi, B. incrassata, Reussella szjanochae, Globorotalites* sp., *Dorothia* sp., *Gyroidina* spp., and *Pleurostomella* sp. Because this fauna is characteristic of outer shelf environments, a shallower water depth is suggested for the Cretaceous sequence, in comparison with the Paleogene. This is consistent with the abundant occurrence of *Inoceramus* prisms in the upper Maestrichtian samples.

Benthic specimens in the Campanian and older sediments occur in low abundance and diversity and have not been identified because of poor preservation.

Diatoms

Diatoms were examined from Cores 119-738A-1H and 119-738B-1H through 119-738B-10H. Diatoms are abundant and moderately to well preserved in samples examined from the uppermost section. Slides prepared for radiolarians from below Core 119-738B-10H were also examined and found to be barren of diatoms. The diatom assemblages from Site 738 consist of pelagic species characteristic of the Southern Ocean and the middle to low latitudes. Lower Pliocene and upper Miocene diatom assemblages at Site 738 evidently have an abrupt downcore change (also noted at Site 737) from a Southern Ocean diatom assemblage above to more of a temperate diatom assemblage dominated by *Thalassionema* spp., which was observed at Site 737 in the upper lower Pliocene (around 3.9 Ma).

Because of the poor preservation and paucity of the biosiliceous component, samples were not prepared and examined from the remainder of Hole 738B or from Hole 738C.

Diatoms were observed in the lower Oligocene, upper Miocene, lower Pliocene, and Quaternary sediments recovered. The occurrence of abundant *Nitzschia kerguelensis,* common *Actinocyclus ingens,* and rare *Coscinodiscus elliptopora* allow Samples 119-738A-1H-CC and 119-738B-1H-CC to be assigned to the *Coscinodiscus elliptopora/Actinocyclus ingens* Zone used by Ciesielski (1983).

Samples 119-738B-2H-CC and 119-738B-3H-1, 140 cm, are placed in the *Nitzschia angulata* Zone based on the presence of *N. angulata* and the absence of *Nitzschia interfrigidaria.* Sample 119-737B-3H-1, 140 cm, is notable for the common occurrence of the temperate silicoflagellate *Distephanus crux.*

The absence of *N. angulata* and *N. praeinterfrigidaria* in Sample 119-738B-3H-2, 62 cm, combined with the presence of *Thalassiosira gracilis,* place that sample in the upper part of the *Nitzschia reinholdii* Zone. Sample 119-738B-3H-2, 148 cm, contains the low-latitude diatoms *Thalassiosira miocenica, Thalassiosira convexa aspinosa,* and *Thalassiosira praeconvexa,* signaling a relatively brief warm interval in the latest Miocene between 6.1 and 5.8 Ma, which has been recognized throughout the middle-latitude northeastern Pacific by J. Barron (unpubl. data). Thus, this sample falls in the middle part of the *N. reinholdii* Zone and is at least 1 m.y. older (5.8 Ma vs. younger than 4.8 Ma) than Sample 119-738B-3H-2, 62 cm, suggesting the possibility of a hiatus between the two samples. Sample 119-738B-3H-3, 21 cm, also is assigned to this same interval based on the presence of *T. convexa aspinosa* and *T. miocenica;* both samples contain common reworked lower upper Miocene diatoms as well as sparse reworked lower Oligocene diatoms.

Samples 119-738B-3H-3, 43 cm, 119-738B-3H-3, 53–55 cm, and 119-738B-3H-3, 110 cm, are placed in the upper part of the *Denticulopsis hustedtii/Denticulopsis lauta* Zone based on the occurrences of *D. hustedtii, Denticulopsis dimorpha,* and *Thalassiosira* cf. *nativa* without *Thalassiosira burckliana.* Sample 119-738B-3H-3, 110 cm, is notable because of the presence of the warm-water silicoflagellate *Dictyocha.* These samples are also distinguished by the presence of relatively common nanno-

fossils and are probably separated from the overlying *N. rein-holdii* Zone samples by an unconformity marked by a color change at 25 cm in Section 119-738A-3H-3. This hiatus encompasses at least the interval from 8.4 to 6.1 Ma and is equivalent to the interval of the combined widespread Neogene hiatuses NH5 and NH6.

Sample 119-738B-3H, 110 cm, contains a lower Oligocene assemblage consisting of *Pyxilla gracilis, Hemiaulus polycystinorum, Azpeitia oligocenica, Stephanopyxis grunowii,* and *Rouxia granda.* The other samples examined contain rare, poorly preserved diatoms or are barren of diatoms.

Radiolarians

Radiolarians are consistently present and well preserved in Miocene to Pleistocene sediments and sporadically present and moderately preserved in Oligocene, Eocene, and Cretaceous sediments recovered from Site 738. Hole 738A yielded a single core, from which the core-catcher sample can be placed in the NR2 Zone.

Radiolarians are abundant and well preserved in Cores 119-738B-1H to 119-738B-3H, although they are overwhelmed by an abundant diatom flora. Species diversity is high, and all the stratigraphic markers are present. Sample 119-738B-1H-CC is related to the upper part of the NR3/NR4 interval because of the occurrence of *Stylatractus universus* and *Phormostichoartus pitomorphus.* Deep-living forms are present, although they remain rare. Phaeodarian debris is common. The radiolarian assemblage in Sample 119-738B-2H-CC is assigned to the NR7 Zone (early Pliocene) because of the abundance of *Desmospyris spongiosa, Prunopyle titan,* and *Helotholus praevema.* These datums suggest a hiatus spanning most of the upper Pliocene and the lower Pleistocene. Because of the low rates of sedimentation, additional samples to that from the core catcher were processed for Core 119-738B-3H. Sample 119-738B-3H-2, 52–53 cm, is assigned to the NR8 Zone because of the absence of *D. spongiosa.* Sample 119-738B-3H-3, 52–53 cm, is tentatively related to the NR9 Zone (occurrence of *S. peregrina*). The radiolarian population from this sample is composed mostly of large specimens and many reworked individuals of Eocene age (*Lophocyrtis biaurita* or *Lithomitrella* sp. are recognized). All these observations suggest a strong winnowing. Sample 119-738B-3H-3, 130–132 cm, is assigned to the NR10 Zone (late to middle Miocene) because of the occurrence of *Actinomma tanyacantha.* Sample 119-738B-3H-4, 53–55 cm, contains an Oligocene assemblage including the high-latitude variety of *Cyclampterium milowi, Calocyclas semipolita,* and some undescribed specimens of *Eucyrtidium* and *Lithomelissa.* No zonal assignment can be made due to the absence of tropical stratigraphical markers. The occurrence of this Oligocene assemblage just on top of Section 119-738B-3H-4 suggests an important hiatus spanning significant parts of the lower and middle Miocene between 14.8 and 23.5 mbsf. Oligocene radiolarians are rare and moderately preserved in core-catcher samples from Cores 119-738B-3H and 110-738B-4H.

Core-catcher samples from Cores 119-738B-5H through 119-738B-10H are barren of radiolarians. Rare debris of *L. biaurita* and *Lychnocanoma amphitrite* (Eocene) occur in Sample 119-738B-12H-CC, but no zonal assignment can be made. Samples 119-738B-12H-CC through 119-738B-15X-CC are barren of radiolarians. A well-preserved radiolarian fauna has been found in Samples 119-738B-16X-CC through 119-738B-18X-CC. Assemblage composition indicates a warmer population diagnostic of the *Podocyrtis chalara/Podocyrtis goetheana* Zones (upper middle Eocene). The most useful stratigraphical marker is *P. chalara,* for which this is the first report in high-latitude assemblages. We did not find *P. goetheana.* Tropical species, such as *Amphicraspedum prolixum, Amphymenium splendiarmatum,*

Lithocyclia ocellus, and *Spongatractus pachystylus,* are more abundant than high-latitude forms. Samples 119-738B-19X-CC through 119-738B-21X-CC are barren of radiolarians. Lower middle to upper lower Eocene radiolarians are abundant and well preserved in Sample 119-738B-22X-CC. Many tropical species are common, but most of the *Theocotyle* and *Theocotylissa* species are missing. The absence of *Dictyoprora mongolfieri, Spongatractus balbis,* and *Buryella clinata,* which are common in lower middle Eocene sediments of the northern sector of the Kerguelen-Heard Plateau (P. Caulet, pers. comm., 1988), is diagnostic of the *Theocotyle cryptocephala* Zone. Ebridians are exceptionally abundant, but the population is apparently monospecific. Samples 119-738B-23X-CC and 119-738B-24X-CC are barren of radiolarians.

Very rare and recrystallized Eocene radiolarians were found in core-catcher samples from Cores 119-738C-2R through 119-738C-9R. All other core-catcher samples are barren of radiolarians down to Sample 119-738C-21R-CC, which yielded rare and strongly recrystallized specimens of *Dictyomitra* sp., suggesting a Cretaceous age. In Sample 119-738C-23R-CC, a few moderately preserved radiolarians, such as *Archaeodictyomitra lamellicostata, Amphipyndax stocki,* and *Siphocampe bassilis* gr., are diagnostic of the *Amphipyndax tylotus* Zone (upper Campanian to Maestrichtian). The same assemblage was found in Samples 119-738C-24R-CC through 119-738C-26R-CC, where a single specimen of *A. tylotus* was observed. Samples 119-738C-27R-CC through 119-738C-31R-CC are completely barren of radiolarians.

Palynomorphs

Core-catcher samples from Cores 119-738C-19R through 119-738C-31R were examined for their palynological content but proved to be barren. However, future shorebased studies using full palynological processing techniques may prove more fruitful.

Moderately well-preserved dinoflagellate cyst assemblages of low abundance and diversity were recovered from Samples 119-738C-22R-6, 20–23 cm, 119-738C-22R-4, 69–72 cm, 119-738C-22R-2, 45–48 cm, 119-738C-22R-1, 45–48 cm, and 119-738C-21R-1, 56–59 cm. Stratigraphically significant forms recovered include *Manumulla druggii, Alisocysta curcumtabulata, Alisocysta reticulata, Alisocysta rugolirata,* and *Xenicodinium reticulatum.* The presence of *M. druggii* and *A. circumtabulata* suggest that Cores 119-738C-21R and 119-738C-22R fall within the *Manumulla druggii* Interval Zone of Helby et al. (1987), which has a suggested age of late Maestrichtian–earliest Danian.

PALEOMAGNETICS

Results from Holes 738B and 738C

The magnetic remanence of the sediments drilled at Holes 738B and 738C was measured with the whole-core cryogenic magnetometer. During transit to the site, filling of the cryogenic magnetometer with liquid helium trapped a large magnetic field within the system. In order to reduce this field, the cryogenic magnetometer was thermally cycled after reaching Site 738. This process proved successful, decreasing the field inside the magnetometer to 400 nT.

Sediment cores collected between 50 and 100 mbsf at Hole 738B were fully oriented for use in magnetic reversal studies. The cores were measured and demagnetized at 5 mT within the cryogenic magnetometer using a three-axis demagnetization coil system. The directions determined after demagnetization are shown in Figure 18. As discussed in the previous site chapter, several problems in the cryogenic magnetometer interface and software were discovered during the measurement of these cores. The data have been corrected for all of the identified problems
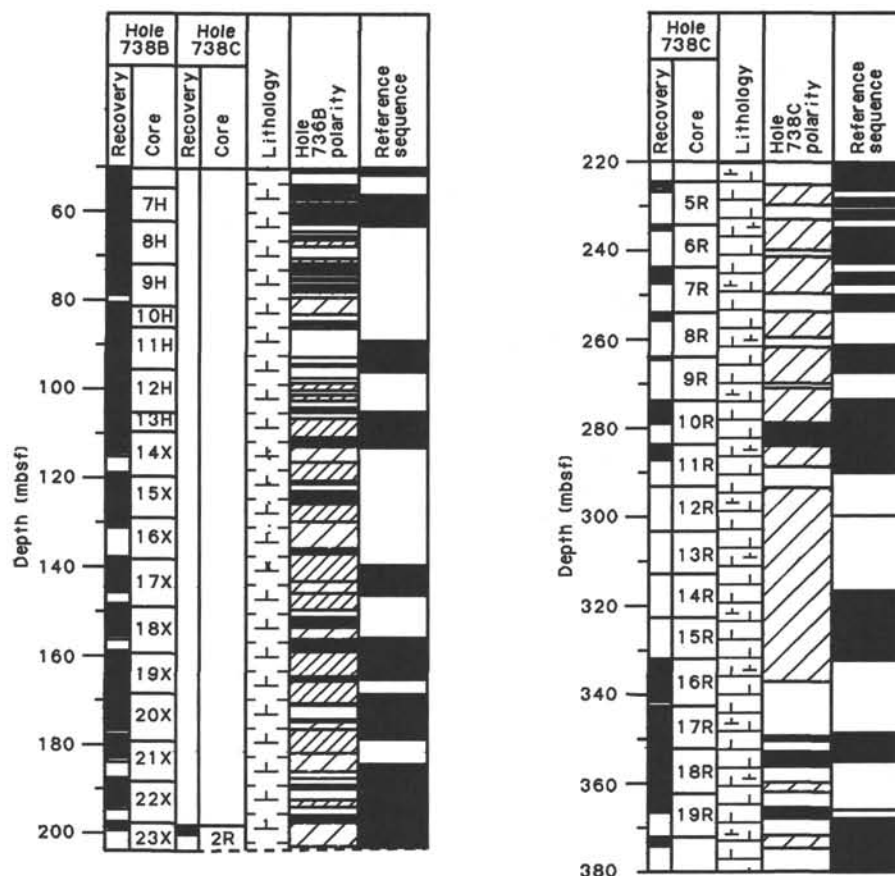
Figure 18. Summary of the magnetic polarity determinations for Holes 738B and 738C. Gaps in the record resulting from poor recovery or uncorrected polarity data are shown by narrow and widely spaced hatched patterns, respectively. The polarity reference column of Berggren et al. (1985) for the corresponding age units is shown, but correlations with this reference sequence are not possible.

except for the undetected flux jumps during measurement. Because the number of flux jumps was not recorded as part of the original computer programs, these data were irretrievably lost, and corrections for this problem were impossible. Therefore, many polarity determinations within large segments of the cores from Holes 738B and 738C have been designated unreliable and are denoted with hatched patterns in the accompanying stratigraphic plots. Gaps resulting from poor core recovery are marked by a closely spaced hatched pattern.

The magnetic polarity could be identified in only approximately 30% of the stratigraphic sequence sampled, with the remainder of the stratigraphic sequence consisting of sampling or data gaps. This paucity of reliable magnetic coverage makes it impossible to correlate the polarity of much of the stratigraphic sequence from Holes 738B and 738C with the reference polarity time scale of Berggren et al. (1985). An important exception, however, is the sequence at the Cretaceous/Tertiary boundary. The results of the paleomagnetic stratigraphic studies are shown in Figure 18. From the reference polarity sequence for the time interval represented, however, no correlation was made with specific polarity zones, except in the case of the Cretaceous/Tertiary boundary. The Cretaceous/Tertiary ages are based upon nannofossil, foraminifer, and radiolarian zonations reported elsewhere in this site chapter ("Biostratigraphy" section).

Discrete, oriented samples were collected from the cores of both Holes 738B and 738C. Unfortunately, the sampling interval was too coarse to be useful in correlating the polarity units with the reference sequence of reversals shown in Figure 18. The

intensities observed in the discrete samples are generally low, with a mean of roughly 0.05 mA/m.

Cretaceous/Tertiary Boundary

Whole-core magnetic measurements were completed on sections of Cores 119-738C-17R through 119-738C-20R. Following measurement of the natural remanent magnetization (NRM), the cores were demagnetized at 5 mT using the built-in three-axis core demagnetization system within the cryogenic magnetometer. The magnetic measurements from this interval are shown in Figure 19. Two long intervals of normal polarity separated by a short interval of reversed polarity were measured in the cores.

SEDIMENTATION RATES

The pelagic sequence recovered at Site 738 is biostratigraphically dated by diatoms and radiolarians in the Neogene and by calcareous nannofossils and planktonic foraminifers in the Paleogene and Upper Cretaceous. The biostratigraphic events recognized are listed in Table 8, and their depth distribution in the recovered cores is shown in Figure 20.

The uppermost 18 m of upper Miocene to Pleistocene diatom ooze was deposited at the slow average rate of 2 m/m.y. A hiatus is present at about 18 mbsf, separating the lower Oligocene from the upper Miocene. The underlying 371 m of continuously deposited upper Maestrichtian to lower Oligocene calcareous sediments was deposited at an average rate of 11.8 m/m.y. The sediments consist of 180 m of middle Eocene to lower Oligocene nannofossil ooze, 170 m of lower Paleocene to lower Eo-
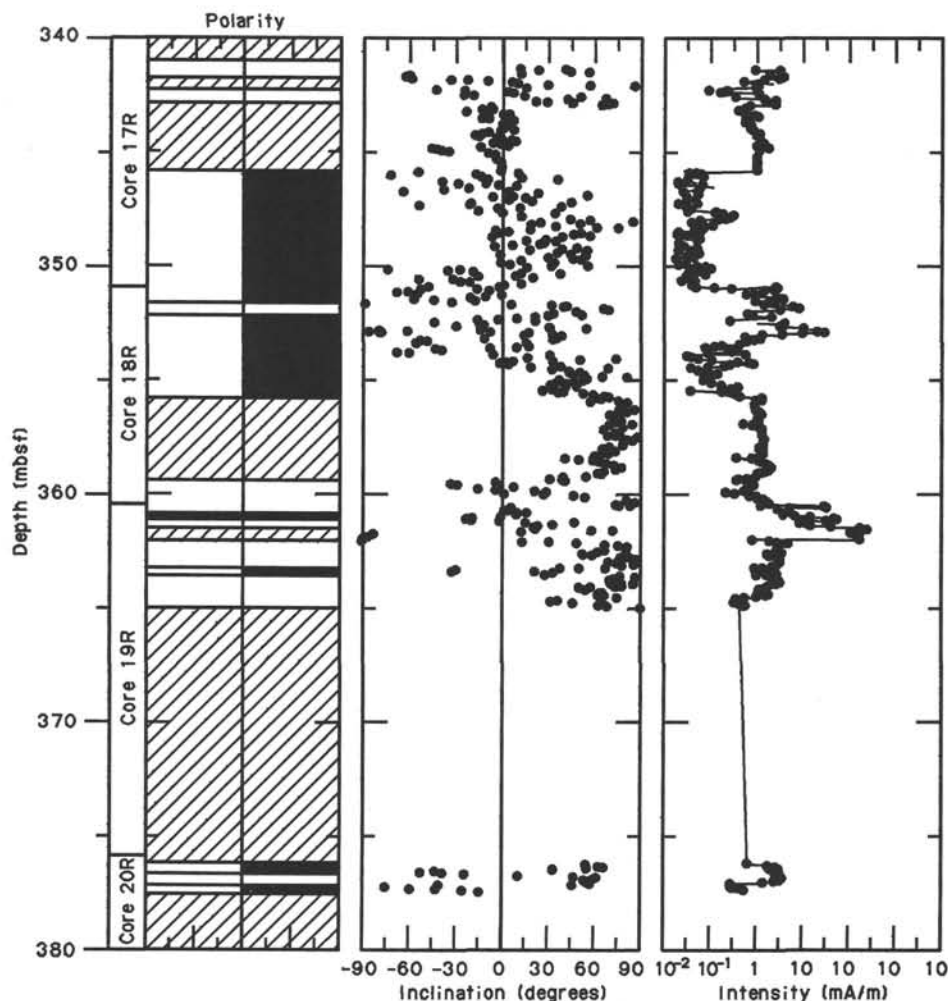
Figure 19. Stratigraphic plot of polarity, sample inclination, and intensity for Cores 119-738C-17R through 119-738C-20R. Black indicates normal polarity, white indicates reversed polarity, and the hatched patterns indicate intervals in which polarity is indeterminate because of the equipment failure described in the text.

cene cherty nannofossil chalks, and 35 m of upper Maestrichtian clayey limestones. A Campanian to late Maestrichtian hiatus of about 9 m.y. duration separates the underlying 70 m of Turonian through Campanian cherty and clayey limestones, which were deposited at an average rate of 4.4 m/m.y.

INORGANIC GEOCHEMISTRY

Whole-round minicores 5 to 10 cm in length were taken from approximately every third core in Holes 738B and 738C for the purpose of interstitial-water chemical studies. A total of 13 interstitial-water samples was obtained from depths of 3 to 396 mbsf.

The composition of the sediments cored at Site 738 sharply contrasts with those cored at Sites 736 and 737. The shallow-water (628 and 564 m at Sites 736 and 737, respectively) sites on the northern Kerguelen Plateau are composed primarily of biosiliceous oozes whereas calcareous sediments predominate at Site 738. All of the interstitial-water samples from Hole 738B were squeezed from nannofossil oozes containing 78% to 97% calcium carbonate (see "Organic Geochemistry" section). Sediment minicores taken from Hole 738C are more lithified nannofossil chalks containing 38% to 95% calcium carbonate and abundant chert nodules (see "Lithostratigraphy, Sedimentology, and Igne-

ous Petrology" section, this chapter). Only one of the sediment minicores contained more than 0.1% organic carbon (Sample 119-738C-16R-4, 140–150 cm, contained 0.13% organic carbon; see "Organic Geochemistry" section). Major lithologic boundaries encountered within the interstitial-water sampling interval at Site 738 include a transition from diatom oozes to nannofossil oozes in Core 119-738B-3R, a transition from nannofossil oozes to nannofossil chalks containing chert nodules in Core 119-738B-24R, and an increase in clay content below Core 119-738C-20R (see "Lithostratigraphy, Sedimentology, and Igneous Petrology" section). We observed several diagenetic features in the sediments cored at Site 738 that may have some bearing on the chemistry of co-existing interstitial waters. Siliceous microfossils (diatoms and radiolarians) are found in abundance only within the first 20 mbsf. Below this level, siliceous microfossils are rare or absent and are always poorly preserved (see "Biostratigraphy" section for more information on microfossil preservation). The first evidence of silica precipitation occurs near 120 mbsf, where the remnants of thin chert beds were recovered. In addition, chert nodules are quite common from around 220 mbsf to the bottom of the sedimentary section at Site 738. With increasing depth, the calcareous oozes (composed primarily of coccoliths and foraminifers) that com-

Table 8. Bioevents identified at Site 738.

Biostratigraphic event[a]	Depth (mbsf)	Age (Ma)
LAD *Stylatractus universus*	0.0–4.0	0.42
LAD *Helotholus praevema*	4.0–13.5	3.9
LAD *Triceraspyris coronata*	13.5–17.0	4.2
FAD *Desmospris spongiosa*	13.5–17.0	4.3
FAD *Thalassiosira miocenica*	16.7–16.9	6.1
LAD *Actinomma tanyacantha*	17.1–17.8	9.5/9.8
LAD *Globigerinatheka index*	32.5–42.0	36.6
LAD *Reticulofenestra reticulata*	39.6–40.6	37.4
FAD *Chiasmolithus oamaruensis*	70.5–71.1	39.8
LAD *Neococcolithes dubius*	46.1–47.6	41.2
LAD *Chiasmolithus solitus*	70.5–71.1	42.3
FAD *Reticulofenestra reticulata*	98.1–99.6	43.6
LAD *Acarinina bullbrooki*	108.2–117.8	43.0
FAD *Reticulofenestra umbilica*	118.4–119.9	44.8
FAD *Globigerinatheka index*	166.2–175.8	45.0
LAD *Tribrachiatus orthostylus*	264.1–264.7	53.7
LAD *Fasciculithus* sp.	274.4–275.9	57.4
LAD *Planorotalites pseudomenardii*	277.1–280.0	58.8
FAD *Discoaster multiradiatus*	273.8–274.4	59.2
FAD *Planorotalites pseudomenardii*	312.3–321.9	61.0
LAD *Morozovella pseudobulloides*	312.3–321.9	61.7
FAD *Discoaster mohleri*	321.9–331.6	60.4
FAD *Morozovella pusilla*	321.9–331.6	62.0
LAD *Planorotalites compressus*	321.9–331.6	61.7
LAD *Cruciplacolithus tenuis*	338.5–339.2	61.8
FAD *Fasciculithus tympaniformis*	340.4–341.3	62.0
LAD *Globoconusa daubjergensis*	341.3–350.9	64.0
FAD *Morozovella pseudobulloides*	350.9–360.5	66.1
FAD *Globoconusa daubjergensis*	370.2–379.9	66.35
FAD *Cruciplacolithus tenuis*	376.3–376.8	66.1
FAD *Zygodiscus sigmoides*	377.0–377.1	66.4
LAD *Globotruncana*	379.9–389.6	66.4
FAD *Nephrolithus frequens*	408.0–409.1	68.0
LAD *Eiffellithus eximius*	413.0–418.6	77.0
FAD *Broisonia parca*	429.2–430.7	81.9
FAD *Zygodiscus anthophorus*	466.6–467.6	86.0
FAD *Micula staurophora*	476.3–477.1	91.0

[a] FAD = first-appearance datum; LAD = last-appearance datum.

prise the sedimentary interval from around 20 to 210 mbsf grade into chalks and limestones in which diagenetic carbonates are the primary calcareous phases. Coccoliths are abundant and moderately well preserved in the Tertiary sediments, but are poorly preserved and generally subordinate to foraminifers in Cretaceous sediments. Foraminifers are well preserved in Cenozoic sediments, but are moderately well to poorly preserved in Cretaceous sediments. Thus, it would appear that the coccoliths may be undergoing preferential dissolution and/or recrystallization relative to foraminifers in the upper 370 m of the sediments and may be the primary source of carbonate cements that become common from around 210 mbsf to the basement at Site 738. Carbonate diagenesis appears to be affecting the preservation state of all calcareous microfossils below 370 mbsf. Clay minerals become abundant at around 200 mbsf and below and are of uncertain origin at the time of this writing.

Methods

All of the interstitial-water samples obtained at Site 738 were analyzed for salinity, chloride, calcium, magnesium, silica, pH, alkalinity, sulfate, ammonium, and phosphate. The analytical methods used are discussed in the "Explanatory Notes" chapter. All of the analyses were completed within one day of the retrieval of the deepest sample.

Results

Data obtained by means of shipboard chemical analyses of Site 738 interstitial-water samples are listed in Table 9. All of the data are reported to the appropriate level of precision for each type of analysis. Each of the following figures represents a composite of data from Holes 738B and 738C.

Salinity and Chloride

Both the salinity and chloride concentration of the interstitial waters analyzed at Site 738 increase slightly with increasing depth (Fig. 21). The total increase is around 3% for both salinity and chloride concentration. Most of the downhole increase occurs in the interval between 142 and 208 mbsf within middle Eocene sediments. This increase may reflect the presence of more saline ancient bottom waters or more recent diagenetic influences, such as the uptake of water by authigenic clay formation.

Magnesium and Calcium

The dissolved magnesium and calcium concentrations and the magnesium to calcium ratios of Site 738 interstitial waters all show nearly linear variations with increasing depth (Fig. 21). The dissolved magnesium concentration decreases 30% from a value similar to average seawater concentrations at 3 mbsf (53.5 mmol/L in Sample 119-738B-1H-2, 145–150 cm) to 38.5 mmol/L at 396 mbsf. Conversely, dissolved calcium concentrations in Site 738 interstitial waters increase 177% from a value similar to average seawater concentrations (11.1 mmol/L in Sample 119-738-1H-2, 145–150 cm) at 3 mbsf to 30.7 mmol/L at 396 mbsf. The magnesium to calcium ratio decreases with increasing depth. All of these trends are dampened near average seawater values in the top 20 mbsf. This may indicate bottom-water influence to a depth of 20 mbsf, where more porous biosiliceous sediments give way to more dense calcareous sediments.

The set of interstitial waters collected at Site 738 is characterized by a linear correlation between dissolved calcium concentrations and dissolved magnesium concentrations. Figure 22 shows the dissolved calcium concentration vs. dissolved magnesium concentration of the Site 738 samples. A regression line through the data points has a slope of −1.27 and a correlation coefficient of −0.9947. A linear correlation between calcium and magnesium concentrations in interstitial waters has been shown to indicate that both cations are behaving in a conservative manner (McDuff and Gieskes, 1976; McDuff, 1978; Gieskes, 1983). Consequently, the concentrations of these two cations in the sediment pore fluids at Site 738 are probably controlled by diffusion processes. The diffusion gradient is set between ocean bottom waters above the sedimentary section and alteration reactions in the basement rocks below the section. Thus, it is likely that dissolved magnesium originates in ocean bottom waters and is lost to the alteration products of the basement rocks (e.g., authigenic clay minerals). Calcium ions may be added to the interstitial waters during the alteration of feldspars and other minerals in the basement rocks and find a sink in carbonate minerals and ocean bottom waters. As these cations appear to behave conservatively in Site 738 interstitial waters, carbonate diagenesis reactions do not greatly affect dissolved calcium and magnesium concentrations.

Silica

Silica concentrations are variable and elevated well above average seawater concentrations (around 89 mmol/L; Stumm and Morgan, 1981) in the interstitial waters collected at Site 738 (Fig. 21). Dissolved silica concentrations decrease from 683 mmol/L at 3 mbsf to 517 mmol/L at 57 mbsf and remain near the latter level to 107 mbsf. This decrease takes place in the same interval in which the dominant lithology changes from biosiliceous oozes above 20 mbsf to nannofossil oozes below and is probably due to a decreasing supply of biogenic silica in this zone. A maximum in the dissolved silica vs. depth profile occurs between 142 and 172 mbsf, where the silica concentration reaches 677 mmol/L. The maximum exists slightly below the
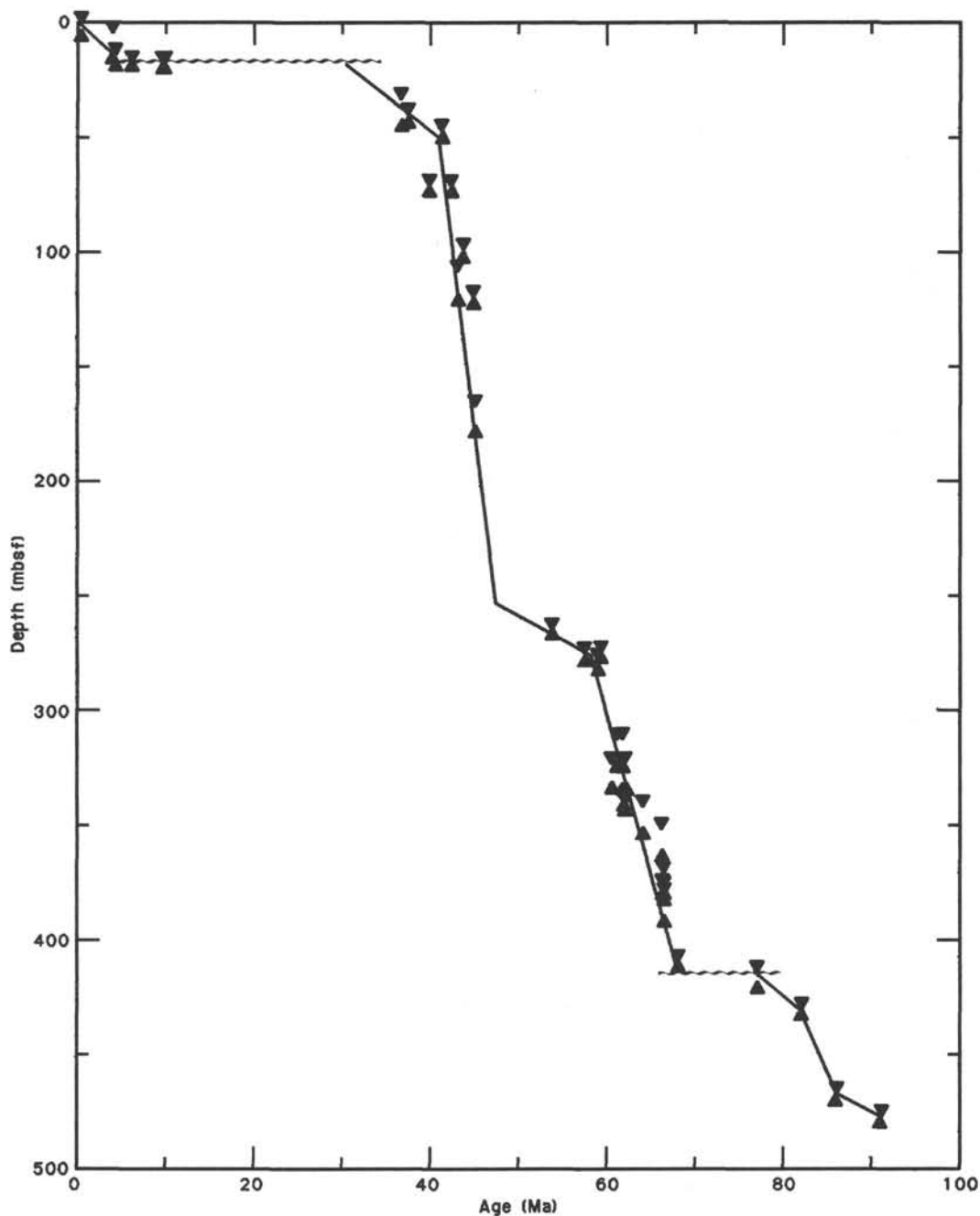
Figure 20. Sedimentation rates at Site 738. Refer to Table 8 for bioevents.

shallowest chert occurrences in Hole 738B (see "Lithostratigraphy, Sedimentology, and Igneous Petrology" section). While this may be indicative of an active zone of silica diagenesis at this depth, it could be merely the dissolution of previously formed silica. From 172 to 396 mbsf interstitial-water silica concentrations show an overall decrease from 677 to 465 mmol/L. This lowermost decrease may indicate the presence of a diffusion gradient between a silica source near the maximum and a silica sink near the bottom of the sedimentary section, where basement-rock alteration results in the precipitation of authigenic silicates. Alternatively, the decrease may be due to the precipitation of additional diagenetic silica within the part of the sedimentary section where chert nodules are common (around 210 mbsf to basement). In the absence of heatflow data for this

site, the presence of cherts at such shallow depths (around 155 mbsf and deeper) seems enigmatic and may indicate that the cherts were formed during an earlier period of time when the sediments were subjected to higher temperatures. These problems will be addressed by more detailed post-cruise research.

pH, Alkalinity, and Sulfate

The pH, alkalinity, and sulfate concentration of Site 738 interstitial waters show only minor variations (Fig. 21). The pH is essentially constant in the upper 396 mbsf of this site. The strong buffering of the pore-water system near a pH of 7.5 is undoubtedly due to the abundance of calcium carbonate in the sediment column. The alkalinity of the interstitial waters decreases around 20% (2.95 to 2.39 mmol/L) in the upper 172 m of sediment at

Table 9. Interstitial-water geochemical data for Site 738.

Core, section, interval (cm)	Depth (mbsf)	Volume (mL)	Salinity (g/kg)	Chloride (mmol/L)	Calcium (mmol/L)	Magnesium (mmol/L)	Mg^{2+}/Ca^{2+}	Silica (μmol/L)	pH	Alkalinity (mmol/L)	Sulfate (mmol/L)	Ammonium (mmol/L)	Phosphate (μmol/L)
119-738B-													
1H-2, 145–150	2.95	47	35.5	556	11.1	53.5	4.8	683	7.6	2.96	25.8	0.02	4
3H-5, 145–150	20.95	40	35.5	559	11.4	53.8	4.7	607	7.6	2.82	25.5	0.01	1
7H-4, 145–150	57.45	40	36.0	560	12.8	53.2	4.2	517	7.5	2.76	22.8	0.02	1
10H-2, 145–150	82.95	35	36.0	560	13.9	51.5	3.7	549	7.5	2.70	23.7	0.02	0
13H-2, 145–150	106.95	40	36.0	562	14.9	50.3	3.4	541	7.4	2.70	23.7	0.01	1
17X-3, 145–150	141.65	30	36.0	562	16.5	48.5	2.9	669	7.4	2.50	24.0	0.01	1
20X-4, 145–150	172.15	30	36.0	568	18.0	47.6	2.6	677	7.4	2.39	24.0	0.01	0
24X-2, 145–150	207.55	28	36.5	568	19.5	47.1	2.4	558	7.4	2.53	23.4	0.01	0
119-738C-													
4R-2, 145–150	218.85	25	36.5	567	20.1	46.7	2.3	592	7.3	2.71	23.7	0.01	1
7R-2, 140–150	247.70	25	36.5	565	21.8	45.2	2.1	547	7.4	2.30	23.4	0.01	0
10R-2, 140–150	276.70	20	36.0	568	23.8	43.2	1.8	498	7.3	2.05	22.8	0.02	0
16R-4, 140–150	337.50	20	36.5	572	28.0	41.0	1.5	532	7.4	2.08	22.8	0.02	0
22R-4, 140–150	395.50	15	36.5	568	30.7	38.5	1.2	465	7.3	1.80	23.7	0.02	0

Site 738, increases to a maximum between 172 and 248 mbsf, and then decreases to 1.80 mmol/L at 396 mbsf. The slight downhole decrease in sulfate concentrations indicates that anaerobic conditions exist below the sediment/water interface, but the small size of the depletion attests to the lack of reactable organic matter in these sediments (see "Organic Geochemistry" section). The variations seen in the alkalinity data indicate that carbonate dissolution and precipitation reactions are occurring throughout the sediment column. Precipitation of calcium carbonate is the most likely cause of the overall decrease in alkalinity with increasing depth. The loss of dissolved calcium by means of carbonate precipitation means that calcium does not behave in an entirely conservative manner within the Site 738 interstitial waters. However, the amount of calcium lost by this process is so small relative to the calcium supply that it does not greatly affect the dissolved calcium vs. depth profile, and calcium appears to behave conservatively.

Ammonium and Phosphate

Ammonium and phosphate are essentially absent in the interstitial waters at Site 738 (Fig. 21). Very low concentrations of phosphate were measured in the shallowest sample analyzed, indicating that some microbial degradation of organic matter is taking place near the sediment/water interface. The small amount of phosphate produced is probably lost to the ocean bottom waters. The lack of organic matter and microbial activity in the sediments at Site 738 indicates that most or all of the organic matter synthesized in the surface waters is recycled in the water column or at the seafloor, before it can be incorporated into the bottom sediments. This interpretation is supported by the low sedimentation rates at this site (see "Lithostratigraphy, Sedimentology, and Igneous Petrology" section).

ORGANIC GEOCHEMISTRY

Organic geochemistry was studied on squeeze-cake samples from the interstitial-water studies of Holes 738B and 738C, as outlined in the "Explanatory Notes" chapter.

Hydrocarbon Gases

The headspace procedure was used approximately every 30 m to determine hydrocarbon gases. One small gas pocket was encountered in Sample 119-738C-20R-2, 70–71 cm. Table 10 is a compilation of the headspace results and the vacutainer sample level. No hydrocarbon gases heavier than methane (C_1) were detected. Most of the samples had methane near or below the mean laboratory air level of 3 ppm.

Sample 119-738B-1H-2, 144–145 cm, had headspace biogenic methane at a level of 1409 ppm. This methane was probably of biogenic origin, as no higher hydrocarbon gases were detected. The interval containing Samples 119-738B-13H-3, 0–1 cm, 119-738B-17X-4, 0–1 cm, and 119-738B-20X-5, 0–1 cm, corresponds to increases in silica concentration (see "Inorganic Geochemistry" section, this chapter). This correspondence might be due to an increase in this interval of microbial activity, thereby increasing methanogenesis and pore-water silica concentration (Claypool and Kvenvolden, 1983).

Carbon Analysis

Inorganic carbon was measured on most core-catcher samples and all of the interstitial-water squeeze-cake samples. Total carbon was measured on all of the interstitial-water squeeze cakes. Total organic carbon (TOC) was calculated for squeeze cakes. See Table 11 and Figures 23 and 24 for tabular and graphic representations of the data. No Rock-Eval pyrolysis was done because the instrument would not detect S3 peaks.

The samples contain no organic matter above 0.1%, with the exception of Samples 119-738C-16R-4, 140–150 cm, and 119-738C-24R-CC, 0–1 cm, which contain 0.13% and 0.65%, respectively.

BIOLOGY AND OCEANOGRAPHY

Physical Characteristics of the Marine Ecosystem

The surface water temperature was 0.8° to 1.0°C at the drill site. Winds were moderately strong (from 13 to 28 kt) from 10 to 13 January, and then decreased to calm to light (0 to 8 kt) on 13 January, remaining moderate during the rest of the occupation of Site 738 (Table 12). Temperature, salinity, and density in the top 200 m of the water column are shown from the self-contained SEACAT CTD (conductivity, temperature, and depth) unit, run 10, 13, and 15 January by the science component on the service vessel, *Maersk Master* (Figs. 25A through 25C). The mixed layer deepened slightly in the first four days of occupation of Site 738 and was shallowing again on the last day. A Secchi disc was used to determine approximate depth of the euphotic zone (considered to be the depth reached by 1% of the incident light at the surface), and this zone deepened from 22 to 27 m between 10 and 14 January, indicating that the water in the mixed layer was somewhat clearer.

Phytoplankton

The phytoplankton was sampled in the water column at Site 738 several ways: (1) horizontal tows and vertical hauls of nets (35-μm mesh) deployed from *Maersk Master*, (2) water samples from Niskin bottles taken from *Maersk Master* for shorebased abundance estimates of species present and chlorophyll *a* for
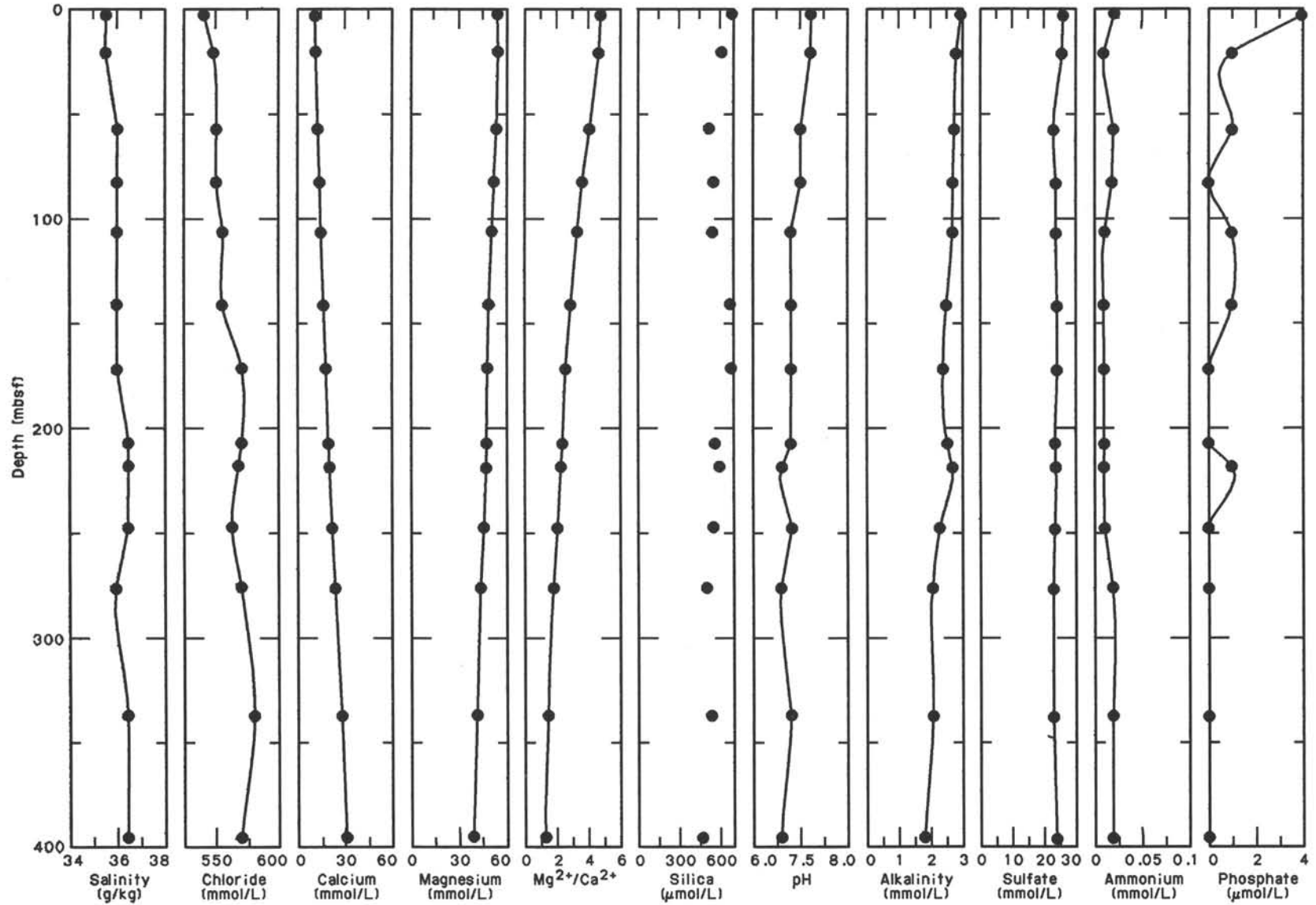
Figure 21. Salinity, chloride, calcium, magnesium, Mg^{2+}/Ca^{2+} ratio, silica, pH, alkalinity, sulfate, ammonium, and phosphate interstitial-water profiles, Site 738.

Figure 22. Calcium concentration vs. magnesium concentration for Site 738 interstitial waters. The regression line passes through data points representing interstitial-water samples in the upper 396 m of sediment and has a slope of −1.27 (r = −0.9947).

Table 10. Hydrocarbon gas analysis, Site 738.

Core, sample, interval (cm)	Depth (mbsf)	C_1 (μL/L)	C_2^a (μL/L)	C_3^a (μL/L)
119-738B-				
1H-2, 144–145	2.94	1409	B.D.	B.D.
3H-5, 119–120	20.69	1	B.D.	B.D.
7H-4, 119–120	57.19	1	B.D.	B.D.
10H-2, 144–145	82.94	2	B.D.	B.D.
13H-3, 0–1	107.00	35	B.D.	B.D.
17X-4, 0–1	141.70	20	B.D.	B.D.
20X-5, 0–1	172.20	20	B.D.	B.D.
24X-2, 119–120	207.29	5	B.D.	B.D.
119-738C-				
4R-3, 0–1	218.90	4	B.D.	B.D.
7R-2, 114–115	247.44	4	B.D.	B.D.
10R-2, 114–115	276.44	4	B.D.	B.D.
16R-4, 114–115	337.24	4	B.D.	B.D.
22R-4, 114–115	395.24	4	B.D.	B.D.
20R-2, 70–71	372.40	^{b}6	B.D.	B.D.

^{a} B.D. = below detection limit.
^{b} Vacutainer sample analyzed on Hewlett Packard.

Table 11. Total carbon, inorganic carbon, organic carbon, and carbonate carbon, Site 738.

Core, section, interval (cm)	Depth (mbsf)	Total carbon (%)	Inorganic carbon (%)	Organic carbon (%)	CaCO$_3$ (%)
119-738B-					
1H-1, 50–51	0.50		7.07		58.9
1H-1, 120–121	1.20		7.14		59.5
1H-1, 145–150	1.45	9.19	9.39	0.00	78.2
1H-2, 50–51	2.00		7.73		64.4
1H-2, 120–121	2.70		9.13		76.1
1H-3, 50–51	3.50		8.76		73.0
1H-CC, 0–1	3.92		8.58		71.5
2H-1, 80–81	4.80		5.41		45.1
2H-2, 80–81	6.30		6.83		56.9
2H-3, 80–81	7.80		5.57		46.4
2H-4, 80–81	9.30		4.66		38.8
2H-5, 80–81	10.80		2.73		22.7
2H-6, 80–81	12.30		0.05		0.4
2H-7, 80–81	13.20		0.02		0.2
2H-CC, 0–1	13.66	0.13	0.05	0.08	0.4
3H-5, 145–150	20.95	11.00	11.14	0.00	92.8
3H-CC, 0–1	22.26		10.94		91.1
4H-CC, 0–1	32.64		11.15		92.9
5H-CC, 0–1	42.19		11.26		93.8
6H-CC, 0–1	50.77		11.57		96.4
7H-4, 145–150	57.45	11.29	11.45	0.00	95.4
7H-CC, 0–1	61.18		11.47		95.6
8H-CC, 0–1	70.59		11.41		95.1
9H-CC, 0–1	77.33		11.35		94.6
10H-2, 145–150	82.95	11.37	11.54	0.00	96.1
10H-CC, 0–1	84.44		11.52		96.0
11H-CC, 0–1	94.25		11.33		94.4
12H-CC, 0–1	103.82		11.28		94.0
13H-2, 145–150	106.95	11.25	11.40	0.00	95.0
13H-CC, 0–1	108.07		11.02		91.8
14X-CC, 0–1	113.22		8.28		69.0
15X-CC, 0–1	126.45		11.42		95.1
16X-CC, 0–1	129.55		11.44		95.3
17X-3, 145–150	141.65	11.42	11.61	0.00	96.7
17X-CC, 0–1	143.62		11.39		94.9
18X-CC, 0–1	153.51		11.52		96.0
19X-CC, 0–1	165.22		11.47		95.6
20X-4, 145–150	172.15	11.52	11.67	0.00	97.2
20X-CC, 0–1	174.89		11.48		95.6
21X-CC, 0–1	179.88		11.45		95.4
22X-CC, 0–1	191.18		11.23		93.6
23X-CC, 0–1	196.50		11.33		94.4
24X-2, 145–150	207.55	11.29	11.31	0.00	94.2
24X-CC, 0–1	208.47		11.26		93.8
119-738C-					
2R-CC, 0–1	198.42		11.18		93.1
3R-CC, 0–1	206.90		11.43		95.2
4R-2, 145–150	218.85		11.35		94.6
4R-CC, 0–1	219.98		11.41		95.1
5R-CC, 0–1	227.88		11.41		95.1
6R-CC, 0–1	236.35		11.29		94.1
7R-2, 140–150	247.70	10.00	9.99	0.01	83.2
7R-CC, 0–1	248.29		11.17		93.1
8R-CC, 0–1	255.73		11.25		93.7
9R-CC, 0–1	264.97		10.71		89.2
10R-1, 29–30	274.09		11.26		93.8
10R-2, 140–150	276.70	10.99	10.92	0.07	91.0
10R-3, 67–68	277.47		11.05		92.1
10R-CC, 0–1	278.72		10.99		91.6
11R-1, 56–58	283.96		10.66		88.8
11R-2, 56–58	285.46	8.37	8.35	0.02	69.6
11R-CC, 0–1	286.65		10.74		89.5
13R-CC, 0–1	302.70		10.99		91.6
14R-CC, 0–1	312.30		11.06		92.1
15R-CC, 0–1	321.90		10.46		87.1
16R-4, 140–150	337.50	10.65	10.52	0.13	87.6
16R-CC, 0–1	340.78		11.33		94.4
17R-CC, 0–1	351.03		11.41		95.1
18R-CC, 0–1	360.47		11.35		94.6
19R-CC, 0–1	365.00		11.32		94.3
20R-CC, 0–1	377.37		11.18		93.1
21R-CC, 0–1	380.59		11.24		93.6

Table 11 (continued).

| Core, section, interval (cm)	Depth (mbsf)	Total carbon (%)	Inorganic carbon (%)	Organic carbon (%)	CaCO$_3$ (%)
119-738C-(Cont.)					
22R-4, 140–150	395.50		11.25		93.7
22R-CC, 0–1	397.49		11.28		94.0
23R-CC, 0–1	403.70		11.15		92.9
24R-CC, 0–1	413.25	8.46	7.81	0.65	65.1
25R-2, 140–150	421.50	10.59	10.65	0.00	88.7
25R-CC, 0–1	423.86		10.35		86.2
26R-CC, 0–1	432.28		9.57		79.7
27R-3, 140–150	442.30		11.10		92.5
27R-CC, 0–1	445.12		10.50		87.5
28R-CC, 0–1	453.41		10.66		88.8
29R-1, 15–16	457.35		10.93		91.1
29R-2, 68–69	459.38		10.96		91.3
29R-CC, 0–1	461.02		9.91		82.6
30R-1, 45–46	467.05		10.67		88.9
30R-1, 119–120	467.79	8.06	8.00	0.06	66.6
30R-CC, 0–1	470.12		4.60		38.3
31R-2, 111–113	478.91	9.83	9.79	0.04	81.6
31R-2, 119–121	478.99	9.21	9.21	0.00	76.7
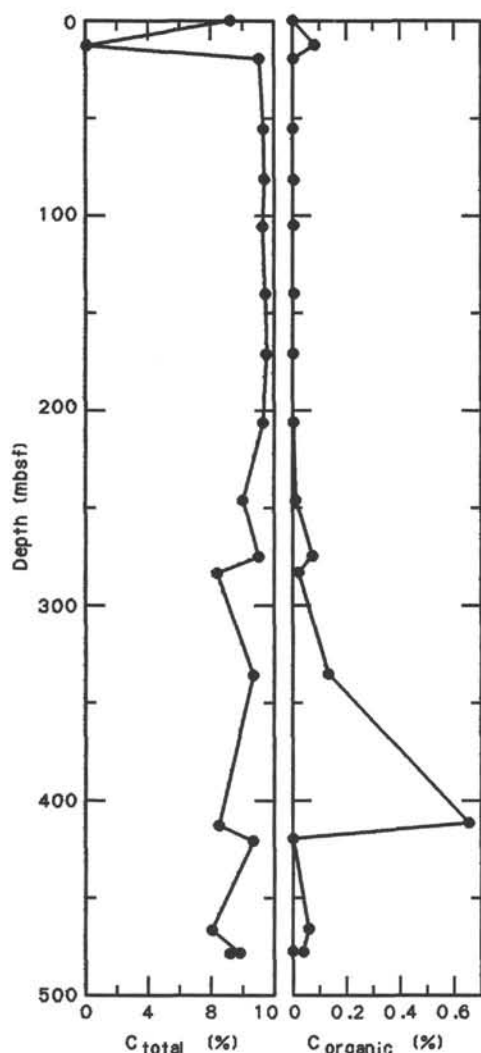
Figure 23. Total carbon (C$_{total}$) and organic carbon (C$_{organic}$) from squeeze-cake and core-catcher sediment samples, Site 738.

biomass estimations, (3) hand-held net (20 μm) off the stern of the drillship in the effluent from the thrusters or towed slowly in surface water from a zodiac boat, and (4) opportunistic collection of colonies of the tunicate *Salpa thompsonii* from surface water adjacent to an iceberg.

The phytoplankton was an Antarctic summer assemblage, dominated by the diatom genera *Rhizosolenia*, *Chaetoceros*, and *Nitzschia* (Table 13). Although many species of the diatom genus *Thalassiosira* were present, they were not abundant. Also present was the cold-water silicoflagellate *Distephanus speculum* and the biflagellate and rosette stage of the prymnesiophyte *Phaeocystis* (Fryxell, in press). Colonies of the bacteriovore choanoflagellate *Parvicorbicula socialis* were present in horizontal net tows and vertical hauls.

Many bleached, empty cells appeared in surface collections, but a healthy population was sampled in the colder water from 50 to 100 m (Fig. 25), with *Corethron inerme* of maximum diameter and prolific production of the flagellate *Solenicola setigera* on the outside of the thecae of *Leptocylindrus mediterraneus*. The only cell of *Coscinodiscus* was found in the 50–100-m net haul. Few fecal pellets were noted above 80 m, along with a continued content of empty cells. Differences were apparent in fecal pellets from the deeper layer with more enclosed cells showing color. Species found only below 80 m include: *Rhizosolenia crassa*, *Stellarima microtrias* (resting spore), *Thalassiosira frenguelliopsis*, *Thalassiosira ritscheri*, and *Tropidoneis antarcticus*.

The most striking aspect of the phytoplankton in the water column was the bundles or rafts of long, slender *Rhizosolenia hebetata* f. *semispina*, with some occurrences as tangled mats in our collections. Many species of *Chaetoceros* were in each collection, including a small, abundant single-celled form that floated on the top of the collection bottles. Also present in all of the collections were species of *Nitzschia*, with many elongate colonies of the needle-shaped cells with overlapping tips. Included in the assemblage were some of the more heavily-silicified *Nitzschia* species forming ribbon-shaped colonies by connection of valve faces.

Of particular interest in this latter group were species present in the collection from the gut contents of salps. The nonselective feeding mode of salps resulted in a diverse diatom assemblage, representing the waters through which the salps had migrated. Dominating in the ingested assemblage were the nannoplanktonic *Nitzschia pseudonana* and the ice-related *Nitzschia cylindrus* and *Nitzschia curta*.

In contrast to the northern form of *Eucampia antarctica* reported from Sites 736 and 737 (cf. Priddle and Fryxell, 1985), specimens were found in single or doublet cells, dorsal/ventrally flexed, with proximal valve surfaces curved under the elevations. Present in the cold-water intrusion were straight-sided winter form doublets or cells germinating from these doublets but retaining the heavily silicified epithecae. The northern form of *E. antarctica*, together with species not found at the southern Site 738, is listed in Table 14. However, the northern form of *Thalassiosira tumida* was still present (as opposed to the southern form found abundantly at the ice edge).

Preliminary assessment of the chlorophyll indicated a fairly low biomass, with the maximum moving from the top 25 to 80 m during the time at the site. Evidently, phytoplankton from the spring increase had sunk into the cold-water intrusion or below, with the abundance of the colonial choanoflagellates indicating recycling of nutrients in a declining, possibly photoinhibited, previously well-grazed, early summer population.

Nitzschia is considered to be a genus that survives even in marginal conditions in these polar waters, whereas *Thalassiosira* is more opportunistic, taking advantage of early spring conditions and water column overturns (Fryxell and Kendrick, 1988).
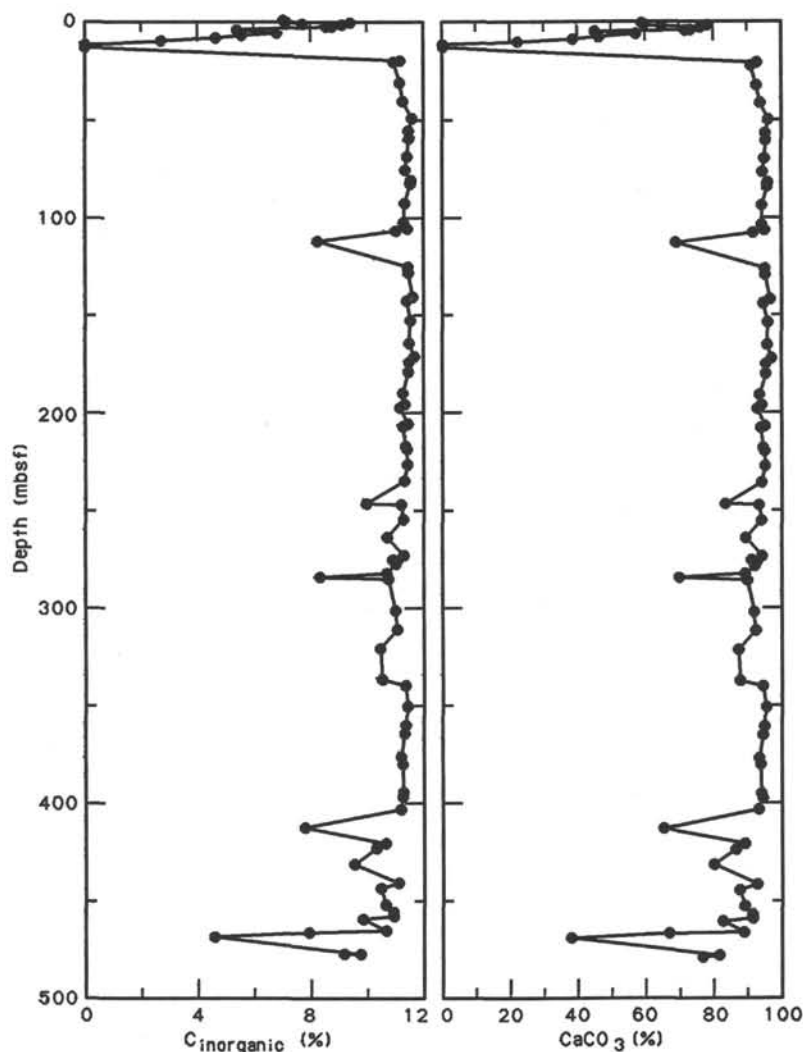
Figure 24. Inorganic carbon and percent calcium carbonate from squeeze-cake and core-catcher sediment samples, Site 738.

No early spring gelatinous colonies or long chains of *Thalassiosira* were noted, although single cells appeared healthy in the cold-water intrusion. Austral summer conditions are indicated in spite of the late thaw of sea ice in this growing season.

Diatoms in Quaternary Sediments

Even analysis of the mud-line Sample 119-738A-1H-1 indicated the presence of a mixed assemblage, although *Nitzschia kerguelensis* and *Thalassiosira lentiginosa* were found. The joint occurrence of *Coscinodiscus elliptopora* and *Actinocyclus ingens* in Sample 119-738A-1H-CC indicates that the *Coscinodiscus elliptopora/Actinocyclus ingens* Zone (0.62 to 1.58 Ma) of the Quaternary could be represented (Gombos, 1977), if the sediments were not mixed.

PHYSICAL PROPERTIES

The objectives of the physical-properties program at Site 738 were to provide continuous depths profiles of (1) index properties (water content and porosity, along with bulk and grain densities), (2) undrained shear strength, and (3) compressional-wave velocity throughout the entire section. Because heatflow measurements were not conducted at Site 738, the physical-proper-

ties program did not include measurements of thermal conductivity. Velocity and bulk-density measurements were continued into basement lithologies, the latter property by means of 2-min GRAPE counts on discrete samples. Techniques and laboratory procedures used are discussed in the "Explanatory Notes" chapter.

Hole 738A consisted of only one core. This same interval was recovered in Hole 738B and is, therefore, not included in the Site 738 physical-properties data. Hole depths and drilling methods are specified in the "Operations" section, this chapter. Visual inspection of split-core sections found some coring disturbance, particularly in XCB cores from Hole 738B and the upper cores of Hole 738C. Obviously disturbed intervals were avoided during physical-properties sampling. Sample disturbance became less significant with increasing lithification in Hole 738C. The physical-properties data for Site 738 are presented in Tables 15 through 19 and Figure 26.

Results

Based on the measured physical properties, the section drilled at Site 738 can be divided into six geotechnically distinguishable units, G1 to G6. All divisions between units may not be obvious

Table 12. Weather summary for *JOIDES Resolution* at Site 738 (67.4°S, 82.5°E).

Time (hr)/date (Jan. 1988)	Winds (kt)	Sea surface temperature (°C)	Waves (m)	Sky
00–15/10	N 13–18	0.6–1.1	3–4	Overcast with light rain/snow showers in the area. Pressure begins to fall at 06 hr.
16/10 to 09/11	NE 22–28, slowly backing to the north	0.8–1.0	4–5	Low overcast with light rain mixed with snow. Pressure still falling.
10/11 to 21/11	NW 22–28	0.8	4	Overcast with fog and drizzle. Pressure rising.
22/11 to 09/13	N 18–22, decreasing to 10–15 by 13 hr	0.8–1.1	3–4	Overcast with occasional to light fog. Pressure low but steady, falling slightly near the end of the period.
10–21/13	N to NW 4–8	0.9–1.1	2–3	Overcast with occasional snowshowers, some very heavy. Pressure low and steady.
22/13 to 09/14	<5, calm to light and variable	1.0	2–3	Overcast with occasional snowshowers. Pressure steady.
10/14 to 15/15	Light and SE to 4–8, increasing to 12–15 by 06 hr, 15 January	0.9–1.0	3–4	Mostly cloudy to overcast with periods of light snow (occasionally very heavy). Pressure rising slightly.
16/15 to 21/16	S to SW 12–18	0.6–1.0	2–3	Overcast with occasional light snow. Pressure rising.
22/16 to 02/17	SE 5–10 and decreasing to near calm	1.2	2–3	Overcast with occasional light snow. Pressure rising.

Note: Numerous icebergs were observed during the measurement period. A maximum of 83 icebergs, with bergy bits and growlers, was observed at 02 hr, 16 January.

by each individual parameter, but with all of the properties taken together the units are well defined. The geotechnically defined units correspond roughly with the lithologic units (see "Lithostratigraphy, Sedimentology, and Igneous Petrology" section).

Unit G1, 0 to 20 mbsf, corresponds to lithologic Unit I, a diatom ooze with dispersed clasts (presumably ice-rafted detritus) of metamorphic and igneous rocks, and lithologic Unit II, a nannofossil ooze with decreasing diatom content.

Unit G2, 20 to 135 mbsf, corresponds to lithologic Unit III, a white, silty nannofossil ooze that may be chalky in parts.

Unit G3, 135 to 210 mbsf, corresponds to lithologic Unit IV, a white nannofossil ooze and chalk with some chert.

Unit G4, 210 to 410 mbsf, corresponds to lithologic Units IV and V. Unit V is a nannofossil ooze with chert nodules, and Unit V is a clayey, bioturbated chalk with chert nodules.

Unit G5, 410 to 485 mbsf, corresponds to lithologic Unit VI, a clayey limestone that is silicified in parts and contains chert nodules.

Unit G6, 485 to 533 (total depth) mbsf, corresponds to the volcanic rock units, which consist mostly of breccias, with varying degrees of alteration.

Index Properties

The index-property profiles distinguish the six geotechnical units by exhibiting relatively clear changes in the range of values and trends with depth (Table 15 and Fig. 26). Geotechnical unit G1 is characterized by a considerable scatter for all the index properties and no apparent change with depth. Grain and wet-bulk densities average 2.65 and 1.45 g/cm^3, respectively. Average water content, and porosity are correspondingly relatively high, around 55% and 75%, respectively.

The index properties show a well-defined break at the upper contact of geotechnical unit G2. Values of bulk density, water content, and porosity show little scatter and have normal depth-related trends (i.e., increasing bulk density and decreasing porosity and water content) within the unit. The latter two index properties vary from 65% to 60% and from 40% to 35%, respectively. Bulk density ranges from 1.7 to 1.9 g/cm^3. Grain density also shifts abruptly at the upper contact, from about 2.65 to 2.9 g/cm^3, and remains relatively constant with depth, which is typical of nonsiliceous, pelagic sediments.

Geotechnical unit G3 is defined by the depth profiles of wet- and dry-bulk densities, porosity, and water content, which show slight, but distinct, changes in gradient. The density values also have a small, abrupt drop at the top of the unit. Values range from 1.8 to 1.9 g/cm^3 (wet-bulk density), 35% to 30% (water content), and 65% to 55% (porosity). Grain densities show an abrupt decrease to about 2.8 g/cm^3 and no trend with depth.

The upper contact of geotechnical unit G4 is gradational and is also indicated by a slight change in the gradient of index-property depth profiles. The continuity and overall character of this trend is somewhat uncertain because of the absence of data for the interval from 290 to 340 mbsf, as a result of poor core recovery. Water content ranges from 30% to 20%, porosity from 55% to 40%, and wet-bulk density from 2.0 to 2.2 g/cm^3. Values of all index properties for geotechnical unit G4 show normal depth related trends and somewhat more scatter relative to unit G3.

Geotechnical unit G5 is defined by an abrupt upper contact with a sharp increase in wet-bulk density to around 2.5 g/cm^3 and a decrease in water content and porosity to about 10% and 20%, respectively.

Index properties measured on the volcanic rocks of geotechnical unit G6 show an abrupt shift. The average bulk density on both index-properties and GRAPE profiles shows an increase to around 2.65 g/cm^3, with corresponding decreases in water content and porosity. Grain density increases to 3.00 g/cm^3.
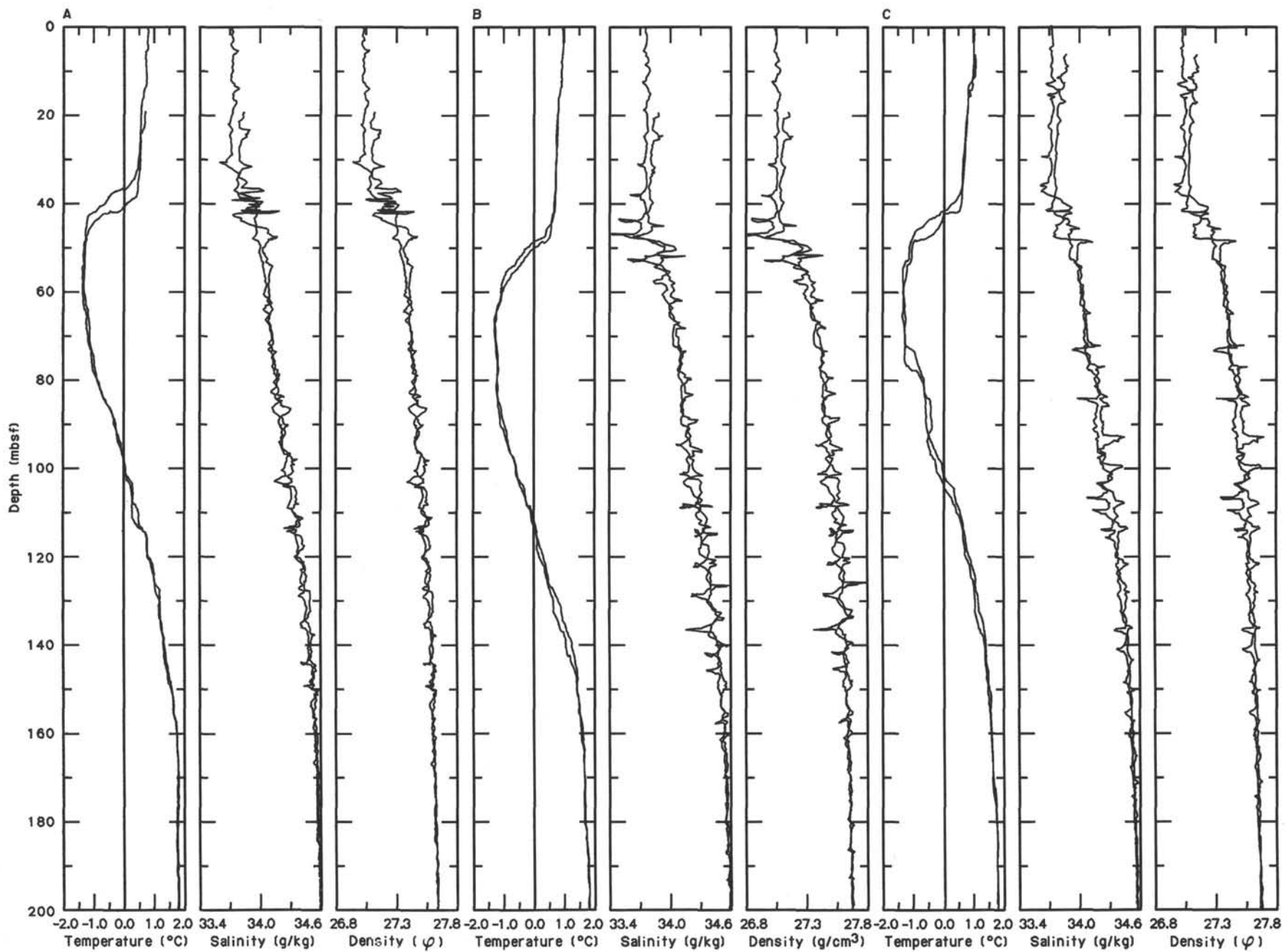
Figure 25. Conductivity, temperature, and depth profiles in the top 200 m of water in the vicinity of Site 738. The double traces show the record going down and back up to the surface (the surface signal showed noise upon entry into the water, and the top 10–20 m of the downgoing traces was removed). The temperature minimum is between 50 and 100 m. **A.** CTD-1: 10 January 1988, operation 175, 1525–1536 hr (local time); 62°43.5′S, 82°51′E. **B.** CTD-2: 14 January 1988, operation 187, 1246–1256 hr (local time); 62°44′S, 82°49.5′E. **C.** CTD-3: 15 January 1988, operation 196, 2049–2144 hr (local time); 62°43.5′S, 82°45.5′E.

Table 13. Diatom species in the water column, Site 738.

^a*Actinocyclus actinochilus*
Asteromphalus hookeri
Asteromphalus hyalinus
Asteromphalus parvulus
Chaetoceros atlanticus
Chaetoceros bulbosus
Chaetoceros castracanei
Chaetoceros convolutus
^b*Chaetoceros criophilus*
Chaetoceros curvisetus
^b*Chaetoceros dichaeta* (Section *Phaeoceros*)
^b*Chaetoceros* sp. cf. *dichaeta* (Section *Hyalochaete*)
^b*Chaetoceros flexuosus*
^c*Chaetoceros neglectus*
Chaetoceros pendulus
Chaetoceros peruvianus
^{b,c}*Chaetoceros* sp. cf. *wighamii*
Corethron inerme
Corethron criophilum?
^a*Coscinodiscus oculoides*
^a*Dactyliosolen antarcticus*
^b*Dactyliosolen tenuijunctus*
^c*Eucampia antarctica* (variety flexed dorsal/ventrally)
Haslea sp.
^b*Leptocylindrus mediterraneous* with ^b*Solenicola setigera*
Navicula directa
^{a,b}*Nitzschia angulata*
Nitzschia closterium
^{a,b}*Nitzschia curta*
^b*Nitzschia cylindrus*
Nitzschia heimii
^a*Nitzschia kerguelensis*
Nitzschia lecointei (may be mixing with *Nitzschia subcurvata*)
Nitzschia lineola? (*Pseudonitzschia* chains)
^{a,b}*Nitzschia obliquecostata*
^a*Nitzschia ritscherii*
Nitzschia turgiduloides? (*Pseudonitzschia* chains)
^c*Odontella weissflogii*
^b*Pleurosigma* sp.
^c*Porosira pseudodenticulata*
Rhizosolenia alata
Rhizosolenia chunii
Rhizosolenia crassa
Rhizosolenia cylindrus
^a*Rhizosolenia hebetata* f. *semispina*
Rhizosolenia simplex
^b*Stellarima microtrias*
^a*Synedra reinboldii*?
Thalassiosira frenguelliopsis
Thalassiosira gracilis
^b*Thalassiosira gracilis* var. *expecta*
^a*Thalassiosira lentiginosa*
^b*Thalassiosira maculata*
^a*Thalassiosira oliveranus*
^b*Thalassiosira perpusilla*
^b*Thalassiosira ritscheri*
^a*Thalassiosira trifulta*
^a*Thalassiosira tumida* (northern variety)
^b*Tropidoneis antarctica*
Tropidoneis belgicae
Tropidoneis galcialis

[a] Valves or bands expected to be in the sediment.
[b] Not seen farther north at Sites 736 and 737.
[c] Resting spores could be preserved in the sediment.

The parameter dry-bulk density is included in the index properties (Fig. 26 and Table 15) because it may provide data for calculating accumulation rates. As water content decreases, the dry- and wet-bulk densities converge. However, as grain density shows a slight overall decrease with depth, the two parameters converge more gradually than expected from the changes in water content alone.

Despite the scatter in the bulk-density values obtained by GRAPE measurement (Fig. 26 and Table 16), geotechnical units G1, G2, and G3 are readily identified based on the same criteria as in the gravimetrically measured bulk densities. Unit G4 data

Table 14. Diatom species found only at the northern sites, Leg 119.

Actinocyclus ehrenbergii
Azpeitia tabularis
Chaetoceros constrictus
Coscinodiscus curvatulus
Eucampia antarctica (northern variety; flexed in broad girdle view)
Nitzschia separanda
Pleurosigma sp.
Rhizosolenia curvata
Thalassionema nitzschioides
Thalassiosira gravida
Thalassiosira scotia

suffer from poor core recovery around 300 mbsf. Furthermore, between 330 and 380 mbsf, whole-round cores were measured by continuous GRAPE runs, as opposed to 2-min counts on discrete samples for the rest of the lithified section. The values from this interval tend to be too low and fall below the trend, probably because of the reduced sample diameter relative to the core liner. Units G5 and G6 are evident from increasing values and larger scatter.

Undrained Shear Strength

Measurements of undrained shear strength were obtained down to 200 mbsf with the vane shear device and to 225 mbsf with fall cone penetrometer (Tables 17 and 18 and Fig. 26). Sediments below these depths were too lithified to use these instruments.

The character and trends with depth of undrained shear strength are well correlated for the two methods. Fall cone data are slightly more scattered, have higher values, and show a slightly steeper depth gradient. This character was also observed at Sites 736 and 737.

The shear-strength profiles support division of the section into distinct geotechnical units. The division between geotechnical units G1 and G2 is not distinct in the vane shear data, but occurs in the fall cone data as an increase from values from about 5 to 15–20 kPa in unit G2. Unit G2 also shows a larger scatter in values than in unit G1. Unit G2 values have an expected downhole increase with depth. The transition into geotechnical unit G3 is seen as an increase in both the gradient and the scatter of the shear-strength values. A few fall cone measurements were obtained in unit G4 material, but because of the increasing lithification in this unit, values from these measurements are dubious. However, the trend serves to illustrate the large increase in strength of the material.

The higher shear-strength values of the fall cone measurements in comparison to the vane shear data were noted by Keller and Bennett (1971). A possible explanation is that the almost instantaneous penetration of the cone—as opposed to the relatively slow rotation of the vane—generates high pore-water pressures in the immediate vicinity of the cone. High insertion pore pressures have been recorded for *in-situ* penetrometers in sediments from the Gulf of Mexico. The high pore pressures may momentarily tend to counter the weight of the cone, thereby reducing penetration and resulting in an apparently higher undrained shear strength.

Compressional-Wave Velocity

Sonic velocities—with the exception of the contact between geotechnical units G1 and G2—show a strong correlation with unit boundaries established from index-property and shear-strength profiles (Table 19 and Fig. 26). Velocity is fairly constant with depth at 1500 m/s within units G1 and G2. A slight
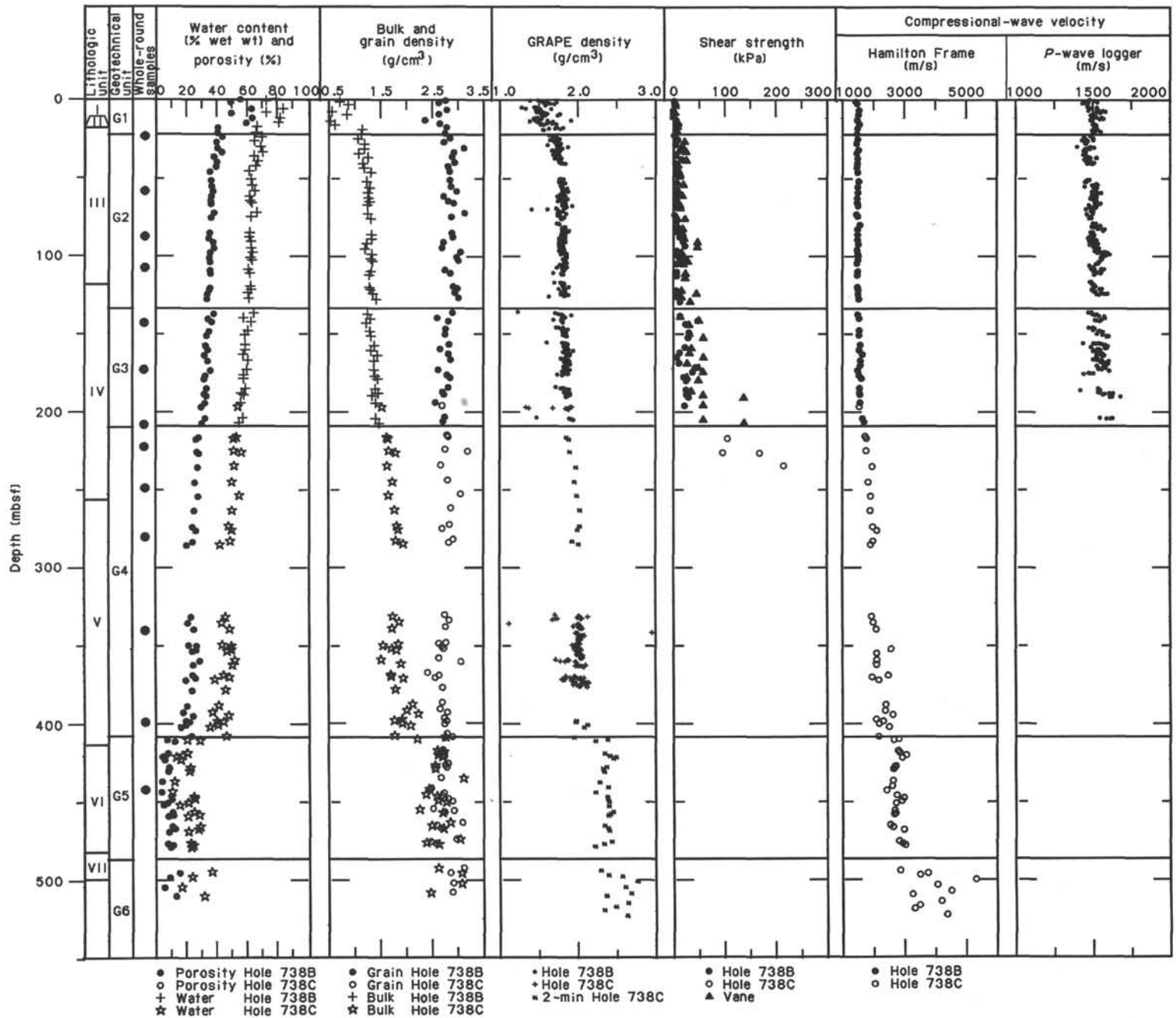
Figure 26. Physical-property profiles, Site 738. GRAPE data are filtered for values < 1.0 and > 3.0 g/cm³ and blocked in 0.2-m averages.

Table 15. Water content, porosity, bulk density, dry-bulk density, and grain density, Holes 738B and 738C.

Table 15 (continued).

Core, section, interval (cm)	Depth (mbsf)	Water content (%)	Porosity (%)	Bulk density (g/cm^3)	Dry-bulk density (g/cm^3)	Grain density (g/cm^3)
119-738B-						
1H-1, 90	0.90	54.67	76.81	1.45	0.66	2.77
1H-3, 81	2.31	48.13	70.73	1.55	0.81	2.63
2H-3, 140	6.90	61.38	81.54	1.38	0.53	2.79
2H-4, 83	9.33	48.54	71.07	1.54	0.79	2.63
2H-7, 10	13.10	62.11	79.49	1.38	0.52	2.37
3H-2, 75	16.75	58.36	78.69	1.42	0.59	2.65
3H-4, 70	18.70	40.28	64.94	1.72	1.03	2.78
3H-CC, 5	22.31	40.13	64.52	1.70	1.02	2.75
4H-2, 75	25.25	43.04	68.02	1.71	0.97	2.85
4H-4, 72	28.22	39.33	63.64	1.77	1.08	2.73
4H-7, 20	38.20	39.93	67.08	1.79	1.08	3.11
5H-2, 88	34.88	42.73	68.26	1.72	0.98	2.92
5H-4, 68	37.68	37.79	63.41	1.83	1.14	2.89
5H-6, 97	40.97	39.71	65.54	1.75	1.06	2.93
6H-2, 29	43.82	39.20	64.11	1.75	1.07	2.81
6H-4, 89	46.94	35.17	60.33	1.82	1.18	2.84
7H-1, 132	52.82	36.35	61.64	1.76	1.12	2.85
7H-4, 81	56.81	36.71	62.19	1.81	1.15	2.87
7H-6, 108	60.08	37.26	63.55	1.82	1.14	2.97
8H-2, 96	63.46	36.42	60.57	1.80	1.15	2.72
8H-4, 84	66.34	36.16	61.23	1.81	1.16	2.82
8H-5, 93	67.93	36.00	61.87	1.77	1.13	2.92
9H-3, 72	74.22	37.77	65.19	1.83	1.14	3.13
9H-5, 47	76.97	36.38	61.84	1.85	1.18	2.87
11H-2, 77	87.27	35.54	61.04	1.84	1.19	2.88
11H-4, 92	90.42	35.04	60.67	1.83	1.19	2.90
11H-6, 97	93.47	37.43	61.63	1.79	1.12	2.72
12H-2, 97	96.97	37.92	61.92	1.75	1.09	2.70
12H-4, 95	98.95	35.93	62.82	1.85	1.19	3.05
12H-6, 100	103.00	35.49	61.73	1.83	1.18	2.97
13H-1, 90	104.90	35.68	62.17	1.88	1.21	3.00
14X-2, 117	110.87	35.70	60.19	1.85	1.19	2.76
14X-4, 27	112.97	35.98	61.31	1.81	1.16	2.86
15X-3, 91	121.71	35.92	61.70	1.82	1.16	2.91
15X-4, 82	123.12	35.47	61.95	1.84	1.18	3.00
15X-6, 45	126.75	34.21	60.17	1.85	1.22	2.95
16X-3, 28	129.34	34.05	60.52	1.91	1.26	3.01
17X-1, 126	138.46	38.01	63.71	1.82	1.13	2.90
17X-3, 110	141.30	34.39	57.32	1.79	1.18	2.60
17X-CC, 10	143.72	36.99	62.04	1.77	1.12	2.82
18X-2, 94	149.24	35.18	59.68	1.81	1.17	2.76
18X-4, 76	152.06	33.75	58.15	1.80	1.19	2.76
19X-2, 73	158.73	33.02	57.95	1.84	1.23	2.83
19X-4, 78	161.78	34.37	57.86	1.81	1.19	2.66
19X-6, 72	164.72	32.26	56.98	1.89	1.28	2.82
20X-2, 80	168.50	34.44	59.71	1.87	1.23	2.86
20X-6, 75	174.45	36.22	59.48	1.94	1.24	2.62
21X-2, 65	177.89	32.83	57.47	1.85	1.25	2.80
21X-4, 36	179.76	32.35	57.41	1.90	1.29	2.86
22X-1, 77	186.17	33.70	58.59	1.91	1.26	2.82
22X-3, 80	189.20	32.45	56.20	1.93	1.30	2.71
22X-4, 72	190.62	33.45	57.60	1.82	1.21	2.74
23X-1, 74	195.74	32.82	55.31	1.87	1.26	2.57
24X-1, 72	206.32	32.87	57.05	1.90	1.27	2.75
24X-3, 26	207.86	30.75	54.40	1.89	1.31	2.72
119-738C-						
4R-1, 121	217.11	28.68	52.57	2.00	1.43	2.80
4R-2, 92	218.32	27.13	50.81	2.00	1.45	2.82
5R-1, 83	226.43	27.63	50.94	2.02	1.46	2.76
5R-2, 50	227.60	28.76	55.92	2.22	1.58	3.19
6R-1, 104	236.24	28.20	50.95	2.01	1.44	2.68
7R-1, 112	245.92	26.48	49.94	2.07	1.52	2.81
8R-1, 80	255.20	28.68	54.70	2.05	1.46	3.05
9R-1, 52	264.62	25.96	49.80	2.11	1.56	2.87
10R-1, 87	274.67	24.77	47.94	2.12	1.59	2.84
10R-3, 29	277.09	27.01	49.59	2.22	1.62	2.70
11R-1, 94	284.34	24.84	48.64	2.10	1.58	2.91
11R-3, 6	286.46	20.84	42.28	2.15	1.70	2.83
16R-2, 73	333.83	23.95	46.02	2.02	1.53	2.75
16R-5, 7	337.67	21.72	43.59	2.09	1.63	2.83
17R-1, 50	341.80	25.61	48.38	2.04	1.52	2.76
17R-CC, 19	351.22	22.26	43.85	2.09	1.62	2.77
18R-1, 108	351.98	27.20	49.30	1.88	1.37	2.63

Core, section, interval (cm)	Depth (mbsf)	Water content (%)	Porosity (%)	Bulk density (g/cm^3)	Dry-bulk density (g/cm^3)	Grain density (g/cm^3)
119-738C-(Cont.)						
18R-3, 7	353.97	27.20	49.80	2.08	1.51	2.69
18R-5, 190	355.10	24.90	47.00	2.11	1.59	2.72
19R-1, 74	361.24	29.40	51.90	1.89	1.34	2.63
19R-3, 60	364.10	25.30	50.40	2.22	1.66	3.05
20R-1, 43	370.63	25.20	44.60	2.01	1.50	2.42
20R-2, 45	372.15	26.50	48.30	2.05	1.50	2.63
20R-3, 57	373.77	20.40	39.30	2.14	1.70	2.56
21R-1, 20	380.10	24.20	46.00	2.07	1.57	2.70
22R-1, 20	389.80	21.30	41.90	2.37	1.86	2.70
22R-3, 125	383.85	18.90	37.80	2.17	1.76	2.65
22R-5, 70	396.30	25.00	47.90	2.58	1.94	2.79
23R-1, 30	399.50	20.51	41.05	2.11	1.68	2.74
23R-1, 110	400.30	22.96	44.59	2.03	1.56	2.74
23R-2, 129	401.99	20.47	41.22	2.11	1.68	2.77
23R-3, 144	403.64	17.41	36.35	2.20	1.82	2.75
24R-1, 74	409.64	23.88	46.35	2.03	1.55	2.79
24R-2, 112	411.52	8.67	21.23	2.62	2.39	2.89
24R-3, 42	412.32	13.44	29.53	2.22	1.92	2.74
25R-1, 120	419.80	9.29	21.43	2.48	2.25	2.71
25R-2, 121	421.31	7.88	18.69	2.56	2.36	2.73
25R-3, 49	422.09	6.27	14.90	2.41	2.26	2.66
25R-4, 63	423.73	7.30	17.52	2.52	2.34	2.74
26R-1, 87	423.07	9.98	23.46	2.46	2.21	2.81
26R-2, 22	429.92	10.17	23.51	2.47	2.22	2.76
26R-3, 28	431.48	9.70	22.73	2.46	2.22	2.78
27R-1, 94	438.36	5.50	13.30	2.84	2.68	2.67
27R-5, 75	444.65	5.20	11.90	2.32	2.11	2.49
28R-1, 20	447.80	11.30	25.40	2.33	2.07	2.72
28R-2, 25	449.35	11.90	26.30	2.54	2.24	2.70
28R-3, 100	451.60	9.20	21.80	2.49	2.26	2.81
28R-4, 97	453.07	6.50	16.50	2.56	2.40	2.89
29R-1, 46	457.66	12.20	25.60	2.23	1.96	2.51
29R-2, 60	459.30	12.60	29.20	3.46	3.03	2.92
29R-3, 5	460.25	9.30	21.60	2.53	2.34	2.74
30R-1, 20	466.80	12.20	29.70	2.80	2.46	3.08
30R-2, 15	468.25	13.50	28.40	2.49	2.15	2.58
30R-3, 40	470.00	9.50	21.60	2.58	2.34	2.66
31R-1, 104	477.34	9.60	23.50	2.90	2.62	2.96
31R-2, 70	478.50	12.20	25.20	2.35	2.07	2.47
31R-3, 27	479.57	11.10	24.10	2.56	2.27	2.57
33R-1, 49	496.09	16.40	37.50	2.72	2.27	3.11
33R-3, 89	499.35	10.40	24.60	2.96	2.65	2.85
34R-1, 48	505.68	7.10	18.00	2.85	2.65	2.91
34R-5, 37	511.44	14.40	32.30	2.50	2.14	2.89

increase in the gradient, with values up to about 1600 m/s, between 135 and 200 mbsf correlates with geotechnical unit G3. Within unit G4, the velocity increases from 1600 to about 2200 m/s. Within this unit, the cherts were avoided during sampling because they are to scattered to be considered significant for the velocity distribution. However, two measurements on cherts gave values of 5700 and 3800 m/s, demonstrating overall high, but varying, velocity in the cherts. The contact between units G4 and G5 is clearly evidenced by an abrupt increase in velocity to an average value of 2800 m/s, with only a slight increase with depth deeper in the section. The values within geotechnical unit G5 show a relatively large scatter. Velocities in the volcanic rocks of the lowermost unit G6 have values ranging from 2800 to 5300 m/s, with an average of about 4000 m/s.

Several samples within geotechnical units G4 and G5 were measured both normal to and parallel to the core axis. Although there were differences, the variations showed no trend indicative of consistent velocity anisotropy. Most of the measurements were performed parallel to core axis (i.e., normal to bedding planes).

The continuous P-wave logger (PWL) was used only down to 210 mbsf. Below this depth RCB coring caused poor liner-to-sample contact. The PWL data from this site merely serve to

Table 16. Bulk density from 2-min GRAPE counts of discrete samples, Hole 738C.

Core, section, interval (cm)	Depth (mbsf)	GRAPE density (g/cm³)
4R-1, 122	217.12	1.85
4R-2, 93	218.33	1.88
5R-1, 83	226.43	1.89
6R-1, 104	236.24	1.97
7R-1, 112	245.92	1.95
8R-1, 80	255.20	1.98
9R-1, 52	264.62	2.02
10R-1, 87	274.67	2.02
10R-3, 29	277.09	1.99
11R-1, 95	284.35	1.92
11R-3, 7	286.47	2.00
23R-1, 31	399.51	1.97
23R-1, 111	400.31	1.96
23R-2, 130	402.00	2.11
23R-3, 145	403.65	2.07
24R-1, 76	409.66	1.94
24R-2, 113	411.53	2.37
24R-3, 43	412.33	2.22
25R-1, 121	419.81	2.34
25R-2, 122	421.32	2.41
25R-3, 50	422.10	2.48
25R-4, 65	423.75	2.45
26R-1, 88	429.08	2.36
26R-2, 23	429.93	2.32
26R-3, 29	431.49	2.33
27R-1, 46	438.36	2.27
27R-3, 90	441.80	2.38
27R-5, 75	444.65	2.22
28R-1, 20	447.80	2.37
28R-2, 25	449.35	2.38
28R-3, 100	451.60	2.39
28R-4, 97	453.07	2.39
29R-1, 46	457.66	2.44
29R-2, 60	459.30	2.41
29R-3, 5	460.25	2.38
30R-1, 20	466.80	2.33
30R-2, 15	468.25	2.37
30R-3, 40	470.00	2.39
31R-1, 104	477.34	2.42
31R-2, 70	478.50	2.32
31R-3, 27	479.57	2.21
33R-1, 49	496.09	2.28
33R-2, 131	498.33	2.38
33R-3, 89	499.35	2.56
33R-5, 84	502.22	2.76
34R-1, 48	505.68	2.60
34R-3, 144	509.60	2.67
34R-5, 37	511.44	2.35
35R-1, 70	515.50	2.63
35R-3, 58	518.35	2.47
35R-5, 28	520.71	2.32
36R-1, 18	524.48	2.62

Table 17. Undrained shear strength from vane measurements, Hole 738B.

Core, section, interval (cm)	Depth (mbsf)	Undrained shear strength (kPa)
1H-1, 90	0.90	3.1
1H-2, 81	2.31	3.9
2H-2, 140	6.90	0.4
2H-4, 83	9.33	0.4
2H-7, 10	13.10	7.0
3H-2, 75	15.75	11.6
3H-4, 70	18.70	5.8
3H-CC, 5	22.31	2.7
4H-2, 75	25.25	10.8
4H-4, 72	28.22	5.6
4H-7, 20	32.20	14.1
5H-2, 92	34.92	5.4
5H-4, 69	37.69	16.6
5H-6, 95	40.95	4.6
6H-2, 28	43.81	7.9
6H-4, 92	46.97	6.6
7H-1, 131	52.81	7.2
7H-4, 84	56.84	7.4
7H-6, 106	60.06	8.3
8H-2, 95	63.45	5.8
8H-4, 86	66.36	7.0
8H-5, 92	67.92	6.6
9H-3, 72	74.22	4.1
9H-5, 47	76.97	8.1
10H-1, 136	81.36	8.1
10H-3, 87	83.87	8.1
11H-2, 76	87.26	13.2
11H-4, 94	90.44	20.5
11H-6, 96	93.46	22.8
12H-2, 94	96.94	7.2
12H-4, 93	99.93	8.7
12H-6, 101	103.01	13.4
13H-1, 91	104.91	7.7
14X-2, 119	110.89	7.4
14X-4, 26	112.96	8.1
15X-3, 91	121.71	6.6
15X-4, 84	123.14	12.2
15X-6, 42	125.72	6.2
16X-3, 26	129.32	14.9
17X-1, 126	138.46	13.9
17X-3, 110	141.30	48.0
17X-CC, 10	143.72	24.4
18X-2, 94	149.24	30.8
18X-4, 76	152.06	29.4
19X-2, 73	158.73	23.4
19X-4, 78	161.78	12.4
19X-6, 72	164.72	6.4
20X-2, 80	168.50	12.4
20X-4, 80	171.50	43.1
20X-6, 75	174.45	37.6
21X-2, 65	177.89	21.6
21X-4, 36	179.76	26.2
22X-1, 77	186.17	25.2
22X-3, 60	189.20	26.6
22X-4, 72	190.62	29.8
23X-1, 74	195.74	22.0

confirm the velocities measured in the Hamilton Frame of about 1500 m/s in the upper 135 m of sediment, geotechnical units G1 and G2. Unit G3 is defined in the PWL data as a slightly larger scatter in the values.

Discussion

Index-property, shear strength, and velocity profiles for Site 738 are consistently correlative with each other and with changes in lithology (see "Lithostratigraphy, Sedimentology, and Igneous Petrology" section) and demonstrate the correspondence between geotechnical stratigraphy and lithologic stratigraphy. The use of geotechnical stratigraphy in defining lithologic boundaries has been established by Taylor (1984).

The geotechnical units, G1 through G6, can be defined on the basis of the index properties water content, porosity, bulk density, and grain density. Shear strength and compressional-wave velocity, however, give additional background for the divisions and, in some cases, may show the boundaries better than the index properties (e.g., the boundary between units G3 and G4).

The characteristics of geotechnical unit G1, with high water content and porosity and low bulk density, seem to be typical for diatom oozes. Because unit G1 is a relatively thin interval, depth trends within it are uncertain. However, the similarity to siliceous intervals at Sites 736 and 737 (see "Physical Properties" sections, "Site 736" and "Site 737" chapters, this volume) suggests that the observed absence of any increase in density with depth is a real trend, indicative of the ability of sediments with abundant biogenic silica to resist the effects of overburden pressure, at least at relatively shallow burial depths. Reasons for the large scatter in parameter values are uncertain at present. How-

Table 18. Undrained shear strength from fall cone measurements, Holes 738B and 738C.

Core, section, interval (cm)	Depth (mbsf)	Undrained shear strength (kPa)
119-738B-		
1H-1, 90	0.80	3.3
1H-2, 81	2.31	3.7
2H-2, 140	6.80	2.5
2H-4, 83	9.33	0.4
2H-7, 10	13.10	8.1
3H-2, 75	15.75	9.0
3H-4, 70	18.70	9.0
3H-CC, 5	22.31	6.6
4H-2, 75	25.25	27.0
4H-4, 72	28.22	21.0
4H-7, 20	32.20	30.0
5H-2, 88	34.38	6.6
5H-4, 71	37.71	31.0
5H-6, 98	40.88	9.8
6H-2, 30	43.83	11.0
6H-4, 88	46.93	16.0
7H-1, 133	52.83	24.0
7H-4, 81	56.81	11.0
7H-6, 108	60.08	22.0
8H-2, 96	63.46	7.7
8H-4, 84	66.34	16.0
8H-5, 94	67.34	17.0
9H-3, 74	74.34	7.7
9H-4, 49	75.49	28.0
10H-1, 137	81.37	22.0
10H-3, 89	83.39	21.0
11H-2, 78	87.28	27.0
11H-4, 92	90.42	58.0
11H-6, 98	93.48	58.0
12H-2, 96	96.56	19.0
12H-4, 91	99.81	25.0
12H-6, 99	102.89	35.0
13H-1, 89	104.89	24.0
14X-2, 123	110.83	30.0
14X-4, 24	112.84	30.0
15X-3, 92	121.72	20.0
15X-4, 83	123.13	56.0
15X-6, 46	125.76	20.0
16X-3, 28	129.34	41.0
17X-1, 126	138.46	17.0
17X-3, 110	141.30	62.0
17X-CC, 10	143.72	39.0
18X-2, 94	149.24	39.0
18X-4, 76	152.06	74.0
19X-2, 73	158.73	44.0
19X-4, 78	161.78	39.0
19X-6, 72	164.72	74.0
20X-2, 80	168.50	34.0
20X-4, 80	171.50	62.0
20X-6, 75	174.45	74.0
21X-2, 65	177.89	34.0
21X-4, 36	179.76	62.0
22X-1, 77	186.17	44.0
22X-3, 80	189.20	74.0
22X-4, 72	190.62	175.0
23X-1, 74	195.74	74.0
24X-1, 72	205.32	74.0
24X-3, 26	207.86	175.0
119-738C-		
4R-1, 64	218.04	135.0
5R-1, 83	226.43	123.0
5R-2, 40	227.50	215.0
6R-1, 56	235.76	275.0

Table 19. Compressional-wave velocity determined with the Hamilton Frame, Holes 738B and 738C.

Core, section, interval (cm)	Depth (mbsf)	Compressional-wave velocity (m/s)
119-738B-		
1H-1, 90	0.90	1471.9
1H-2, 81	2.31	1507.0
2H-2, 140	6.90	1565.6
2H-4, 83	8.33	1545.8
2H-7, 10	13.10	1511.3
3H-2, 75	15.75	1575.1
3H-4, 70	18.70	1522.3
3H-CC, 5	22.31	1510.5
4H-2, 75	25.25	1522.4
4H-4, 72	28.22	1486.1
4H-7, 20	32.20	1546.6
5H-2, 84	34.84	1493.5
5H-4, 66	37.66	1516.2
5H-6, 97	46.97	1510.1
6H-2, 32	43.85	1494.2
6H-4, 88	46.93	1515.7
7H-1, 134	53.84	1557.8
7H-4, 80	56.80	1527.6
7H-6, 108	68.08	1532.7
8H-2, 97	63.47	1513.8
8H-4, 84	66.34	1513.3
8H-5, 94	67.94	1528.8
9H-3, 74	74.24	1500.0
9H-4, 49	75.49	1526.4
10H-1, 137	81.37	1594.9
10H-3, 89	83.89	1520.5
11H-2, 78	87.28	1523.5
11H-4, 92	90.42	1519.0
11H-6, 98	93.48	1530.8
12H-2, 97	98.97	1498.6
12H-4, 91	98.91	1523.0
12H-6, 99	102.99	1523.2
13H-1, 89	104.89	1503.9
14X-2, 123	110.93	1526.7
14X-4, 24	112.94	1516.2
15X-3, 92	122.72	1524.7
15X-4, 78	123.08	1537.2
15X-6, 46	125.76	1531.2
16X-3, 20	128.26	1558.0
17X-1, 126	138.46	1530.0
17X-3, 110	141.30	1560.2
18X-2, 94	145.24	1567.0
18X-4, 76	152.06	1559.0
19X-2, 73	158.73	1595.5
19X-4, 78	161.78	1565.0
19X-6, 72	164.72	1662.1
20X-2, 80	168.50	1596.4
20X-4, 80	171.50	1603.4
20X-6, 75	174.45	1530.4
21X-2, 65	177.89	1562.2
21X-4, 36	178.76	1645.0
22X-1, 77	186.17	1583.7
22X-3, 80	189.20	1576.4
22X-4, 72	190.62	1593.9
23X-1, 74	195.74	1592.2
24X-1, 72	205.32	1666.7
24X-3, 26	207.86	1730.8
119-738C-		
2R-1, 137	197.97	1570.8
4R-1, 122	217.12	1750.0
4R-2, 93	218.33	1802.7
5R-1, 83	226.43	1782.0
6R-1, 104	236.24	1979.7
7R-1, 112	245.92	1859.8
8R-1, 80	255.20	1932.4
9R-1, 52	264.62	1918.5
10R-1, 87	274.67	1993.9
10R-3, 29	277.09	2127.1
11R-1, 95	284.35	1997.2
11R-3, 7	286.47	1932.4
16R-2, 73	333.83	1954.2

ever, because the continuous GRAPE measurements confirm this scatter, measurement errors and insufficient sampling intervals are excluded as probable explanations.

The boundary between geotechnical units G1 and G2 is a major hiatus (upper Miocene to lower Oligocene) at which there is an abrupt decrease in water content and porosity and an in-

Table 19 (continued).

Core, section, interval (cm)	Depth (mbsf)	Compressional-wave velocity (m/s)
119-738C-(Cont.)		
16R-5, 7	337.67	2009.7
17R-1, 50	341.80	2107.7
18R-3, 7	353.97	2590.0
18R-5, 6	356.96	2127.0
19R-1, 74	361.24	2132.0
19R-3, 60	364.10	2126.0
20R-1, 43	370.63	2492.0
20R-2, 45	372.15	1973.0
20R-3, 57	373.77	2194.0
22R-1, 20	389.80	2408.0
22R-3, 125	393.85	2402.0
22R-5, 70	396.30	2651.0
23R-1, 31	399.51	2097.0
23R-1, 111	400.31	2335.6
23R-2, 130	402.00	2194.9
23R-3, 145	403.65	2523.9
24R-1, 76	409.66	2181.8
24R-2, 113	411.53	2836.1
24R-3, 43	412.33	2677.2
25R-1, 121	419.81	2828.1
25R-2, 122	421.32	2875.0
25R-3, 50	422.10	3093.7
25R-4, 65	423.75	2956.1
26R-1, 88	429.08	2746.2
26R-2, 23	429.93	2721.4
26R-3, 29	431.49	2674.2
27R-1, 46	438.36	2649.6
27R-3, 90	441.80	2622.0
27R-5, 75	444.65	2432.4
28R-1, 20	447.80	2771.4
28R-2, 25	449.35	3000.0
28R-3, 100	451.60	2924.0
28R-4, 97	453.07	2740.7
29R-1, 46	457.66	2703.9
29R-2, 60	459.30	2720.0
29R-3, 5	460.25	2685.7
30R-1, 20	466.80	2543.1
30R-2, 15	468.25	2633.6
30R-3, 40	470.00	2988.5
31R-1, 104	477.34	2841.6
31R-2, 70	478.50	2954.1
31R-3, 27	479.57	3036.0
33R-1, 49	496.09	2872.0
33R-2, 131	498.33	3772.0
33R-3, 89	499.35	3523.0
33R-5, 84	503.22	5333.0
34R-1, 48	505.68	4085.0
34R-3, 144	509.60	4533.0
34R-5, 37	511.44	3268.0
35R-1, 70	515.50	4206.0
35R-3, 58	518.35	3505.0
35R-5, 28	520.71	3338.0
36R-1, 18	524.48	4395.0

crease in bulk density. The change may, however, be accounted for by the change in lithology from a diatom ooze to a nanno-fossil ooze over the interval from about 16 to 20 mbsf (see "Lithostratigraphy, Sedimentology, and Igneous Petrology" section). Velocity shows no apparent increase across the boundary, and the increase in shear strength is small. These trends point toward nondeposition rather than the removal of significant amounts of sediment.

Causes for the division between units G2 and G3, particularly as evidenced in the velocity profile, are not obvious from the lithology. However, slight diagenetic variations could be one cause. Although concentrations are small, a slightly elevated silica level is shown by the interstitial-water chemistry for this interval (see "Inorganic Geochemistry" section).

The transition from geotechnical units G3 to G4 corresponds to the transition from nannofossil ooze to nannofossil chalk,

and the distinct change in the physical properties is ascribed to the change in lithification. The Cretaceous/Tertiary boundary, situated in unit G4 at about 377 mbsf, does not involve any apparent changes in physical properties.

The next major geotechnical boundary, between geotechnical units G4 and G5, corresponds to the change from chalk to a clayey limestone. The wide scatter in index properties and velocities characteristic of unit G5 may be attributed to variations in bioturbation, sand content, and lithification (see "Lithostratigraphy, Sedimentology, and Igneous Petrology" section).

The volcanic breccias vary greatly in degree of alteration. This is reflected in the large density and velocity variations seen in geotechnical unit G6, with reddish, apparently highly altered sections typically showing velocities and densities of about 3000 m/s and 2.3 g/cm^3, respectively.

LOGGING

Operations

Two logging runs were completed from 97 to 457 mbsf at Hole 738C. The first logging run was recorded with the seismic stratigraphic combination (Fig. 27) and the second logging run with the lithoporosity combination (Fig. 28) (see "Explanatory Notes" chapter and "Logging" section, "Site 737" chapter).

The seismic stratigraphic combination was rigged at 0645 hr on 16 January after 100 bbl of gel mud was pumped into the hole and then displaced with seawater. A bridge was encountered at 457 mbsf, preventing the tool from going to the bottom of the hole at 532 mbsf. The logging run began at 0800 hr from the bridge at 457 mbsf and continued up to the base of the pipe at 97 mbsf, ending at 1150 hr.

The lithoporosity tool was rigged at 1230 hr. The same interval from 457 to 97 mbsf was logged from 0130 to 0330 hr.

With the exception of the caliper record and short sections of the sonic density and porosity records, most of the logs are of good quality. The logs are shown in Figures 27 through 30.

Caliper

The caliper tool (MCD) did not work properly and appears as a straight line at 31 cm on the record. Thus, a measurement of the hole diameter was not obtained from these two runs.

Density

The density quality curve (Fig. 29) reads too high (more than 0.05 g/cm^3) at 230–270, 344, 370–380, and 400–405 mbsf in the logged interval, indicating that a substantial correction is being applied to the density measurement. In these sections the litho-density tool gives incorrect low density values corresponding to caved or washed-out zones.

Sonic

Cycle skipping (see "Logging" section, "Site 737" chapter) and incorrect transit time corresponding to very high (e.g., >5000 m/s) or very low velocities (e.g., <1000 m/s) occur on several sections of the logged interval, mainly between 417 and 430 mbsf (Fig. 27).

Porosity

The porosity values measured by the neutron tool within the high-porosity zone from 97 to 250 mbsf are about 10% lower than those calculated from the density tool measurements (Fig. 30). As is usual in high-porosity intervals, the neutron measurement is saturated and appears almost as a straight line at 52% of porosity whereas the porosity calculated from density measurements decreases from 64% to 52%. The higher porosity values (i.e., >54%) are similar to those measured on cores (see "Physical Properties" section).
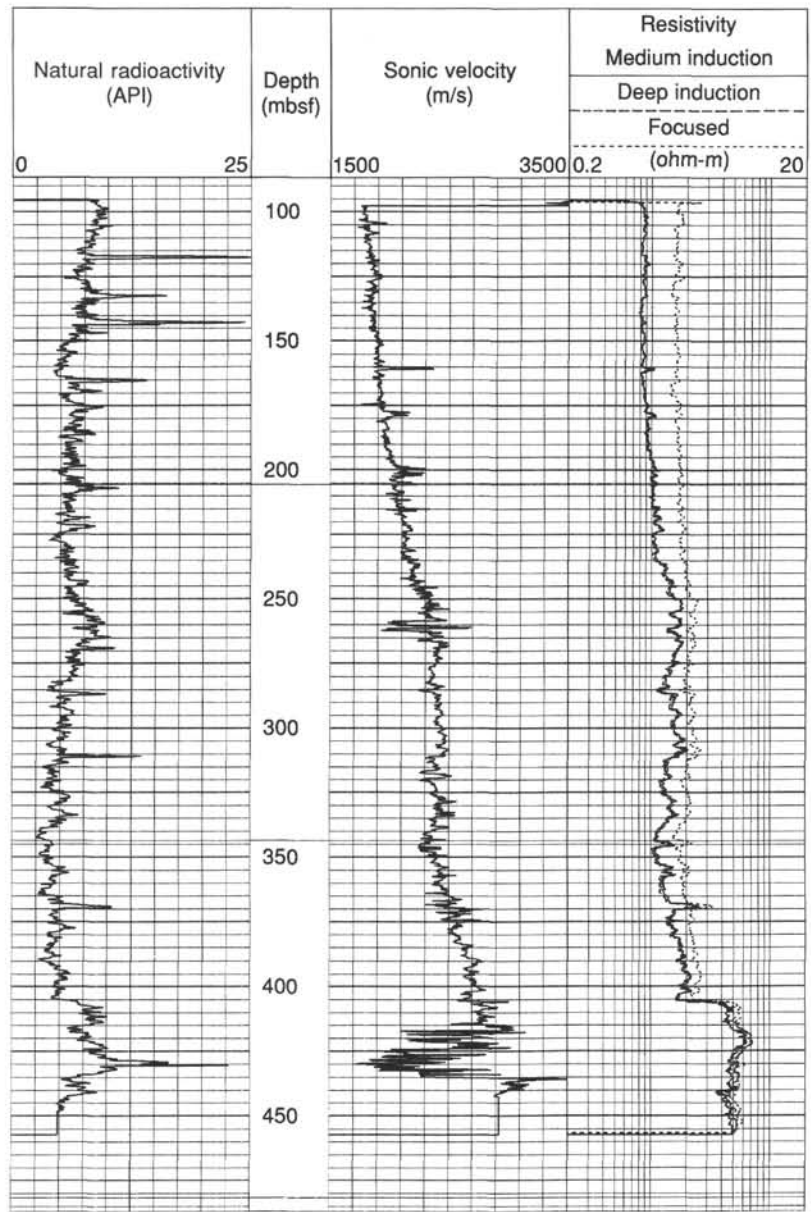
Figure 27. Downhole logs for the seismic stratigraphic combination: gamma ray, sonic, and resistivity for the interval from 97 to 457 mbsf, Hole 738C.

Interval of Poor Core Recovery (195 to 330 mbsf)

The interval between 195 and 330 mbsf was generally not well sampled by drilling, and no rocks were recovered between 287 and 330 mbsf. The interval from 287 to 330 mbsf has constant logging parameters in logging unit 2, indicating no major change in the dominant lithologic section. The interval from 195 to 287 mbsf was better recovered and consists of the lower part of lithologic Unit IV and upper part of lithologic Unit V. The logging records for the interval from 195 to 287 mbsf appear as straight lines that confirm, like for the interval from 287 to 330 mbsf, that the lithology of the recovered sections is the same as that in the nonrecovered sections (nannofossil ooze above 250 mbsf and chalk below 250 mbsf). Between 200 and 225 mbsf, peaks of low values (ranging from 3.5 to 2) occur on the photoelectric effect curve, indicating a more siliceous material. These peaks correspond to high-velocity peaks on the sonic velocity curve, which suggests thin layers of chert.

Logging Units

Logging Unit 1 (97 to 250 mbsf)

Logging unit 1 is characterized by a uniform increase downhole in resistivity, density, and sonic velocity and a uniform decrease downhole in porosity (Fig. 31): (1) resistivity increases from 0.9 to 2 ohm-m, (2) sonic velocity increases from 1806 to 2390 m/s; (3) density increases from 1.3 to 1.9 g/cm^3; and (4) porosity measured with the neutron tool or calculated from the density log decreases from 64% to 46%. Logging unit 1 consists mainly of nannofossil ooze and chalk (see "Lithostratigraphy, Sedimentology, and Igneous Petrology" section). The preceding
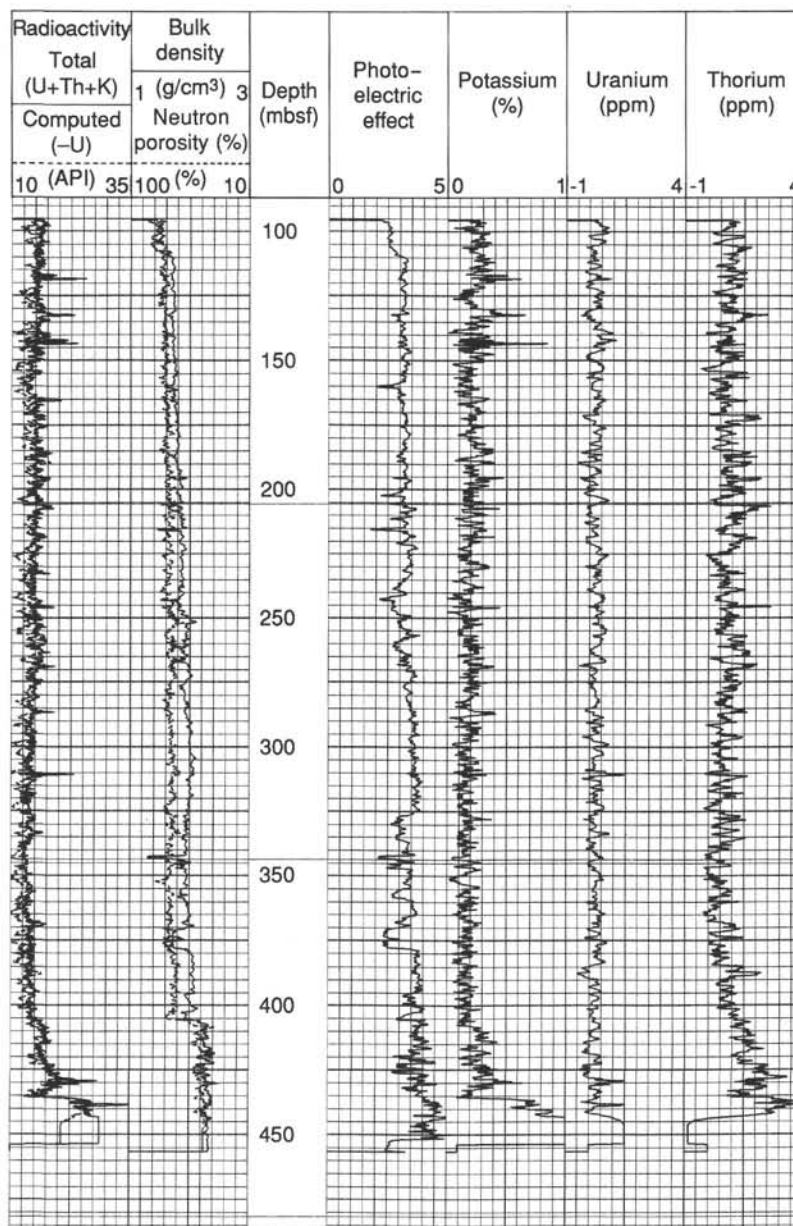
Figure 28. Downhole logs for lithoporosity combination: total gamma ray (uranium, thorium, and potassium), computed gamma ray, density, neutron porosity photoelectric effect, and potassium, uranium, and thorium, for the interval from 97 to 457 mbsf, Hole 738C.

changes in sonic velocity, density, resistivity, and porosity with depth in the nannofossil ooze and chalk formations result from compaction. The rate of compaction in logging unit 1 corresponds to an average decrease in porosity of 0.12%/m. The compaction of the nannofossil ooze and chalk at Site 738 is different from the compaction of the diatom ooze at Site 737, where velocity, density, resistivity, and porosity do not change in the downhole logs with increasing depth. The different degree of compaction between diatom ooze and nannofossil ooze and chalk at similar burial depths results from the different sizes of the microfossils. Diatoms have relatively large, porous frustules with a high surface-to-volume ratio that form an internal structure resistant to the overburden load. Nannofossils, however, are small, clay-size organisms with fragile skeletal structures that compact readily.

Logging Unit 2 (250 to 344 mbsf)

Logging unit 2 is characterized by nearly uniform sonic velocity, density, resistivity, and porosity values throughout the interval (2400 m/s, 2 g/cm³, 1.5 ohm-m, and 46%, respectively) (Fig. 31). Unit 2 corresponds to the upper part of the chalk (see "Lithostratigraphy, Sedimentology, and Igneous Petrology" section). The uniform values of velocity, density, resistivity, porosity in logging unit 2 show that sediment compaction by overburden load is not the only controlling process. The boundary between logging units 1 and 2 is a diagenetic front corresponding to the transformation of the nannofossil ooze to chalk. This transformation seems to be only an early step in the diagenetic process because water content (see "Physical Properties" section) and porosity remain high in this interval.

271
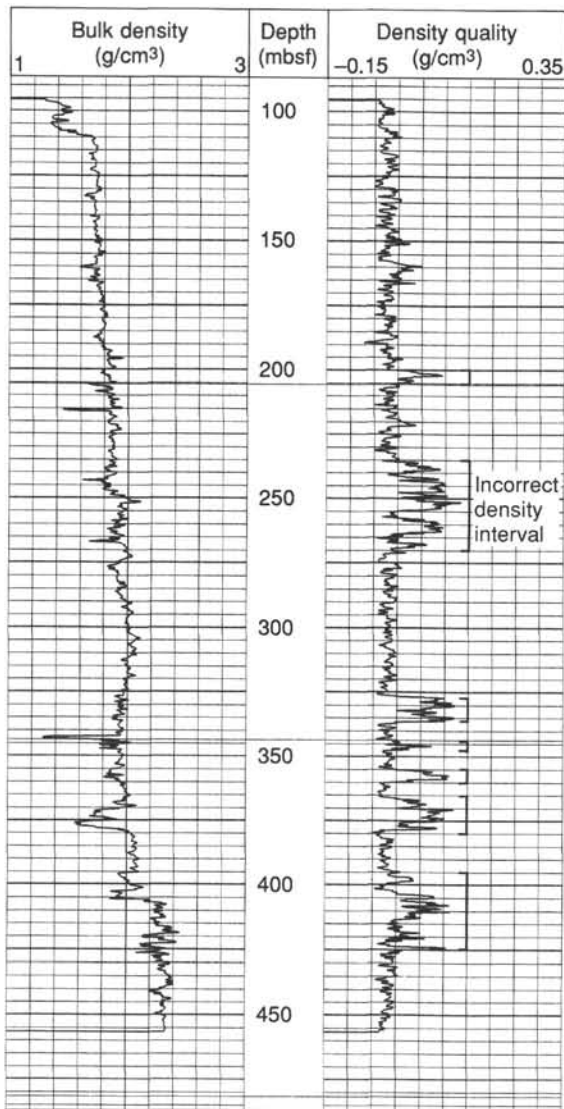
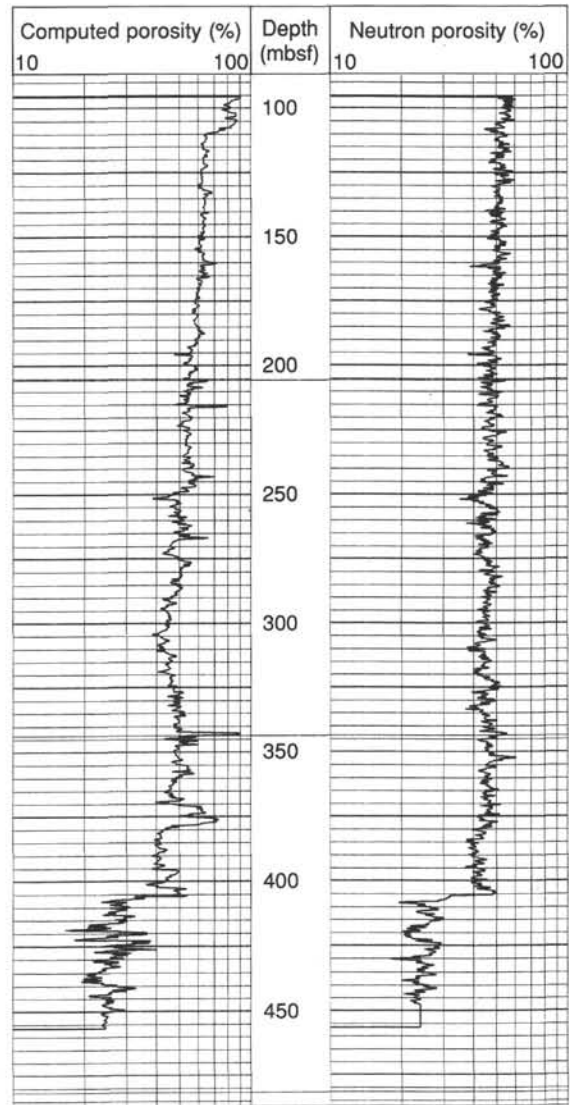Figure 29. Downhole density and density quality curve logs for the interval from 97 to 457 mbsf, Hole 738C.

Figure 30. Comparison of density porosity (computed from the lithology tool) and neutron porosity (observed) for the interval from 97 to 457 mbsf, Hole 738C.

Logging Unit 3 (344 to 405 mbsf)

Logging Unit 3 corresponds to the lower part of the chalk unit (Fig. 31) and is defined by a uniform increase in resistivity, density, and sonic velocity from the top of the unit at 344 mbsf to the bottom of the unit at 405 mbsf: (1) resistivity increases from 1.5 to 2.2 ohm-m, (2) sonic velocity increases from 2400 to 2700 m/s, and (3) density increases from 2 to 2.17 g/cm³. Neutron porosity and porosity calculated from density decrease from 46% to 41% from top to bottom in the unit. As in logging unit 1, compaction of the sedimentary column as a result of the expulsion of water by the weight of the overlying rocks is the dominant process recorded by the porosity, density, resistivity, and sonic velocity measurements. Logging unit 3 represents a further step in the diagenesis of the chalk from that of logging unit 2.

Logging Unit 4 (405 to 455 mbsf)

The boundary between logging units 3 and 4 is marked by an abrupt increase in sonic velocity, resistivity, density, and radioactivity and an abrupt decrease in porosity: (1) resistivity jumps from 2.2 to about 5.5 ohm-m, (2) sonic velocity increases from

2700 to 2850 m/s, (3) density increases from 2.0 to 2.3 g/cm³, (4) natural radioactivity increases from 4 to 6 API units, and (5) porosity decreases from 46% to 28%. This abrupt change in the characteristics of the logging parameters suggests that logging unit 4 consists of highly compacted material (Fig. 31). Below 405 mbsf, the logging parameters (sonic velocity, resistivity, density, radioactivity, and porosity) are nearly uniform, and no distinct increase or decrease with increasing depth appears in the unit. The log characteristics of logging unit 4 fit fairly well with the description of the silicified limestones (see "Lithostratigraphy, Sedimentology, and Igneous Petrology" section). Isolated peaks occurring at different depths correspond to some minor variations in the lithology. Natural radioactivity is higher in logging unit 4 than in the overlying units which suggests a higher clay content than in logging units 1 through 3.

Logging Units and Apparent Sedimentation Rate

The boundaries between downhole logging units 1 through 4 for Hole 738C correspond either to unconformities or changes in sedimentation rates (see "Sedimentation Rates" section and
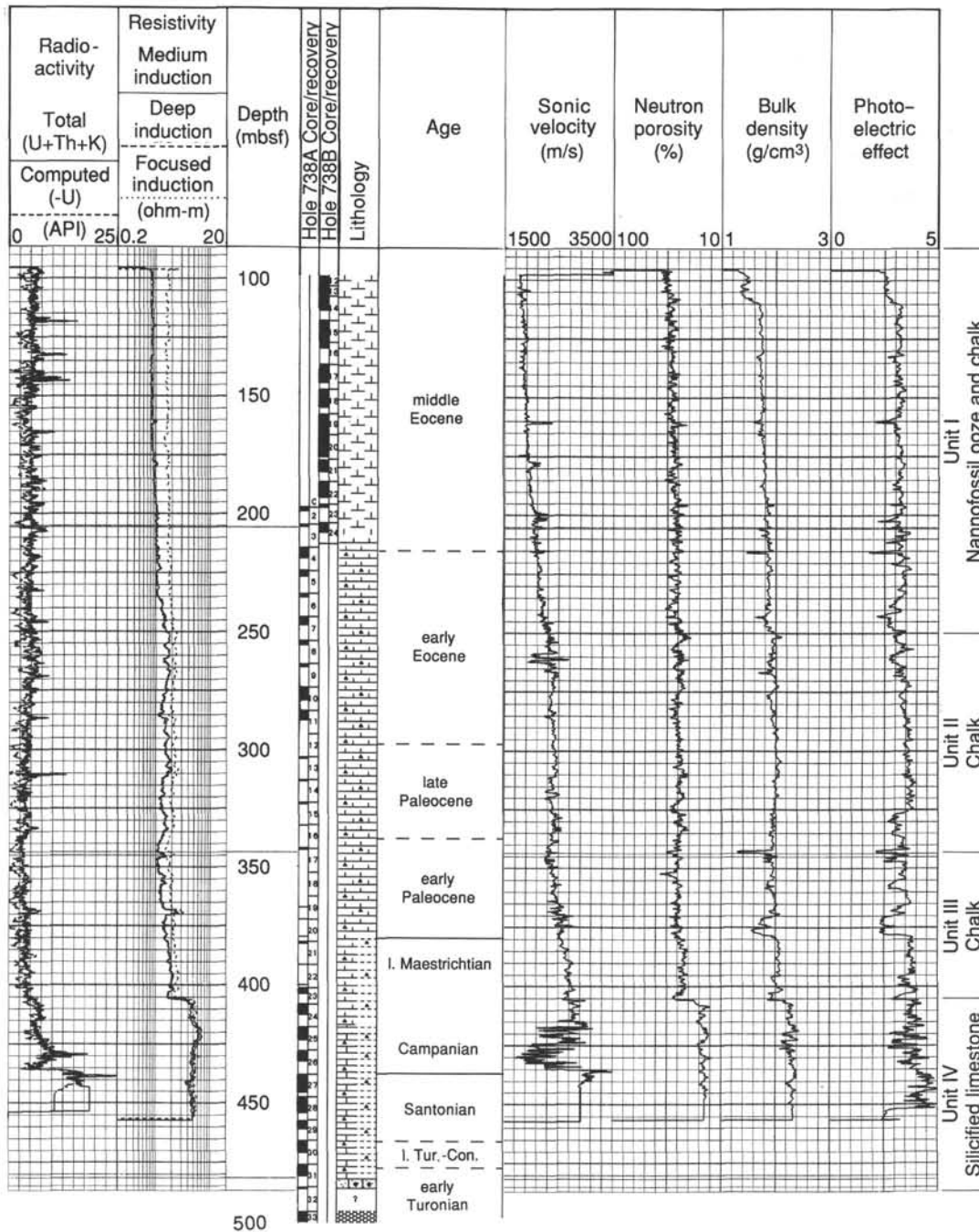
Figure 31. Summary compilation of important downhole logs used to define the four logging units at Site 738.

Fig. 32). Intervals of low apparent sedimentation rates correspond to uncompacted or unlithified units from 97 to 250 mbsf and from 344 to 405 mbsf. Intervals of high apparent sedimentation rates correspond to compacted or lithified units from 250 to 344 mbsf and from 405 to 455 mbsf. The agreement between boundaries in the logging units and breaks in apparent rates of sedimentation at Site 738 confirms that two factors control the apparent sedimentation rate. The first factor is the true rate of sedimentation, and the second is the loss of sedimentary volume resulting from compaction.

Synthetic Seismogram

Synthetic seismograms were computed for Site 738 using sonic and density logs to accurately correlate drill cores with seismic-reflection data over the site (Fig. 33). The seismograms cover only the logged interval, 100 to 460 mbsf. Deeper and shallower parts of the hole are not included because laboratory measurements of velocity and density for these depths are either too sparse and variable (below 460 mbsf) or too small (by about 20% above 100 mbsf) to give reliable results on the synthetic seismogram.

Two seismograms were computed (Fig. 33). The first one is based only on the short-sonic-velocity (spacing = 2 m) log, and the second is computed from the short-sonic-velocity and density logs. The two seismograms are similar, but the seismogram based on velocity only gives a slightly better correlation because of less noise in the profile. The velocity, density, and acoustic impedance curves used to compute the synthetic seismograms are

273
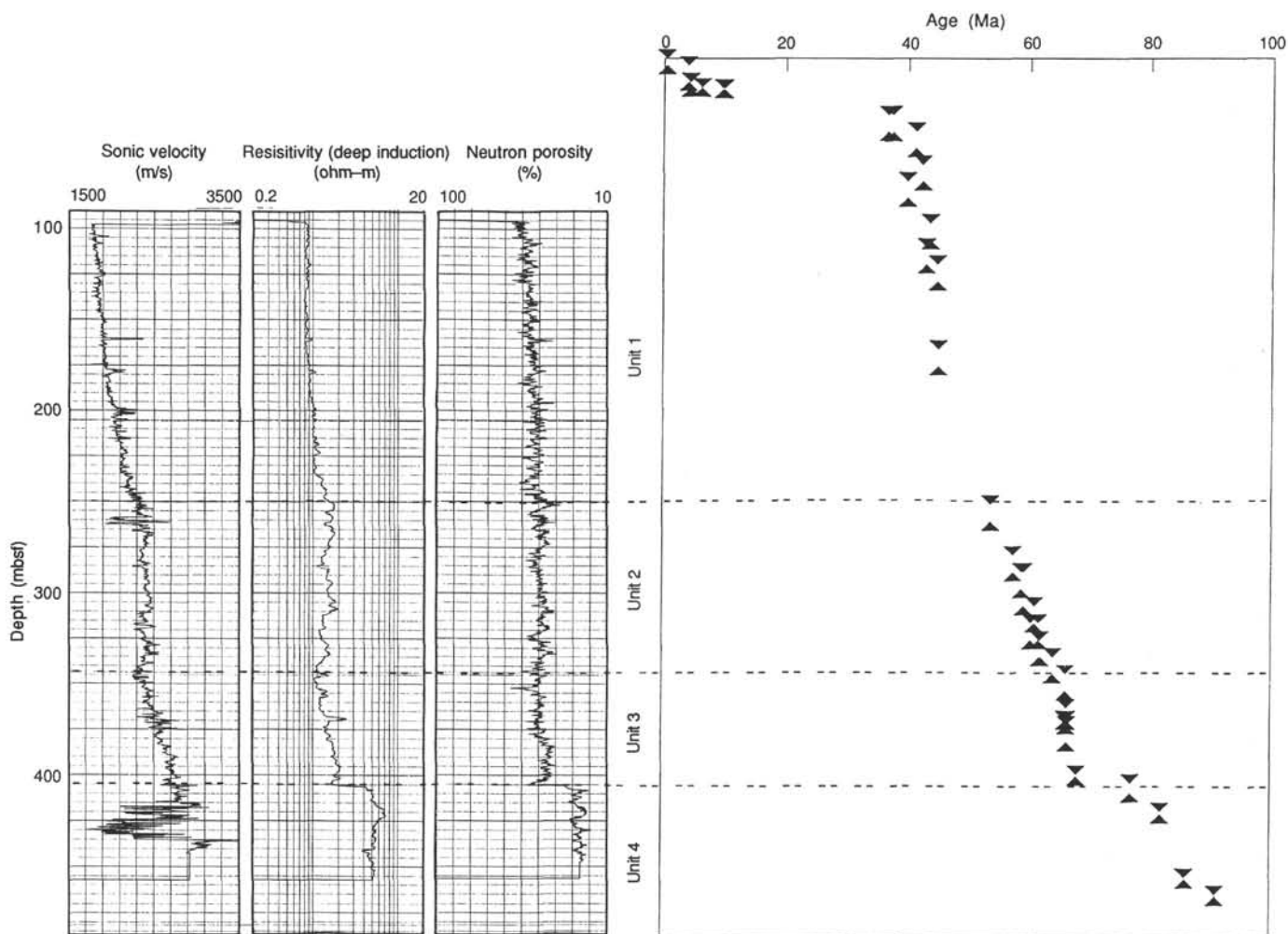
Figure 32. Comparison of the boundaries between downhole logging units 1 through 4 (derived in part from the sonic velocity, resistivity, and neutron porosity logs shown) and the sedimentation rate plot, Hole 738C.

shown in Figure 33. The velocities from sonic logs, laboratory measurements, and sonobuoy seismic are compared in Figure 34.

The short-sonic values were selected instead of long-sonic values (log spacing = 3.5 m) for the synthetic seismogram because they gave greater resolution and fewer errors in the rapidly varying lithologies at the site. Velocity measurements were good throughout the hole, with possible exception of noisy measurements from a low-velocity interval from 415 to 435 mbsf.

Downhole density measurements were edited to remove bad values (about 10%) caused by apparent washed-out zones in the hole. Densities in these zones were anomalously low, causing spurious reflections in the synthetic seismogram. The laboratory density measurements (see "Physical Properties" section) were not used because they are too sparse and variable to give a reliable synthetic seismogram (i.e., sparse sampling of small density variations gives spurious reflection events).

The synthetic seismogram illustrates several important points:

1. The location of prominent reflectors and bands of reflectors is more strongly controlled by the position of thin (<5-m-thick) high-velocity layers than by the degree of lithification and compaction in thick (50–150-m) units.

2. In the upper 200 m of the hole, where only a few local velocity variations (i.e., lithologic variations) are found, the synthetic seismogram has low-amplitude reflections with small peaks over the isolated high-velocity layers.

3. The large isolated and banded reflections at 200 to 300 mbsf occur where thin layers of high-velocity chert? are interbedded in lower velocity rocks.

4. A prominent reflection at 430 mbsf corresponds with a 15-m-thick low-velocity zone.

Comparison of the synthetic seismogram with vertical-incident seismic-reflection data recorded over Site 738 is shown in Figure 35. The accuracy of the correlation is predicated on the assumption that the seismic-reflection profile was recorded directly above the drill site, as shown. Location errors of up to 50–100 m (2–4 traces) are possible, and the observed reflectors could move up or down by up to 10–30 ms over this distance. The good correlation of the synthetic trace with the banded reflection events at 200–300 mbsf and with a distinct reflector at about 420 mbsf suggests that navigational errors are not large (or that lateral variations in geology are small).

In general, the synthetic and observed seismic traces can be correlated at Site 738 (Fig. 35). The widths of reflection peaks are affected, in part, by the band-pass filters used; however, the agreement between observed and synthetic data for location of isolated peaks and bands of reflections can only be explained by real variations in acoustic impedance (i.e., lithology). Reflection amplitudes, which are more sensitive to the relative change in acoustic impedance than to the absolute magnitude of the impedance, change abruptly at about 200 and 425 mbsf. At 200
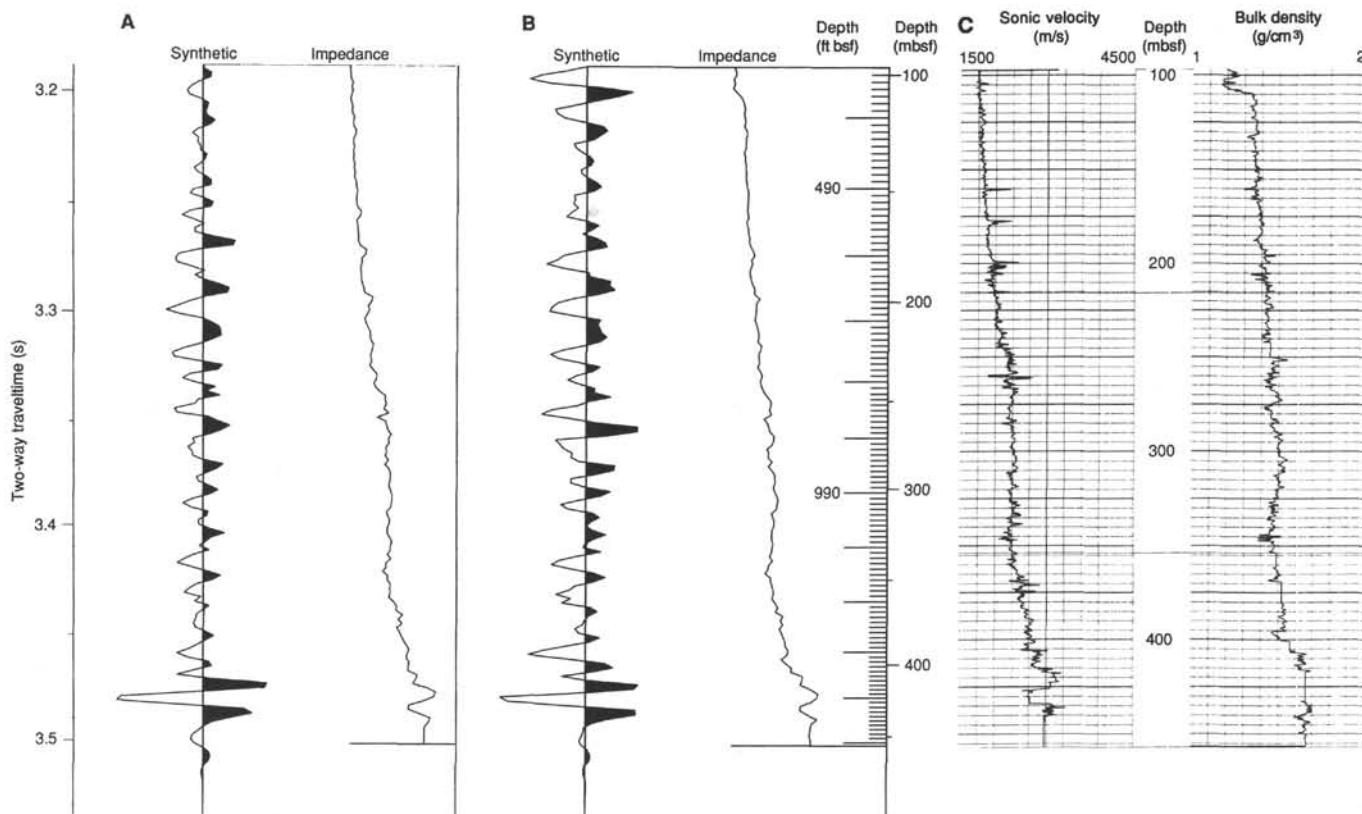
Figure 33. **A.** Synthetic seismic traces computed from downhole logs using only velocity data (**A**) and velocity and density data (**B**); the corresponding impedance curves are shown to the right of the synthetic traces. **C.** Values of density and velocity (inverse of sonic log values) used to compute impedance for synthetic seismic traces (see text).

mbsf, the locally high impedance contrasts between the nanno-fossil oozes (2.0 km/s) and the thin interbedded chert and calcareous layers (2.2–2.5 km/s) produce the major zone of reflectors. In contrast, a similar zone of reflectors at Site 737 (see "Logging" section, "Site 737" chapter) is caused by gradual oscillations of about 0.3 km/s over distances of 5–10 m instead of by abrupt velocity changes in thin (< 5 m) discrete layers.

Reflection amplitudes directly above and below the banded reflections (e.g., 200–300 mbsf) are small in the vertical-incidence seismic data, but are larger in the synthetic data. The difference in amplitude is indirectly related to noise in the logging data, which introduces spurious small peaks in the synthetic data. Below 400 mbsf, waveforms in the observed seismic data are more complex, indicating either minor sediment deformation or a sequence of thin beds of differing lithology. The downhole logging indicates that the seismic wave complexity below 400 mbsf may also result from differing degrees of lithification (e.g., alternating layers of hard, high-velocity rock and soft, low-velocity sediment).

The depths to major seismic reflections for the interval from 100 to 430 mbsf generally do not coincide with the depths for the boundaries between the four logging units described in this section. Boundaries for the logging units (250, 344, and 405 mbsf) occur at depths where the slopes of two or more parameter curves (e.g., velocity, resistivity, etc.) change, signifying different lithologic units. With one possible exception (405 mbsf), these boundaries do not generate reflection arrivals. In addition, the logging units do not have a specific acoustic character; however, they contain a mixture of reflection types.

The misfit between the logging units and the seismic-reflection character is best exemplified by logging unit 1 (Figs. 31 and

36). Logging unit 1 (100–250 mbsf) is characterized by uniformly increasing velocity, density, and resistivity (decreasing porosity) and by narrow (i.e., thin layer), isolated velocity peaks. In the seismic data, the unit contains low-amplitude reflections (100–200 mbsf) and high-amplitude banded reflections (200–250 mbsf). The change in acoustic character from low- to high-amplitude reflections is caused by the occurrence of thin high-velocity chalk layers (197–215 mbsf) within the Eocene nannofossil oozes. In addition, a distinct reflection does not occur between logging units 1 and 2, the disconformity at the middle to upper Eocene boundary in nannofossil oozes (and chalks).

The apparent discrepancy between the logging units and seismic-reflection data illustrates a common pitfall of seismic-reflection interpretation: the assumption that major reflection events always signify major lithologic (or age) boundaries (Fig. 36). Although major boundaries are commonly associated with reflection events, other factors such as diagenesis, facies changes, and variations in depositional environment can result in major reflections, as at Site 738.

Summary

In summary, a suite of 10 downhole logs was successfully recorded at Site 738, leading to the identification of four distinct logging units. These units indicate that the composition, compaction, and diagenesis of the calcareous ooze, chalk, and limestone section are the principal processes controlling the changes in downhole log responses. Strong reflections in the sedimentary section occur both within a broad zone and as isolated events. The reflections are caused principally by thin interbedded layers within logging units instead of by abrupt changes of lithology at the boundaries of the logging units. The apparently
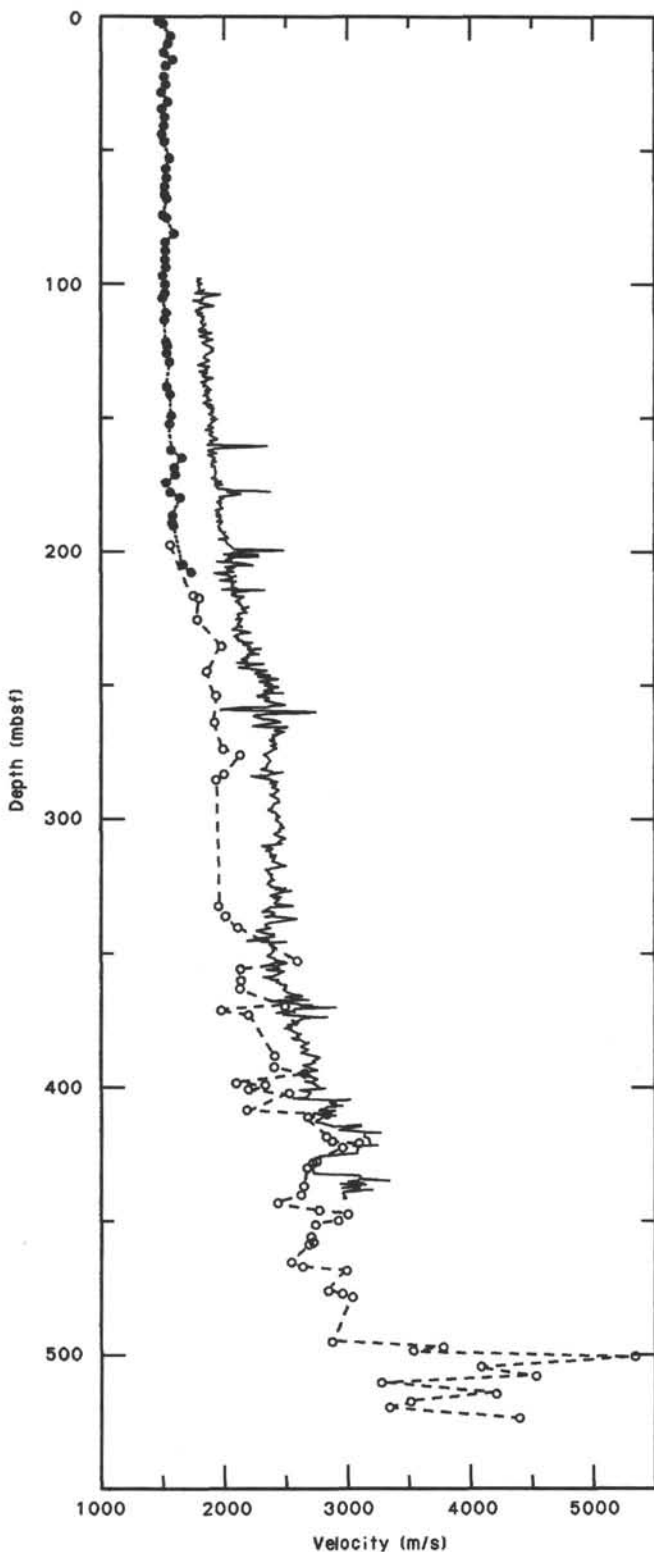
Figure 34. Comparison of velocities from sonic logs (short-dashed line), laboratory measurements (solid line), and sonobuoy seismic (long-dashed line) for Site 738.

poor correlation between major reflections and logging unit boundaries is surprising because important unconformities occur at each of the logging boundaries. The unconformities are therefore not easily identifiable and traceable in the seismic-reflection profile across Site 738.

SEISMIC STRATIGRAPHY

The synthetic seismograms based on downhole logging do not demonstrate a detailed correlation between the seismic reflectors and the stratigraphic boundaries established in the coring at Site 738 (see Figs. 35 and 36 in "Logging" section). However, we attempted to use the stratigraphy known for Site 738 to derive for a more general estimate of the age and lithology of seismic units observed in the single-channel seismic line recorded by *JOIDES Resolution* (Fig. 4) and the multichannel lines MD 47-07 (Fig. 37) and MD 47-08 recorded by *Marion Dufresne* (R. Schlich and M. Munschy, unpubl. data).

A direct comparison between the single-channel record and the lithologic/stratigraphic sequence observed at Site 738 suggests the following seismic units:

1. Seismic Unit I is a thin upper unit. The base is at 18 mbsf, probably marking the observed hiatus between lower Oligocene and upper or uppermost Miocene.

2. Seismic Unit II is characterized by wavy low-amplitude reflectors of low continuity. The top of unit may be erosionally truncated, and the bottom of unit is at 200–210 mbsf, probably marking the diagenetic change from calcareous ooze above to chalk below. At Site 738 this change is close to the lower Eocene/middle Eocene boundary.

3. Seismic Unit III is characterized by fairly strong, wavy reflections of good continuity. The base of the unit is not well defined on the seismic record, but abrupt changes in sonic velocity and density in shipboard measurements suggest a boundary at 410 mbsf.

4. Seismic Unit IV is characterized by more flat-lying and more high-frequency reflectors than in the preceding unit. Continuity is medium, and definition is better northwest of Site 738. Unit IV probably reflects the Cretaceous limestones with a varying content of chert and silicified layers. The bottom of the unit is at approximately 500 mbsf.

5. Seismic Unit V (basement) is marked by a strong uneven reflection with many point refractions. This suggests an uneven surface, possibly with local sediment deposits.

The uppermost seismic unit is not distinguishable at Site 738 because of the long bottom pulse, but it is clear upslope toward the northwest. However, shipboard measurements of samples document a marked increase in density but not in sound velocity (Fig. 26) at 18 mbsf, suggesting the presence of a reflecting surface. It is uncertain whether this reflector is related to the base of the uppermost Miocene–Quaternary diatom ooze, to the hiatus between lower Oligocene nannofossil ooze and middle Miocene diatomaceous nannofossil ooze, or to a combination.

Seismic Units I through III and the basement reflector V are recognized on the crossing multichannel line MD 47-07, shotpoint 3890. Seismic Unit III is underlain by a zone characterized by low-amplitude reflections, which is not recognized in the single-channel profile; however, regionally this zone is included in seismic Unit III. Seismic Unit IV is represented on the multichannel profile by one or two strong continuous reflections above the basement, but a detailed fit of the Unit III/Unit IV boundary seen in the single-channel profile is not possible. Seismic Unit IV is associated with a reeflike structure about 50 km northwest of Site 738. This reef may correlate with a layer of algal calciclastic limestone in Hole 738C at 485 mbsf, just above the volcanics.

Site 738 is near the top of a 1.5-km-high broad basement ridge, the core of the southernmost part of the southern Kerguelen Plateau. According to Coffin et al. (1986), this ridge is
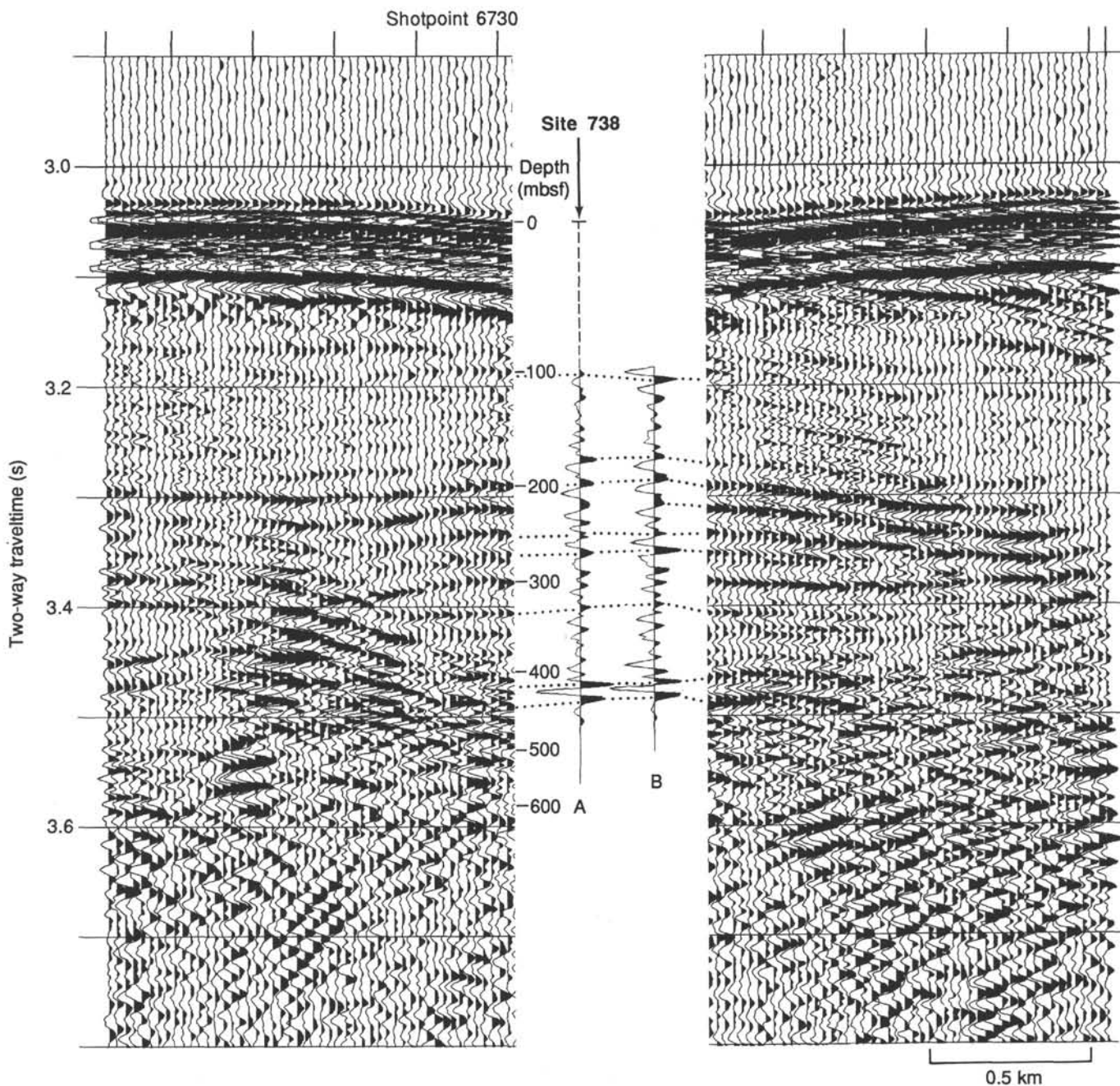
Figure 35. Comparison of vertical-incident seismic-reflection data recorded over Site 738 with synthetic seismic-reflection traces computed from downhole measurements of (A) velocity data and (B) velocity and density data.

the southern end of a 1200-km-long broad arch that extends almost to Heard Island and thus forms the backbone of the southern Kerguelen Plateau. The coring at Site 738 provided the first *in-situ* samples of basement which proved that basement consists of pre-Turonian age volcanic rocks that were probably subaerially erupted. This agrees with conclusions of Bassias et al. (1987) and Leclaire et al. (1987), based on sparse dredged samples from the central Kerguelen Plateau.

The basement arch is covered with 500–4000 m of sediments. Colwell et al. (in press) recognized six major seismic stratigraphic sequences in the Raggatt Basin on the southern Kerguelen Plateau, approximately 500 km northeast of Site 738. The sequence includes a basal unit F, which fills minor lows in the basement, and a thick unit E, which shows clear onlapping onto the basement. Unit E fills the larger basins and shows a mounded upper

surface (carbonate or volcanic mounds). Unit D fills small depressions in unit E and is locally related to debris from the mounds. A thick unit C covers most of the Raggatt Basin and is partly of middle to late Eocene age. Unit B shows characteristic low-amplitude reflections, and the covering unit A is relatively thin and more limited in areal extent; both units A and B are of post-Eocene age. Houtz et al. (1977) identified three major reflectors ("A," "B," and "C") on single-channel seismic. According to Colwell et al. (in press), the unconformity between sequences D and E is equivalent to the "A" reflector of Houtz et al. (1977), and the top of the basement at the base of unit F correlates with "B." Layering within the basement complex is equivalent to reflector "C."

The available seismic lines do not allow a direct tracing of the seismic units from the Raggatt Basin to the sedimentary se-
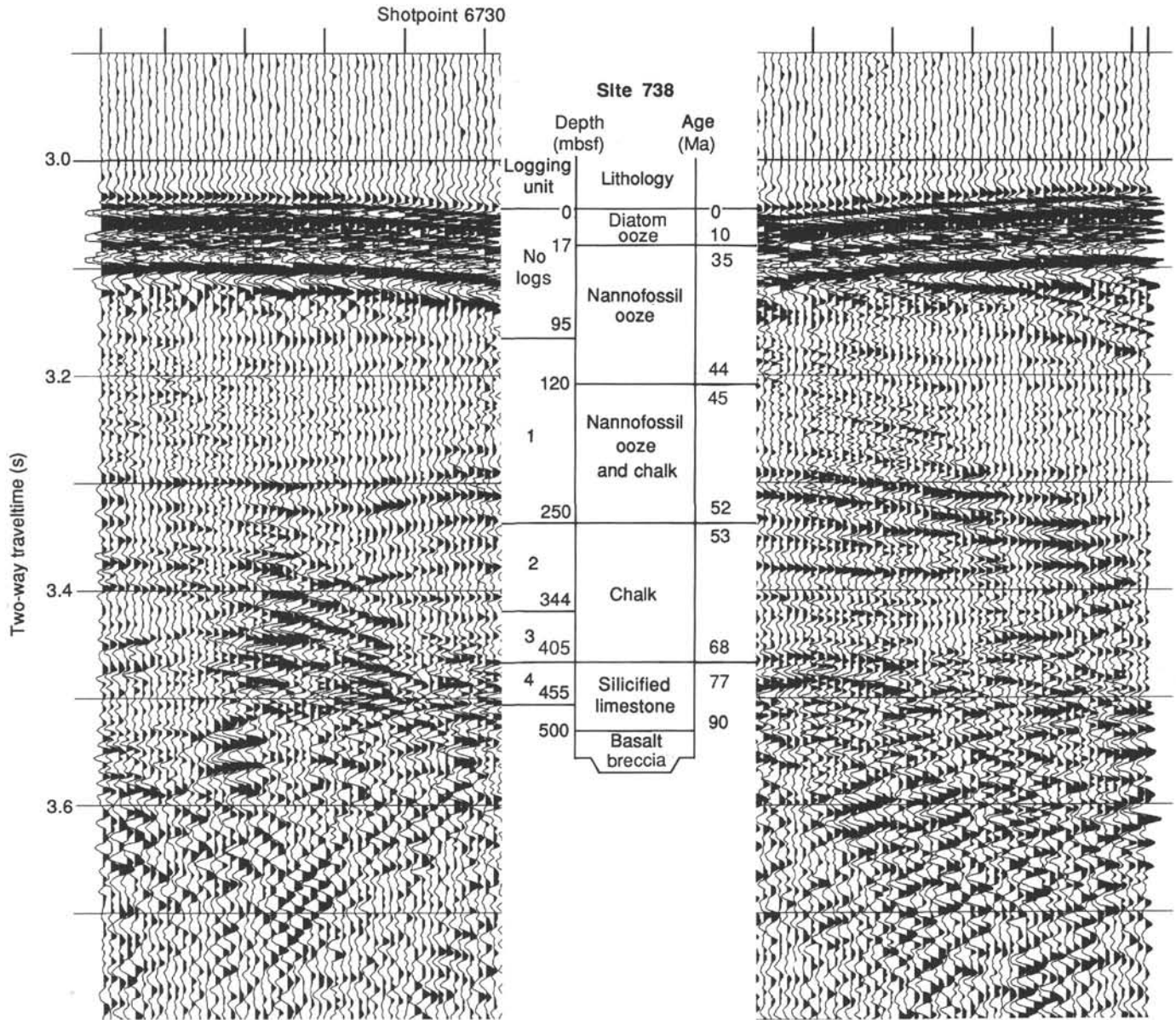
Figure 36. Seismic section over Site 738 showing depths to major lithologic and logging units. Depths are from synthetic seismic traces of Figure 33.
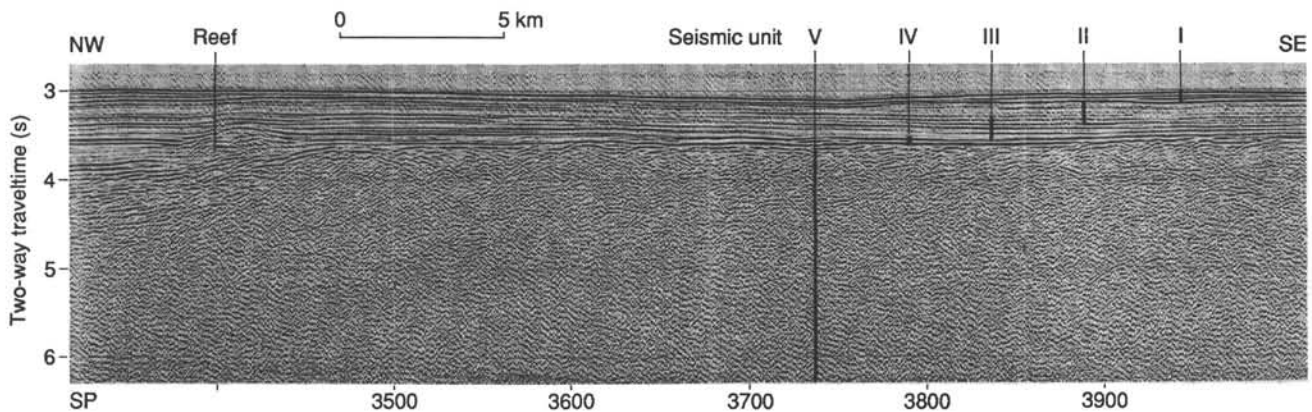

Figure 37. Part of multichannel seismic section MD 47-07, courtesy of M. Munschy and R. Schlich. Crossing of single-channel seismic tie line to Site 738 and seismic units is shown.

quence on the southwestern flank of the plateau and to Site 738. The units have been tentatively correlated, as shown in Table 20.

Seismic Unit IV is approximately 50 m thick at Site 738 but increases considerably both to the northwest (Fig. 37) and to the northeast downslope of the southern Kerguelen Plateau. It is probably underlain by older sediments of unknown age.

SUMMARY AND CONCLUSIONS

A 486-m-thick lower Turonian through Quaternary sediment section overlying 38 m of volcaniclastic rock and altered basalt was cored at Site 738 on the southern tip of the Kerguelen Plateau. The sediment section records shallow deposition on the inner shelf during the early Turonian, followed by deepening to depths equivalent to near the shelf break by the end of the Cretaceous, and continued deepening and deposition at depths at or below the present-day water depth (2252.5 m) throughout most of the Cenozoic. Biogenic carbonate (nannofossil oozes, chalks, and limestones) dominates the Cretaceous and Paleogene section whereas biogenic silica (diatoms and radiolarians) is more evident in the abbreviated section of Neogene sediments recovered at the site. Two changes in sedimentation occur in the lower Oligocene, possibly attesting to a marked increase in Antarctic cooling or glaciation: (1) diatoms become a consistent component of the sediments and (2) pelagic deposition becomes sporadic, probably reflecting an intensification of bottom water flow across the site. Seismic stratigraphic studies by Leclaire et al. (1987) and our site survey both indicate that the seismic unit overlying the top of the main body of the lowermost Oligocene to Cretaceous section varies in thickness regionally on the southern Kerguelen Plateau and displays scouring and fill relationships on the older unit.

Lithostratigraphy

Eight lithologic units are recognized at Site 738: Unit I (0–16.8 mbsf) is a Quaternary to upper Miocene diatom ooze with minor proportions of foraminifers, calcareous nannofossils, radiolarians, and clay; Unit II (16.8–17.7 mbsf) is a upper Miocene nannofossil ooze with minor diatoms; Unit III (17.7–120.8 mbsf) is a lower Oligocene to middle Eocene homogeneous nannofossil ooze; Unit IV (120.8–254.4 mbsf) is a middle Eocene nannofossil ooze and chalk, with chert layers and concretions in some parts; Unit V (254.4–418.6 mbsf), a lower Eocene to Campanian calcareous chalk with chert nodules and fragments, is moderately to intensively bioturbated and includes trace fossils in its Cretaceous lower part; Unit VI (418.6–479.7 mbsf) is a Campanian to lower Turonian partially silicified limestone that contains burrowing trace fossils and *Inoceramus* fragments; Unit VII (479.7–486 mbsf) consists of an algal calciclastic limestone with basaltic pebbles and a basaltic breccia; and Unit VIII (495.6–533.8 mbsf) includes alternating volcaniclastics and massive, aphyric basalts, which are moderately to highly fractured and altered. The occurrence of dull red volcaniclastics in four intervals, the abundance of vesicles, and the lack of chilled mar-

Table 20. Tentative correlation between seismic units from the southernmost Kerguelen Plateau (Site 738 plus line MD 47-07) and Raggatt Basin (Colwell et al., in press).

Southernmost Kerguelen Plateau	Raggatt Basin
Seismic Unit I (late Miocene to Quaternary)	Units A and B (post-Eocene)
------------------------- Hiatus -------------------------	
Seismic Unit II (middle to late Eocene)	Unit C (partly middle to late Eocene)
---------------- Diagenetic boundary ----------------	
Seismic Unit III (early Eocene to Maestrichtian)	Units D + (and part of Unit E)
---------------- Diagenetic boundary ----------------	??? ---------- Local unconformity ----------
Seismic Unit IV (Campanian–Turonian)	Unit E in part
---------------- Hiatus? --------------------< < < < < <Units E + F (not at Site 738)	
Seismic Unit V Basement (pre- to late Turonian)	Basement (age ?)

gins suggest that these basalts were erupted in shallow water or a subaerial environment.

The lowermost occurrence of significant terrigenous material in the post-Cretaceous pelagic section lies in the uppermost part of Unit III in the lower Oligocene (120 cm in Section 119-738B-3H-3 to 35 cm in Section 119-738B-3H-5). This interval contains traces (<1%) of exotic, sand-sized particles, which were probably ice rafted.

Biostratigraphy and Paleoceanography

The Turonian to Quaternary sediment section cored at Site 738 can be readily correlated to existing microfossil zonations. In general, Southern Ocean or middle-latitude zonations are most applicable; however, low-latitude biostratigraphy can be applied to parts of the Cretaceous and Paleogene section. The abbreviated Neogene section (0–17.7 mbsf) contains a consistent reworked component from the Paleogene and parts of the Neogene, whereas reworking is quite rare in the Paleogene and Cretaceous section.

Two prominent unconformities are recognized in the Site 738 sediment section: a hiatus at 17.7 mbsf separates lower upper Miocene sediments from lower Oligocene sediments and a Campanian to upper Maestrichtian hiatus between Cores 119-738C-23R and 119-738C-24R (408.9 mbsf) has a duration of 9 m.y. Leclaire et al. (1987) suggested that another, possibly subaerial, unconformity separates the basalt and volcaniclastic rock from the marine sediment section, because they dated dredged basalt in the southern Kerguelen Plateau area at 114 ± 1 Ma (Barremian), or at least 20 m.y. older than early Turonian.

The Cretaceous/Tertiary boundary at Site 738 is complete, occurring in a 15-cm-thick laminated claystone at 377.1 mbsf. The fine fraction of the laminated claystone consists of 95% microcarbonate particles and few to rare nannofossils. Magnetostratigraphy identifies lowermost Tertiary magnetic anomalies 27 and 28 in Cores 119-738C-17H (341.3–350.9 mbsf) and 119-738C-18H (350.9–360.9 mbsf), further evidence of the completeness of the lowermost Tertiary at Site 738. In the interval from 80 to 85 cm in Section 119-738C-20R-5 (377.05–377.00 mbsf), Danian taxa increase from less than 1% to 50% of the assemblage, with the remainder consisting of Cretaceous taxa. Because this gradual replacement of Cretaceous by early Tertiary age nannofossils occurs in a laminated claystone, the transition cannot be explained by bioturbation processes, but must be truly gradational or the result of a lateral influx of older Cretaceous material.

Another significant paleontological finding at Site 738 is the occurrence of the low-latitude diatoms *Thalassiosira convexa aspinosa*, *Thalassiosira miocenica*, and *Thalassiosira praeconvexa* in Samples 119-738B-3H-2, 148 cm (16.48 mbsf), and 119-738B-3H-3, 62 cm (17.12 mbsf), which coincides with a latest Miocene warm interval between 5.8 and 6.1 Ma.

Geotechnical Stratigraphy

The six geotechnically distinguishable units recognized at Site 738 correspond in part to the lithologic units. The first geotechnical unit is characterized by a high water content and low bulk density, which is typical of diatom oozes. A second geotechnical unit between 17.7 and 135 mbsf has a bulk density, water content, and porosity that show little scatter in values and normal depth-related trends (i.e., increasing bulk density and decreasing porosity and water content with depth). The third geotechnical unit (135–210 mbsf) corresponds to an interval with a distinct change of gradient in porosity and water content with depth, which may indicate an increase in diagenesis that is not apparent in the lithostratigraphy. Interstitial-water chemistry shows a slight increase in dissolved silica in this middle Eocene interval, and radiolarians are relatively common, although highly spo-

radic. A fourth geotechnical unit (210–410 mbsf) is basically chalk, and it is marked by a new downhole gradient in index-property depth profiles. The base of the fourth geotechnical unit and the top of the fifth geotechnical unit (410 mbsf) correspond with an unconformity between the upper Maestrichtian and Campanian. This horizon is marked by an abrupt downhole increase in wet-bulk density and a decrease in water content and porosity. A final geotechnical unit between 485 and 533 mbsf is composed of the volcaniclastic rocks and basalt and is marked by large variations in density and velocity, probably reflecting different degrees of alteration.

Logging

Logging was completed between 97 and 457 mbsf at Site 738, and four logging units are recognized: unit 1, 97–250 mbsf; unit 2, 250–344 mbsf; unit 3, 344–405 mbsf; and unit 4, 405–455 mbsf. The upper three logging units correspond to intervals that display the same general downhole trends in resistivity, density, sonic velocity, and porosity, whether those parameters are uniform, increasing, or decreasing within the interval. The top of the fourth logging unit is marked by an abrupt increase in sonic velocity, resistivity, density, and radioactivity and an abrupt decrease in porosity. The boundaries between logging units 1 and 2 and logging units 3 and 4 correspond respectively to the boundary between lithologic Units IV and V (lower Eocene/middle Eocene boundary) and to the Campanian/upper Maestrichtian unconformity, which also marks a geotechnical unit boundary. The 2/3 logging unit boundary at 344 mbsf falls within the lower Paleocene and is not marked by either a lithologic or a geotechnical change.

Seismic Stratigraphy and Tectonic History

Recent seismic work in the southern Kerguelen Plateau, especially in the Raggatt Basin north of Site 738, identifies six major regional reflectors: a basal unit F, which fills depressions in the basement; a thick unit E, which has a mounded upper surface and is dated as Late Cretaceous; a depression-filling unit D, which is undated; a thick unit C, which is middle to upper Eocene in part; and two post-Eocene units A and B, which are relatively thin and more limited in areal extent than the underlying sequences (Colwell et al., in press; Leclaire et al., 1987; Bassias et al., 1987). Although no attempt was made to trace these reflectors south to the area of Site 738, it is possible to compare the ages of the seismic units recognized at Site 738 with those of the Raggatt Basin.

The upper seismic unit at Site 738 consists of the abbreviated Neogene biosiliceous sequence (0–17.7 mbsf = geotechnical unit G1), and it appears to be an age-equivalent of Colwell et al.'s (in press) seismic units A and B. A second seismic unit at Site 738 consists of lower Oligocene to middle Eocene nannofossil ooze (17.7–210 mbsf), which is equivalent to logging unit 1 and geotechnical units G2 and G3. This seismic unit is correlative, at least in part, with Colwell et al.'s (in press) seismic unit C. Between 210 and 410 mbsf, a third seismic unit that corresponds with logging units 2 and 3 and geotechnical unit G4 is a middle Eocene to upper Maestrichtian chalk. The upper boundary of this seismic unit appears to be a diagenetic boundary, and it is unclear whether this unit has a correlative equivalent in the Raggatt Basin. A fourth seismic unit at Site 738 (410–480 mbsf) is Campanian to Turonian limestone, which is equivalent to geotechnical unit G5 and logging unit 4. This seismic unit may be equivalent to parts of either or both of Leclaire et al.'s (1987) units E and F.

Leclaire et al. (1987) suggest that arching of the Kerguelen Plateau occurred at the top of their seismic unit E, which they date as latest Cretaceous. It is possible that the unconformity between upper Maestrichtian chalk and Campanian limestone (410 mbsf), which also marks seismic, geotechnical, and logging unit boundaries at Site 738, resulted from this tectonic event. A final seismic unit recognized at Site 738 is the volcaniclastics and altered basalt flows encountered between 495.6 and 533.8 mbsf (sixth geotechnical unit).

The Cretaceous and Paleogene geologic history of Site 738 resembles the geologic history proposed by Leclaire et al. (1987) and Colwell et al. (in press) for the southern Kerguelen Plateau. Nearshore to subaerial volcanism in the pre-Turonian was accompanied by deposition of volcaniclastic rocks. Subsidence during the Turonian to Maestrichtian coincided with deposition of limestone in a shelf environment. During the earliest Paleocene to the earliest Oligocene, Site 738 underwent subsidence to water depths at or near the present depth (2252.5 m). Unlike the northern and central parts of the Kerguelen Plateau, however, there is no evidence that Site 738 was uplifted and subaerially eroded after the Eocene. Instead, deposition of the abbreviated Oligocene and Neogene section of the site was influenced by strong bottom currents, which caused erosion and/or nondeposition.

If the Turonian limestone at Site 738 was deposited near sea level, the surface of the basaltic basement has subsided 2742 m in approximately 90 m.y. Roughly 150 m of this subsidence is probably due to isostatic compensation of the 500-m-thick pile of sediments, estimated at one-third of the sediment thickness (van Andel et al., 1977). The present depth of the basement at Site 738 and its minimum age of 90 Ma agree well with the subsidence curve for aseismic ridges published by Detrick et al. (1977; Fig. 38). This suggests that the subsidence of Site 738 may be due mainly to thermal contraction of a cooling lithosphere, occurring at the same rate as that of oceanic crust located on aseismic ridges or on other volcanic ridges. Assuming that the site was near sea level at 90 Ma and discounting eustatic changes in sea level, one would expect water depths at Site 738 at the end of the Campanian to be about 1200 m. However, upper Maestrichtian benthic foraminifers suggest a considerably shallower paleodepth near the outer shelf (400–600 m), arguing that additional tectonic factors may also be responsible for the subsidence history of Site 738.

REFERENCES

Barker, P. F., Kennett, J. P., et al., 1988. *Proc. ODP, Init. Repts.*, 113: College Station, TX (Ocean Drilling Program).

Barron, J. A., and Keller, G., 1982. Widespread Miocene deep-sea hiatuses: coincidence with periods of global cooling. *Geology*, 10:577–581.

Bassias, Y., Davies, H., Leclaire, L., and Weis, D., 1987. Basaltic basement and sedimentary rocks from the southern sector of the Kerguelen-Heard Plateau: new data and their Meso-Cenozoic paleogeographic and geodynamic implications. *Bull. Mus. Natl. Hist. Nat.*, 9: 367–403.

Berggren, W. A., and Aubert, J., 1976. Eocene benthonic foraminiferal biostratigraphy and paleobathymetry of Orphan Knoll (Labrador Sea). *Micropaleontology*, 22:327–346.

Berggren, W. A., Kent, D. V., Flynn, J. J., and Van Couvering, J. A., 1985. Cenozoic geochronology. *Geol. Soc. Am. Bull.*, 96:1407–1418.

Bolli, H. M., and Saunders, J. B., 1985. Oligocene to Holocene low latitude planktonic foraminifera. *In* Bolli, H. M., Saunders, J. B., and Perch-Nielsen, K. (Eds.), *Plankton Stratigraphy*: Cambridge (Cambridge Univ. Press), 155–262.

Ciesielski, P. F., 1983. The Neogene and Quaternary diatom biostratigraphy of subantarctic sediments. *In* Ludwig W. J., Krasheninnikov, V. A., et al., *Init. Repts. DSDP*, 71: Washington (U. S. Printing Office), 635–665.

Claypool, G. E., and Kvenvolden, K. A., 1983. Methane and other hydrocarbon gases in marine sediments. *Annu. Rev. Earth Planet. Sci.*, 11:299–327.

Coffin, M. F., Davies, H. L., and Haxby, W. F., 1986. Structure of the Kerguelen Plateau province from SEASAT altimetry and seismic reflection data. *Nature*, 324:134–136.

Colwell, J. B., Coffin, M. F., Pigram, C. J., Davies, H. L., Stagg, H.M.J., and Hill, P. J., in press. Seismic stratigraphy and evolution of the Raggatt Basin, southern Kerguelen Plateau. *Mar. Petrol. Geol.*

Corliss, B. H., 1979. Recent deep-sea benthonic formainiferal distributions in the southeast Indian Ocean: inferred bottom-water routes and ecological implications. *Mar. Geol.*, 31:115–138.

Detrick, J. G., Sclater, J. G., and Thiede, J., 1977. The subsidence of aseismic ridges. *Earth Planet. Sci. Lett.*, 34:185–196.

Dorn, W. U., 1987. Late Miocene hiatuses and related events in the central equatorial pacific: their depositional imprint and paleoceanographic implications [Ph.D. dissert.]. Univ. of Hawaii.

Fluegel, E., 1982. *Microfacies Analysis of Limestones*: Berlin (Springer).

Fryxell, G. A., in press. Antarctic marine phytoplankton at the Weddell Sea ice edge: seasonal changes at the specific level. *Polar Biol.*

Fryxell, G. A., and Kendrick, G. A., 1988. Austral spring microalgae across the Weddell Sea ice edge: spatial relationships found along a northward transect during AMERIEZ 83. *Deep Sea Res., Part A*, 35:1–20.

Gieskes, J. M., 1983. The chemistry of interstitial waters of deep sea sediments: interpretation of deep sea drilling data. *In* Riley, J. P., and Chester, R. (Eds.), *Chemical Oceanography* (vol. 8): New York (Academic Press), 221–269.

Gombos, A. M., Jr., 1977. Paleogene and Neogene diatoms from the Falkland Plateau and Malvinas Outer Basin: Leg 36, Deep Sea Drilling Project. *In* Barker, P. F., Dalziel, I.W.D., et al., *Init. Repts. DSDP*, 36: Washington (U.S. Govt. Printing Office), 575–687.

Helby, R., Morgan, R., and Partridge, A. D., 1987. A palynological zonation of the Australian Mesozoic. *In* Jell, P. A. (Ed.), *Studies in Australian Mesozoic Palynology*: Mem. Assoc. Aust. Palynol., 4:1–85.

Houtz, R. E., Hayes, D. E., and Markl, R. G., 1977. Kerguelen Plateau, bathymetry, sediment distribution and crustal structure. *Mar. Geol.*, 25:95–130.

Jenkins, D. G., 1985. Southern mid-latitude Paleocene to Holocene planktonic foraminifera. *In* Bolli, H. M., Saunders, J. G., and Perch-Nielsen, K. (Eds.), *Plankton Stratigraphy*: Cambridge (Cambridge Univ. Press), 263–282.

Keller, G. H., and Bennett, R. H., 1971. Sediment mass physical properties—Panama Basin and northeastern Equatorial Pacific. *In* van Andel, T. H., Heath, G. R., et al., *Init. Repts. DSDP*, 16: Washington (U.S. Govt. Printing Office), 499–512.

King, T. W., Banerjee, S. K., Marvin, T., and Ozdemir, O., 1982. A comparison of different magnetic methods for determining the relative grain size of magnetite in natural materials: some results from lake sediments. *Earth Planet. Sci. Lett.*, 59:404–419.

Kolla, V., Sullivan, L., Streeter, S., and Langseth, M., 1976. Spreading of Antarctic Bottom Water and its effects on the floor of the Indian Ocean inferred from bottom-water potential temperature, turbidity, and sea-floor photography. *Mar. Geol.*, 21:171–189.

Leclaire, L., Bassias, Y., Denis-Clocchiatti, M., Davies, H., Gautier, I., Gensous, B., and Wannesson, J., 1987. Lower Cretaceous basalt and sediments from the Kerguelen Plateau. *Geo-Mar. Lett.*, 7:169–176.

Martini, E., 1971. Standard Tertiary and Quaternary calcareous nannoplankton zonation. *In* Farinacci, A. (Ed.), *Proc. Planktonic Conf. II Rome 1970*: Rome (Technoscienze), 2:739–785.

Martini, E., and Müller, C., 1986. Current Tertiary and Quaternary calcareous nannoplankton stratigraphy and correlations. *Newsl. Stratigr.*, 16:99–112.

McDuff, R. E., 1978. Conservative behavior of calcium and magnesium in interstitial waters of marine sediments: identification and interpretation [Ph.D. dissert.]. Univ. of California, San Diego.

McDuff, R. E., and Gieskes, J. M., 1976. Calcium and magnesium profiles in DSDP interstitial waters: diffusion or reaction? *Earth Planet. Sci. Lett.*, 33:1–10.

Monechi, S., and Thierstein, H. R., 1985. Late Cretaceous-Eocene nannofossil and magnetostratigraphic correlations near Gubbio, Italy. *Mar. Micropaleont.*, 9:419–440.

Morimoto, N., 1988. Nomenclature of pyroxenes. *Schweiz. Mineral. Petrogr. Mitt.*, 68:95–111.

Okada, H., and Bukry, D., 1980. Supplementary modification and introduction of code numbers to the low-latitude coccolith biostratigraphic zonation (Bukry, 1973; 1975). *Mar. Micropaleont.*, 5:321–325.

Perch-Nielsen, K., 1985. Cenozoic calcareous nannofossils. *In* Bolli, H. M., Saunders, J. B., Perch-Nielsen, K. (Eds.), *Plankton Stratigraphy*: Cambridge (Cambridge Univ. Press), 427–554.

Peterson, L. C., 1984. Recent abyssal benthic foraminiferal biofacies of the eastern equatorial Indian Ocean. *Mar. Micropaleont.*, 8:479–509.

Priddle, J., and Fryxell, G. A., 1985. *Handbook of the Common Plankton Diatoms of the Southern Ocean: Centrales Except the Genus Thalassiosira*: Cambridge (Cambridge Univ. Press).

Roth, P. H., 1978. Cretaceous nannoplankton biostratigraphy and oceanography of the northwestern Atlantic Ocean. *In* Benson, W. E., Sheridan, R. E., et al., *Init. Repts. DSDP*, 44: Washington (U.S. Govt. Printing Office), 731–759.

Scholle, P. A., 1978. *A Color Illustrated Guide to Carbonate Rock Constituents, Textures, Cements, and Porosities*: AAPG Memoir, 27.

Shipboard Scientific Party, 1988. Site 689. *In* Barker, P. F., Kennett, J. P., et al., *Proc. ODP, Init. Repts.*, 113: College Station, TX (Ocean Drilling Program), 89–181.

Stumm, W., and Morgan, J. J., 1981. *Aquatic Chemistry*: New York (Wiley).

Taylor, E., 1984. Oceanic sedimentation and geotechnical stratigraphy: hemipelagic carbonates and red clays [Ph.D. dissert.]. Texas A&M Univ.

Tjalsma, R. C., and Lohmann, G. P., 1983. Paleocene-Eocene bathyal and abyssal benthic foraminifera from the Atlantic Ocean. *Micropaleontology, Spec. Publ.*, 4:1–90.

Toumarkine, M., and Luterbacher, H., 1985. Paleocene and Eocene planktonic foraminifera. *In* Bolli, H. M., Saunders, J. B., and Perch-Nielsen, K. (Eds.), *Plankton Stratigraphy*: Cambridge (Cambridge Univ. Press), 87–154.

van Andel, T. H., Thiede, J., Sclater, J. G., and Hay, W. W., 1977. Depositional history of the South Atlantic Ocean during the last 125 million years. *J. Geol.*, 85:651–698.

Wei, W., and Wise, S. W., Jr., in press. *Discoaster praebifax* n. sp.—possible ancestor of *Discoaster bifax* Bukry (calcareous nannofossil). *J. Paleontol.*
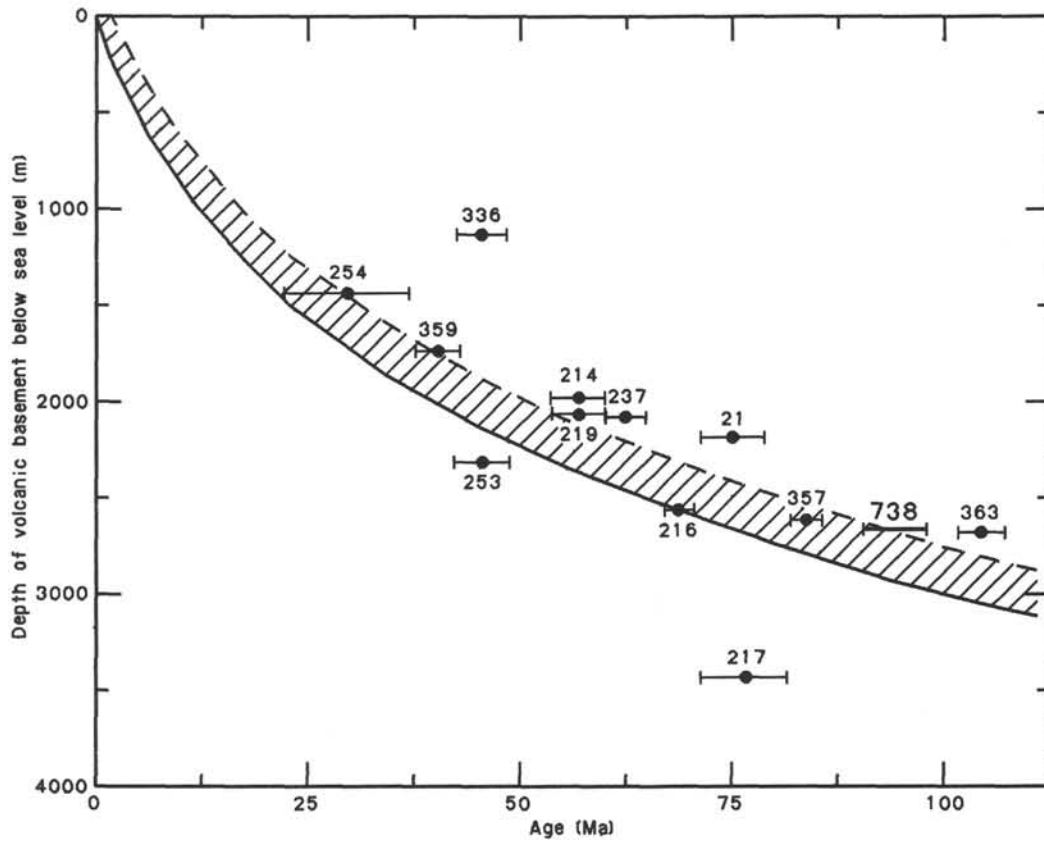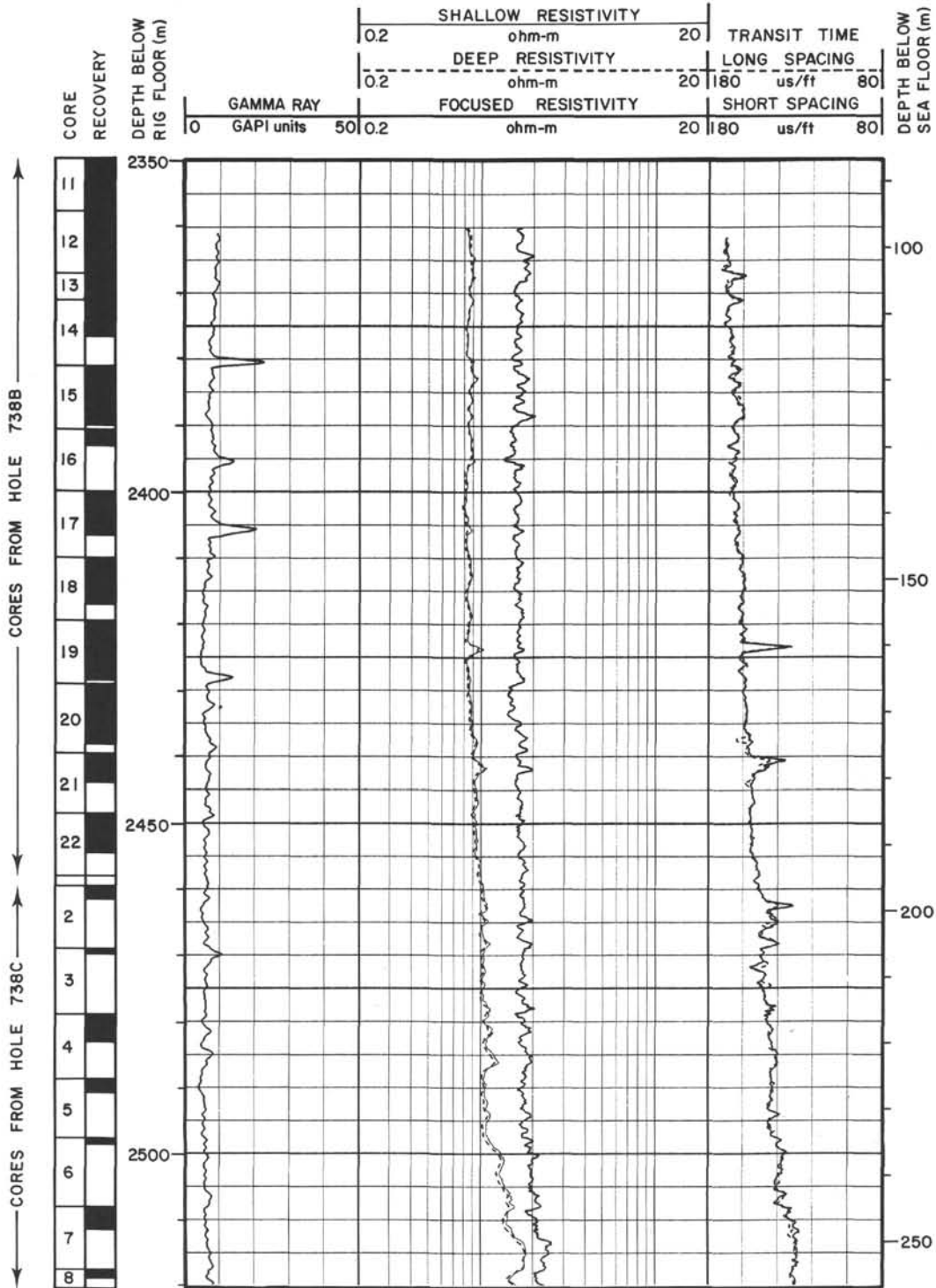
Ms 119A-106

Figure 38. Plot of depth vs. age of DSDP sites on aseismic ridges inferred to have formed near sea level (Detrick et al., 1977). The heavy black line is an empirical curve showing depth range expected on the assumption of normal subsidence. The dashed line is the same curve displaced upward by 300 m.
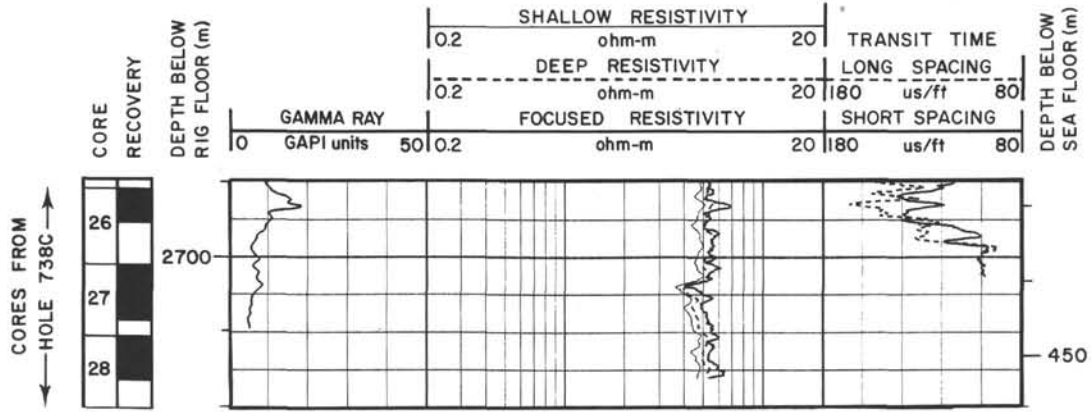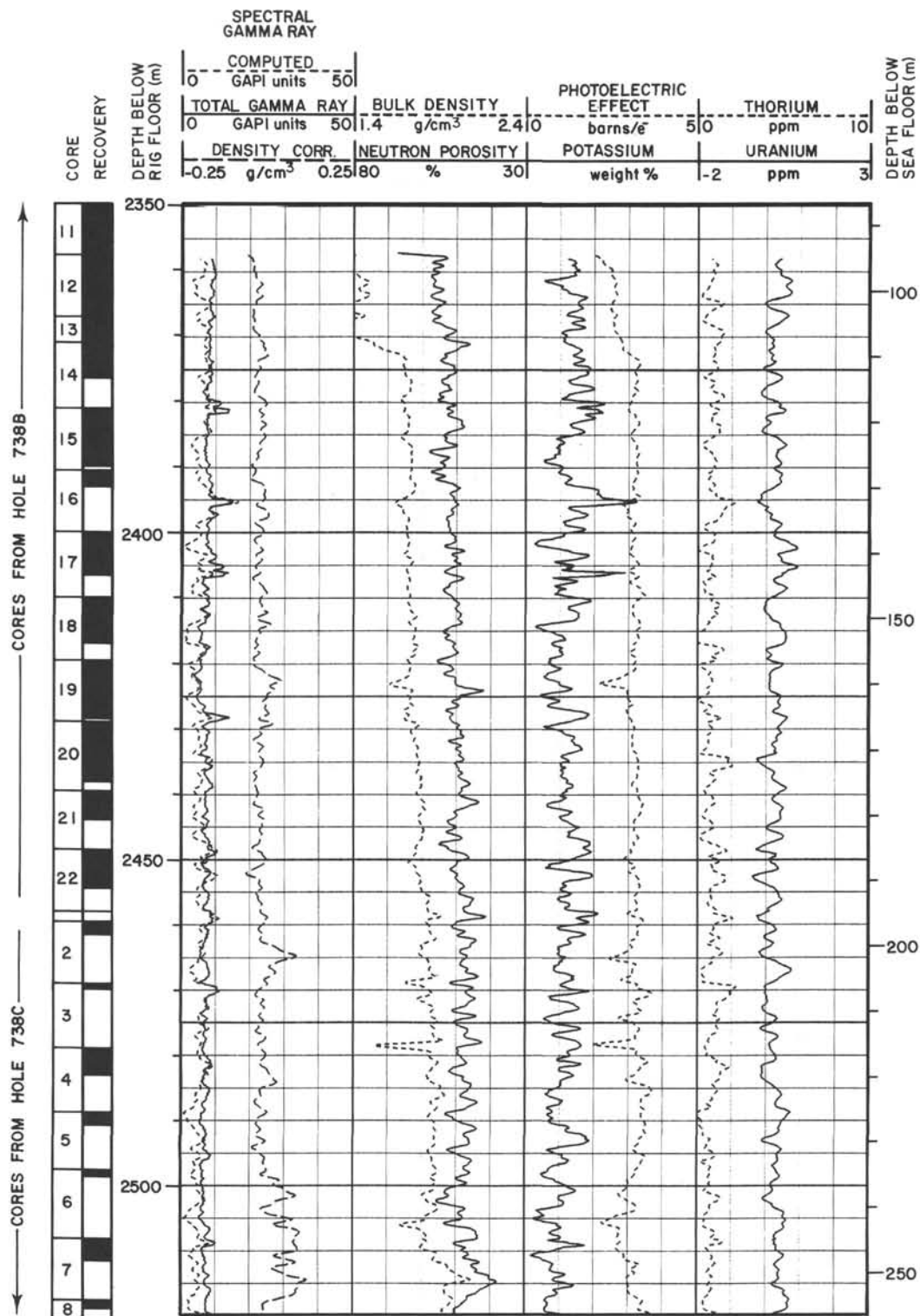
Summary Log for Hole 738C
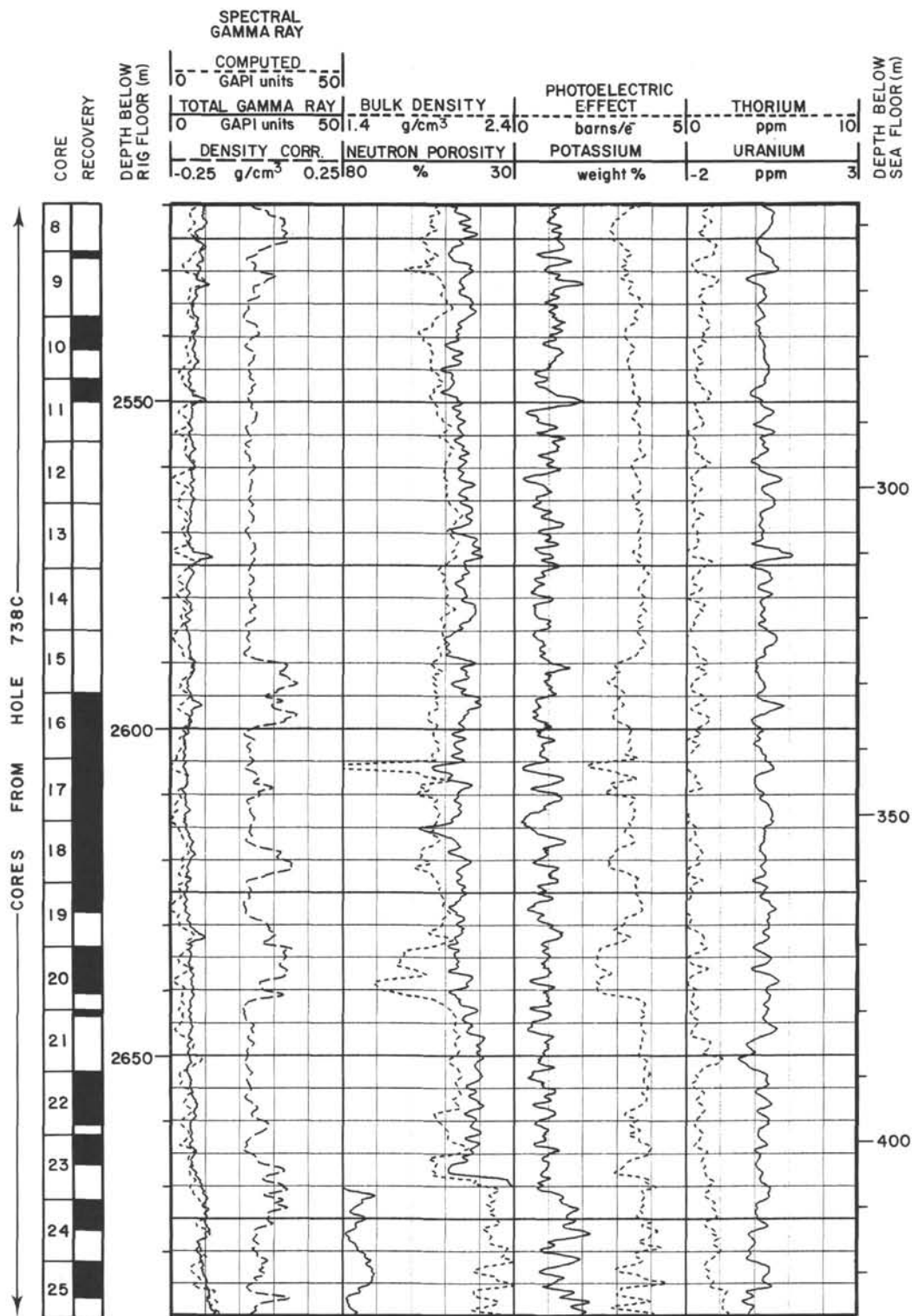
Summary Log for Hole 738C (continued)

Summary Log for Hole 738C (continued)

Summary Log for Hole 738C (continued)

Summary Log for Hole 738C (continued)

Summary Log for Hole 738C (continued)